DISSERTATION

Profilin in *Plasmodium berghei* gliding motility and development

Catherine Anne Moreau

2017

DISSERTATION

submitted to the Combined Faculties for the Natural Sciences and for Mathematics of the
Ruperto-Carola University of Heidelberg, Germany
for the degree of
Doctor of Natural Sciences

presented by
Master of Science Catherine Anne Moreau
born in Troisdorf, Germany
Oral examination: 22.09.2017

Profilin in *Plasmodium berghei* gliding motility and development

Referees:

Prof. Dr. Michael Lanzer,
Center for Infectious Diseases, Parasitology
University of Heidelberg

Prof. Dr. Friedrich Frischknecht,
Center for Infectious Diseases, Integrative Parasitology
University of Heidelberg

Zusammenfassung

Profilin ist ein Aktinbindeprotein und spielt bei Zellbewegungen eine zentrale Rolle. Interessanterweise hat der Stamm der Apicomplexa, zu der mehrere bedeutende Pathogene wie *Toxoplasma* und *Plasmodium* gehören, eine sehr ungewöhnliche Profilinvariante. In diesen Parasiten enthält Profilin drei zusätzliche Strukturmotive, die in anderen Organismen wie Hefe, Pflanzen und Tiere fehlen. Zudem haben zum Stamm der Apicomplexa gehörende Parasiten eine einzigartige Form der Fortbewegung die auf einem Aktin-Myosin-Motor beruht. Dieser Motor befähigt die invasiven Stadien des Parasiten, sich mit hohen Geschwindigkeiten fortzubewegen. Sporozoiten, die Stadien, welche von Moskitos in die Haut des Wirts übertragen werden, bewegen sich am schnellsten.

Eines der zusätzlichen Strukturmotive in Profilin der Apicomplexa ist eine β-Schleife, genannt Armmotiv, die im Verdacht steht an der Aktinbindung beteiligt zu sein, was ich im Rahmen dieser Arbeit durch eine Kombination biochemischer und computergestützter Analysen von Proteinen, Molekulargenetik von *Plasmodium berghei* Parasiten und biophysikalischen Messungen an Sporozoiten aufzeigen konnte. Bestätigt werden konnte nicht nur dass das Armmotiv in der Aktinbindung involviert ist, sondern auch, dass das Armmotiv für die zweidimensionale Zellmotilität eine entscheidende Bedeutung hat. Interessanterweise brachte die Deletion des Armmotivs Sporozoiten mit einer geringeren Virulenz hervor als Wildtyp Sporozoiten. Bestimmte Mäuse waren in der Lage, die sporozoiten-induzierte Infektionen mit der Armdeletion zu überleben und abzuwehren, und waren anschließend gegen den schweren Verlauf der Malaria geschützt und in der Lage, Wildtypinfektionen zu überstehen. Dies weist darauf hin, dass es prinzipiell möglich sein sollte, einen genetisch attenuierten Parasiten zu generieren und ihn für sporozoiten-induzierte Blutstadienimpfungen einzusetzen.

Außerdem fanden wir Hinweise, dass ein weiteres der zusätzlichen Motive, der ‘acidic loop’, zur Orientierung des Armmotivs beiträgt und somit die Aktinbindung beeinflusst. Obwohl angenommen wurde, dass Profilin essentiell sei, gelang es mir einen Profilin-Knockout zu generieren. Im Zuge dessen konnte gezeigt werden dass Profilin im Blutstadium nicht essentiell ist auch wenn die Multiplikationsrate des Profilin-Knockouts signifikant reduziert war. Profilin war jedoch notwendig für die Entwicklung der Moskitostadien, da die Abwesenheit von Profilin zu beschädigten ‘crystalloid bodies’ führte, und, was noch bedeutsamer ist, das Fehlen von Speicheldrüsen-Sporozoiten nach sich zog.

Summary

Profilin is an actin binding protein playing a central role in cell motility. Interestingly, the group of Apicomplexa that contains a number of important pathogens like *Toxoplasma* and *Plasmodium* has a very unusual type of profilin. In these parasites, profilin contains three additional structural motifs that are not found in other organisms like yeast, plants or animals. Additionally, apicomplexan parasites have a unique way of cell locomotion that is based on an unusual actin-myosin motor. This motor enables the invasive stage of the parasite to move with high speeds. In *Plasmodium* the sporozoite, the stage transmitted to the skin of the host by a mosquito, displays the highest speed.

One of the additional structural motifs of apicomplexan profilin, a β-hairpin extension called the arm motif, has been suggested to be involved in actin binding. During this work, I could show through a combination of biochemical and computational analyses of proteins, molecular genetics of *Plasmodium berghei* parasites and biophysical measurements on sporozoites that this assumption is true. Not only could we show that the arm motif is involved in actin binding, but we could show that the arm motif is crucial for 2D gliding motility of sporozoites.

Deletion of the arm motif produced sporozoites that were less virulent than wild type sporozoites. Certain mice were able to survive and clear sporozoites-induced infections with the arm deletion parasites and were later protected against severe malaria and able to clear wild type infections. This indicates, that it should in principle be possible to generate a genetically attenuated parasite for use in sporozoite-induced blood stage vaccinations. We found indications that another additional motif, the acidic loop, is involved in defining the arm motif orientation and thus influences actin binding. Even though profilin was suggested to be essential I was able to generate a profilin knockout. This revealed that profilin is not essential in the blood stage, although the growth rate of the profilin knockout was significantly reduced. However, profilin was necessary during mosquito development, as loss of profilin led to impaired crystalloid body integrity and most significantly, a lack of salivary gland sporozoites.

Table of contents

Abbreviations

ABP	actin binding protein
ADP	adenosine diphosphate
ATP	adenosine triphosphate
BS	blood stage(s)
BSA	bovine serum albumin
CD	Cytochalasin D
cDNA	complementary DNA
(E)CM	(experimental) cerebral malaria
CSP	circumsporozoite protein
DIC	differential interference contrast
dNTP	deoxynucleotide triphosphate
DV	digestive vacuole
F-actin	filamentous actin
FBS	fetal bovine serum
FBT	fresh blood transfer
G-actin	globular actin
GAP	glideosome-associated protein
GAPM	glideosome-associated protein with multiple-membrane spans
gDNA	genomic DNA
HSP70	heat shock protein 70
IMC	inner membrane complex
IP	intraperitoneal(ly)
IV	intravenous(ly)
MLC	myosin light chain
PBS	phosphate buffered saline
PCR	polymerase chain reaction
Pfn	profilin
P_i	inorganic phosphate
PM	plasma membrane
PV	parasitophorous vacuole
(i)RBC	(infected) red blood cell
RT	room temperature
SC	subcutaneous(ly)
T_a	T_{anneal}, annealing temperature of primers
TLR	toll-like receptor
TRAP	thrombospondin-related anonymous protein
U	unit(s)
UTR	untranslated region
WHO	World Health Organization
Wt	wild type

1 Introduction

1.1 Cell motility

Cellular movement is a necessity for many processes in life. For both unicellular and multicellular organisms, it is of an advantage to be able to move. On a macroscopic level, motility is necessary for many animals to avoid predators or seek food and shelter. On a microscopic level, single cells have to be able to move within the body of complex organisms for example during embryogenesis or for immune surveillance.

Nature has achieved a number of different mechanisms that facilitate movement of single cells. For example, extracellular appendages like flagellin-based flagella in bacteria, microtubule-based flagella or cilia in protists and higher eukaryotes enable cells to propel themselves forward or backward and allow directional changes – much like a propeller on a boat (Samatey *et al.*, 2004). This type of movement is dependent on access to a liquid 3D environment, and does not require a solid substrate.

In contrast to that, solid substrates are required for another type of cell motility that doesn't involve appendages but is best described by cell crawling. This is considered the classical type of vertebrate cell motility during which the cell protrudes on one side of the cell and retracts on the other side, thus pulling itself over the substrate (Pollard & Borisy, 2003). During this process, contact areas to the substrate are formed at the leading edge and disengaged at the back end of the cell. The protrusions can be either thin, rod-like filopodia or present themselves as thin sheets called lamellipodia that can stretch along the width of the whole cell (Figure 1). They can occur separately or together – filopodia can protrude more or less from lamellipodia and the space between filopodia can be filled creating a lamellipodium. In any case these structures are highly dynamic and the shape of cells changes drastically during this process. The main component and driver of these protrusions is a protein called actin, whose key ability is polymer formation that drives many motility-related processes.

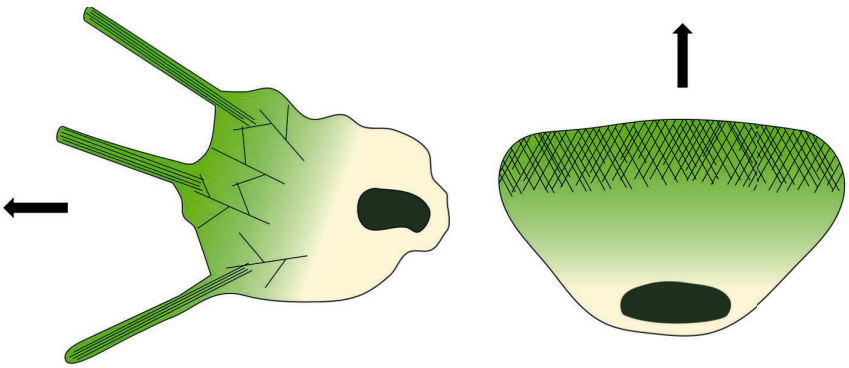

Figure 1: Morphology of cell protrusions created by actin. Left side: Cell displaying filopodia that point towards the direction of movement (arrow). Filopodia are formed by bundled actin filaments. Right side: Cell with an extensive lamellipodium created by a dense network of highly branched actin filaments.

The membrane area that faces the direction of movement is called the leading edge. Different types of cells display different morphologies of their leading edges. For example during movement fish keratocytes do not display filopodia but a very broad 180° lamellipodium that is very stable during motility (Small *et al.*, 1995). The lamellipodium only changes its shape if environmental factors like adhesiveness of the substrate or the temperature are altered (Barnhart *et al.*, 2011, Ream *et al.*, 2003). Other cells (e.g. U2OS cells) form more transient lamellipodia (Hotulainen & Lappalainen, 2006). The growth cones of nerve cells are largely based on filopodia but can fill in the space between them to create a large lamellipodium when growth factors are present (Marsick *et al.*, 2010).

Another type of cellular motility that involved a type of protrusion called plasma membrane blebs is not generated through actin polymerization (Fackler & Grosse, 2008). Instead, the cell generates a local breakdown of the actin cortex that can lead to the inflation of the PM into a spherical protrusion filled with cytoplasm (Charras & Paluch, 2008). Subsequently, the actin cortex is re-established at the new position of the membrane (Fackler & Grosse, 2008). This type of movement has been described for example in zebrafish primordial germ cells (Blaser *et al.*, 2006) and a number of tumors (Lammermann & Sixt, 2009) that migrate in dense 3D meshes.

1.1.1 Classical actin

Many of the proteins that are involved in creating maintaining and changing the structures of and behind the motility-related protrusions have been identified. The major building block of cellular protrusions is a 42-kDa protein called actin. The protein exists in several isoforms that differ only in the first 10 amino acid positions and only in a maximum of four residues at a time (Perrin & Ervasti, 2010). Polymerization of this globular protein into filaments of varying length and orientation is a key driver of typical vertebrate cell motility. For the actin monomers to polymerize they must be bound to ATP. Filaments are formed by adding monomers in head-to-tail fashion and initiated through a nucleation step. The monomers are attached to each other lengthwise in two rows that twist around each other, giving the appearance of beads on two strings that wrap around each other. In this array, each monomer has contact with four other monomers: one above, one below and two on the opposite side (Holmes *et al*., 1990). ATP-actin dimer and trimer (‘nucleus’) formation is an unfavorable step but as soon as it occurs, these nuclei are quickly elongated into filaments. After a half time of 2 seconds inside the filament, the ATP is hydrolyzed to ADP+P_i (Pollard & Borisy, 2003) (Figure 2).

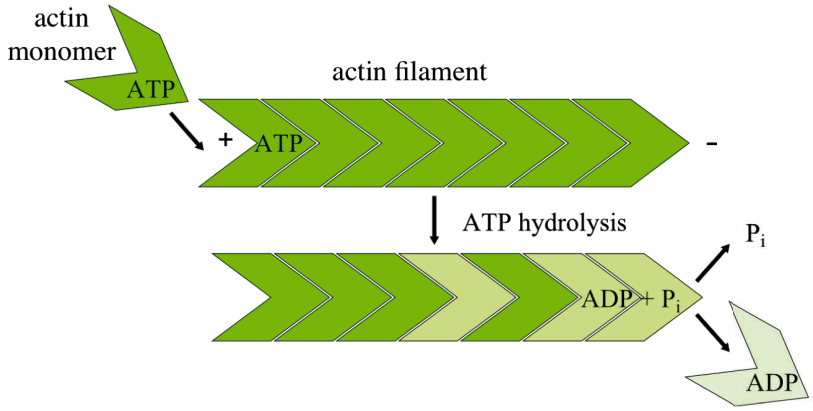

Figure 2: Actin filaments are formed by adding ATP-bound monomers (green) to the barbed or plus end (+) in a head-to-tail fashion. ATP is hydrolyzed but the inorganic phosphate (P_i) stays associated (light green). P_i dissociates later increasing the propensity of ADP-bound monomer (grey) to dissociate from the filament close to the pointed or minus end (-).

In muscle actin filaments, the inorganic phosphate stays associated with ADP actin for much longer (half time of 6 min), however in yeast actin filaments this happens ~50 times faster (Berro *et al.*, 2010). Dissociation of P_i induces a conformational change (Otterbein *et al.*, 2001) that increases the propensity of disassembling the filament (Figure 2). The dissociation of actin monomers from one end (pointed or minus end) and their addition at the other end (barbed or plus end) reaches a seemingly steady-state length in a process called treadmilling (Wegner, 1976). It is thought that growth of actin filaments at their barbed end provides the force to push the leading edge outward. In order for the actin filaments to produce these forces, the actin network has to be highly branched, a process that is enabled by the Arp2/3 complex (Machesky *et al.*, 1994a). Also, only short filaments or branches are stiff enough to produce these forces without buckling, thus special proteins like capping protein block the filament elongation soon after branch formation (Kovar & Pollard, 2004). While actin filaments provides the force to push the leading edge forward, a counteracting force is required in order to result in net forward movement. This can be achieved either via specialized adhesion proteins (adhesins) that establish contact to the substrate and link the cell cortex to the extracellular matrix or by retrograde actin flow (Lammermann *et al.*, 2008) or a combination of both (Renkawitz *et al.*, 2009). Retrograde flow of actin was initially described in photobleaching experiments where the bleached region was flowing towards the cell center with a speed higher than achieved just by the rate of polymerization (Wang, 1985). In other experiments, beads were positioned on top of lamellipodia and also moved towards the cell center (Forscher *et al.*, 1992). Today, we believe that myosins are somehow involved in retrograde flow (Mitchison & Cramer, 1996). Myosins are ATPases that can produce forces through a conformational change when bound to one or several actin filaments. Myosins are mainly thought to provide the force for retracting the rear of the cell during cell motility (Vicente-Manzanares *et al.*, 2009) as they are increasingly concentrated at the back of the cell (Renkawitz *et al.*, 2009). Myosins have also

been reported to be involved in establishing cell polarity for motility and actin disassembly (Wilson *et al.*, 2010, Yam *et al.*, 2007).

In addition to myosins, a myriad of regulatory actin-binding proteins (>160) that affect actin in different ways have been investigated. Many of them are components of the leading edge where they display a high functional diversity and influence the shape of the actin network, giving it a high degree of flexibility and dynamics. Many of them influence actin filaments e.g. filament initiation (nucleation) and/or elongation (formins described below), branching (Arp2/3 as described above), severing, bundling, cross-linking, filament end capping (capping protein also mentioned above) or depolymerization activities. Other proteins act on monomeric actin, like monomer sequestration or delivering monomers to the growing filament. A prominent member of this group of actin monomer binding proteins is profilin.

1.1.2 Profilin

Profilin was first isolated from calf spleen, crystallized in 1976 and found to be in association with actin in a 1:1 complex (Carlsson *et al.*, 1976). The crystal structure revealed the traditional profilin fold where a 7-stranded β-sheet is situated in between two α-helices on both sides. Already one year later, some of its effects on actin polymerization were demonstrated (Carlsson *et al.*, 1977).

Since then, profilin has been shown to be a key player in cell motility-dependent processes: Knocking out profilins led to impaired motility in *Dictostelium discoideum* (Haugwitz *et al.*, 1994) and in *Drosphila melanogaster* (Verheyen & Cooley, 1994). Profilin was also shown to be essential for embryogenesis in mice where homozygous profilin 1 knock out embryos die at the 2-cell stage due to impaired cytokinesis (Witke *et al.*, 2001). While profilin is found in all eukaryotes and even a virus (Machesky *et al.*, 1994b), its amino acid sequence differs considerably between species. Thus, foreign profilins can be powerful antigens and are the underlying basis of many plant allergies for example against birch pollen (Valenta *et al.*, 1992).

Profilin has three different binding partners: Poly-L-prolines (Metzler *et al.*, 1994), phosphoinositolphosphates (PIPs) (Machesky & Poland, 1993) and actin. The poly-L-proline binding site is located at profilins' N- and C-terminus. Poly-proline-stretches are commonly used among actin-binding proteins as a way to bind to each other. Key examples in this regard are formins. These are a special class of proteins that can nucleate filaments and also enhance monomer incorporation during elongation (Otomo *et al.*, 2005). They are associated to the growing end of actin filaments as dimers through homodimeric FH2 domains that together

create a ring structure around the filament (Higashida *et al.*, 2004). Attached to this ring is the formins flexible FH1 domain that functions like a sticky fishing line for G-actin-profilin complexes. The complexes are bound by proline repeat regions (Kursula *et al.*, 2008b) and delivered to the growing end of the filament, increasing the speed of filament elongation considerably (Romero *et al.*, 2004).

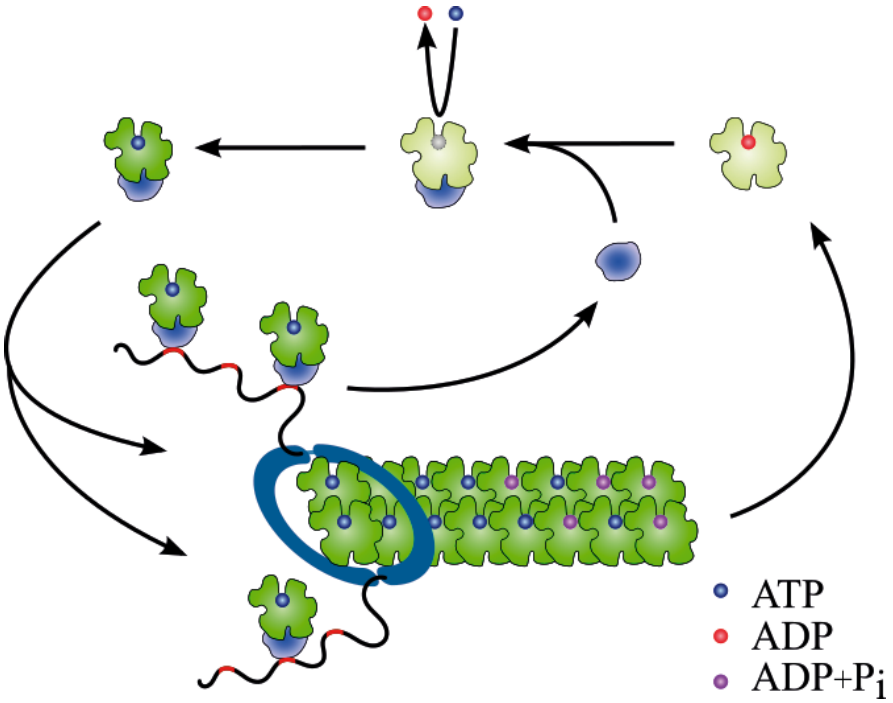

Figure 3: Catalysis of actin filament elongation by profilin and formin. Profilin (blue) catalyzes the exchange from ADP-actin (light green) that dissociates from the filament to ATP-actin (bright green). Dimerized formin FH2 domains (blue ring) are bound to the barbed end of F-actin. Profilin-actin complexes are bound to proline repeat regions (red line) in formins FH1 domains (black line), which incorporate the G-actin into the filament.

Profilin also binds to phosphoinositolphosphates (PIPs) that are part of cellular membranes enabling proteins to associate with membranes; Traditionally profilin binds to phosphatidylinositol - 4, 5-bisphosphate ($PI(4,5)P_2$) and phosphatidylinositol - 3, 4, 5 - triphosphate ($PI(3,4,5)P_3$) and this binding site seems to overlap with both the actin-binding and the poly-L-proline binding-sites (Witke, 2004). PIP binding was actually demonstrated to regulate both actin-binding and poly-L-proline-binding (Witke, 2004). It is still not clear which residues of profilin bind PIPs, but it is known that positively charged amino acids participate in the binding (Chaudhary *et al.*, 1998, Lu & Pollard, 2001, Sohn *et al.*, 1995). Interestingly, all known cellular organelles contain specific types of PIPs (Falkenburger *et al.*, 2010). It is speculated that this enables the cell to recruit certain proteins to organelles with matching PIP profiles (Falkenburger *et al.*, 2010).

The best-known function of profilin is its actin-binding ability. Profilins β-strand 4 and α-helix 4 bind to subdomains 1 and 3 of actin, which leads to an opening of the nucleotide binding cleft of actin, thereby catalyzing the exchange from ADP to ATP (Porta & Borgstahl, 2012, Vinson

et al., 1998). The increase in nucleotide exchange rate highly depends on the species and ranges from zero to 1000-fold (Wolven *et al.*, 2000). As only ATP-bound actin has a much higher affinity for the growing end of filaments than ADP-actin, nucleotide exchange is a key step in providing new polymerizable actin monomers and thus enabling cell motility. The actin-profilin complex is then shuttled to the growing end of actin filaments with the help of formins as described above (Romero *et al.*, 2004).

However, there is still much that we don't know about the role of profilin in complex systems: it is implicated in several different human tumors, but results seem to contradict each other as levels of Pfn-1 and Pfn-2 in some cancer cell types lead to more and in other cells to less invasiveness and metastasis formation (Ding & Roy, 2013, Witke, 2004).

This is just one example of profilin and actin dynamics being involved in disease. However, there are countless other implications of the importance of actin dynamics with regard to disease.

1.2 Malaria

Organisms belonging to the genus of *Plasmodium spp.* are unicellular protists with an obligate parasitic lifestyle involving a mosquito and a vertebrate host. As the causative agent of malaria, these parasites are a heavy health and economic burden: The World Health Organization (WHO) estimates approximately 212 million cases of malaria in 2015, with 90 % occurring in Africa and 7 % in southeast Asia. Of the roughly 430.000 deaths, 70 % represent children under the age of five (WHO, 2016). Currently there is no vaccine available that confers 100 % protection against infection.

The severity of clinical symptoms depends on the species that is causing the infection. There are four main species whose vertebrate hosts are humans: *P. falciparum, P. malariae, P. ovale* and *P. vivax*. Both P. falciparum and P.vivax have been found to be able to infect apes as well (Prugnolle *et al.*, 2010, Ramasamy, 2014). *P. knowlesi*, a species infecting macaques, has been found to be able to infect humans, although mosquitoes only seem to be able to become infected by macaques and not by humans (Ramasamy, 2014). Of the five species infecting humans, *Plasmodium falciparum* is responsible for the majority of severe malaria cases. Typical symptoms include fever, chills, nausea and vomiting, respiratory problems, sweating, headaches and body aches. Many of the severe cases in young children caused by *P. falciparum* include severe anemia and/or neurological impairments that can lead to coma and ultimately death. This latter syndrome is known as cerebral malaria (CM) and is accompanied by a

combination of inflammatory responses from the host as well as parasites obstructing blood vessels. After more than a century of malaria research, we are still without a protective vaccine against *Plasmodium*. The reasons for that include the complexity of the parasite life cycle and also our lack of knowledge of the mechanisms conveying malaria immunity (Stanisic & Good, 2015). We do know, that immunity against symptomatic malaria is slowly acquired with increasing age and is antibody-mediated (Bouharoun-Tayoun *et al.*, 1995, Cohen *et al.*, 1969, Langhorne *et al.*, 2008, Long & Zavala, 2017)} and that protection against severity of disease correlates with the presence of multiple antibodies against several different blood stage epitopes (Osier *et al.*, 2008).

Studies performed in mice have made considerable contributions to our current knowledge and *Plasmodium* strains that infect mice are powerful tools to study *Plasmodium* biology in the laboratory. The best animal model available for CM and severe malaria is *Plasmodium berghei* strain ANKA infection of C57BL/6 mice (de Oca *et al*., 2013), that despite limitations is a very important tool to investigate *Plasmodia* (Langhorne *et al*., 2011, Riley *et al*., 2010, White *et al*., 2010). In addition, several other murine strains are commonly used: *P. yoelii* of which several strains exist that vary with respect to pathology and *P. chabaudi* is used to model uncomplicated malaria (Huang *et al.*, 2015).

1.3 Life cycle

The infection with *Plasmodium* begins with the bite of an infected female mosquito from the genus *Anopheles*. When they bite a vertebrate for a blood meal they inject saliva into the skin of the host while probing for a blood vessel (Ribeiro & Francischetti, 2003). Special proteins in the saliva of *Anopheles* mosquitoes increase vasodilation, prevent blood coagulation and pain reception (Ribeiro & Francischetti, 2003). *Plasmodia* in the form of sporozoites are residing in the salivary glands of female infected mosquitoes. Together with the saliva these sporozoites are transferred into the skin of the host (Menard *et al.*, 2013, Sidjanski & Vanderberg, 1997, Vanderberg & Frevert, 2004). Once inside the dermis, the sporozoites actively migrate to find and invade a blood vessel to be transported to the liver *via* the blood stream (Amino *et al.*, 2006, Douglas *et al.*, 2015). Entering the liver happens in sinusoids through Kupffer cells or endothelial cells (Frevert *et al.*, 2005, Tavares *et al.*, 2013). Once in the liver, the sporozoite traverses several hepatocytes before finally invading the destination cell (Mota *et al.*, 2001). Among others, (CD81, SR-BI) the ephrin A2 receptor on hepatocytes was suggested to be required for establishing an infection (Kaushansky *et al.*, 2015, Vaughan & Kappe, 2017).

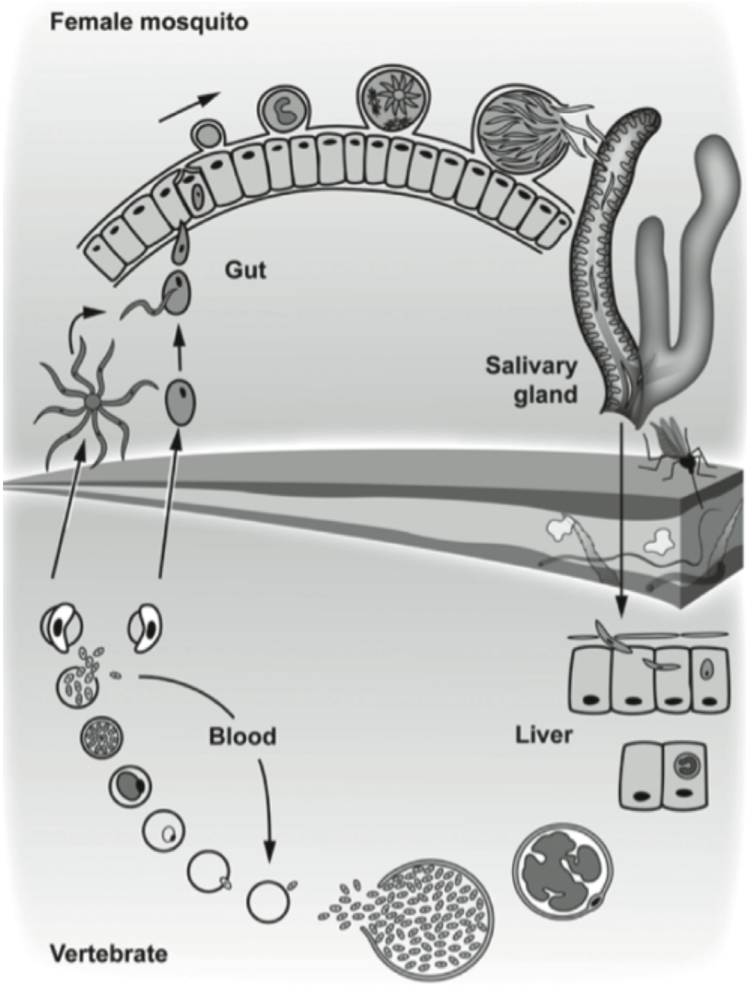

Figure 4: Life cycle of *Plasmodium*. The upper half of the image represents the mosquito and the lower half the vertebrate host. Sporozoites are injected into the skin where they actively move to find and invade a blood vessel. They hitch a ride to the liver in the blood stream. Sporozoites invade the liver and multiply into thousands of merozoites that infect RBCs after leaving the liver. During the blood stage, the parasites multiply with a rate of approximately 10 every day. Some blood stages develop into gametocytes that can fuse once they are taken up by another mosquito. The resulting zygote develops into the motile ookinete that traverses the midgut epithelium of the mosquito and forms an oocyst below the basal membrane of the gut. Oocysts develop and produce thousands of new sporozoites that egress into the hemolymph and invade salivary glands to be transmitted again.

The invasion process involves the formation of a so-called parasitophorous vacuole (PV) inside which the parasite transforms into extra-erythrocytic forms (Mota *et al.*, 2001, Prudencio *et al.*, 2006). The membrane of the PV (PVM) is derived from the host-cell membrane that is extensively remodeled by the parasites. It inserts its own proteins into the PVM some of which have been shown to be essential for liver stage development (Mueller *et al.*, 2005a, Mueller *et al.*, 2005b, van Dijk *et al.*, 2005). Parasites even shed host-cell proteins from the PVM that normally facilitate autophagy (Agop-Nersesian *et al.*, 2017, Grutzke *et al.*, 2014, Prado *et al.*, 2015). In this vacuole, the parasite replicates through schizogony, a specialized form of multiplication that involves several rounds of asynchronous DNA replication and mitosis. Then, in the budding phase, the genome is synchronously undergoing mitosis that is directly followed by cytokinesis. This includes packaging of all other organelles into liver merozoites (Francia & Striepen, 2014). Thousands of merozoites are released into the bloodstream (Prudencio *et al.*, 2006) contained in membranous sacks called merosomes (Sturm *et al.*, 2006) that rupture possibly in the capillaries of the lung (Baer *et al.*, 2007) to release the free

merozoites. Once in the bloodstream, the merozoites invade red blood cells (RBCs) to multiply in the asexual blood stage. Some species preferentially invade reticulocytes, can sometimes switch to infect normocytes, while others directly invade normocytes (Paul *et al.*, 2015). The blood stage is the clinically apparent stage that causes symptoms in the vertebrate host. Again, the parasite establishes a parasitophorous vacuole (PV) during invasion. Inside the PV, the merozoite develops into a ring stage and starts digesting the protein part of hemoglobin in a specialized compartment called the digestive vacuole (DV). Free heme that remains is highly toxic and the parasites protect themselves from it by crystallizing it into hemozoin (Kapishnikov *et al.*, 2012). The new home of the parasite, the RBC is extensively remodeled after the parasite invades (Mbengue *et al.*, 2012). It establishes an elaborate protein export system even creating a special organelle in the RBC cytoplasm to send some of its own proteins to the surface of the RBC (de Koning-Ward *et al.*, 2016). The parasite continues to grow into a trophozoite and finally a blood stage schizont. One major function of parasitic proteins on the RBC surface in *P. falciparum* (PfEMP-1) is cytoadherence of these later stages of infected RBC to endothelial walls of blood vessels to avoid clearance by the spleen (Langreth & Peterson, 1985). After 24 – 72 hours (depending on the species), the newly formed merozoites egress from the PV and the RBC to invade new ones.

Under circumstances such as cell stress caused by host immunity, antimalarial drug treatment, anemia or high parasite density, some schizonts (Justin Boddey, personal communication) form gametocyte-committed merozoites (Meibalan & Marti, 2016). These merozoites are already primed to develop into either female or male gametocytes that activate once they are taken up by a mosquito during its blood meal (Silvestrini *et al.*, 2000). Sexual commitment is dependent on a transcription factor called ApiAP2-G (Kafsack *et al.*, 2014, Sinha *et al.*, 2014). Inside the gut of the mosquito – sensed by the temperature drop, the presence of xanthurenic acid and a drop in pH (Billker *et al.*, 1998, Billker *et al.*, 2000) – both male and female gametocytes egress from the red blood cell. This process involves the secretion of specialized vesicles called osmiophilic bodies that leads to lysis of the PVM and the plasma membrane of the RBC (Bennink *et al.*, 2016, Kehrer *et al.*, 2016). The male gametocyte differentiates into 8 microgametes in a process called exflagellation. Each one can fertilize a female macrogamete and thus form a zygote (Sinden *et al.*, 2010).

The zygote develops into an ookinete that is able to actively traverse the epithelium of the mosquito midgut. This process involves at least a transient PV, and occurs mostly intracellularly (Vlachou *et al.*, 2004). Once it reaches the other side of the gut the ookinete

transforms into an oocyst between the gut epithelium and its surrounding basal lamina (Vlachou *et al.*, 2006). This process might be induced through contact with the basal lamina as hemocoel-injected ookinetes can form early oocysts in *Drosophila* and *Aedes* (Schneider & Shahabuddin, 2000). Inside the oocyst, thousands of sporozoites are formed in a process called sporogony. Once the sporozoites are properly formed, they seem to display motility before they egress from the oocysts (Klug & Frischknecht, 2017), most likely in an active manner (Aly & Matuschewski, 2005). They are passively carried with the mosquito's hemolymph and attach to the salivary glands, which the sporozoites invade actively (Douglas *et al.*, 2015, Pimenta *et al.*, 1994, Sterling *et al.*, 1973). Most of them are stacked at the back end of salivary glands (Pimenta *et al.*, 1994) while some already make it to the salivary duct in which the sporozoites move in sudden bursts of speeds in between longer periods without movement (Frischknecht *et al.*, 2004).

1.4 Vaccination approaches

During its life cycle the parasite comes into contact with the vertebrate host at the stages of sporozoite, liver stage and blood stage. In 1948, Freund showed that heat-killed blood stage parasites failed to elicit sufficient immunity in monkeys (Freund *et al.*, 1948), but two decades later, radiation attenuated sporozoites (RAS) were shown to stop developing at the liver stage and to be capable of inducing protection against subsequent sporozoite infections in mice (Nussenzweig *et al.*, 1967). This was later also shown by using genetically attenuated parasites (GAP), which also arrest development in the liver (Mueller *et al.*, 2005a, Mueller *et al.*, 2005b, van Dijk *et al.*, 2005). Increasing evidence hints towards better protection of late-arresting liver stages that expose the host to more antigens than early-arresting liver stages (Singer & Frischknecht, 2017). In line with this, subunit vaccines like the recently approved RTS,S (based on the major sporozoite surface protein circumsporozoite protein (CSP)) have turned out to be less effective than previously hoped (30-50 % protection after four administrations) (Agnandji *et al.*, 2014, WHO, 2017). Additionally, sterile cryo-preserved RAS injections in humans had to be administered frequently and in very high doses (Seder *et al.*, 2013) or IV (Lyke *et al.*, 2017), leading to concerns about its practicability in the field. Some studies have been able to induce immunity by letting the infection progress past the liver stage to the blood stage and allowing the parasites some replication in the blood before eliminating parasites using antimalarial or antibiotic drugs (Singer & Frischknecht, 2017).

Similar approaches for inducing immunity (radiation or genetic attenuation or infections under drug-cover) have been taken using blood stages (Stanisic & Good, 2015), however, the practicability of injecting infected blood IV into humans on a large scale is a risk that will continue to be a concern.

1.5 Subcellular structures and organelles in *Plasmodium*

It is remarkable how many quite dramatic changes the parasite undergoes throughout its life cycle. Every stage is adapted and primed perfectly to the environment it encounters. The variety of shapes and sizes require a high degree of flexibility, but evolutionary pressure pushes the parasite to be efficient at the same time. This suggests that even though the shapes of the cells are different in the individual stages, the building blocks could be similar. In fact, the invasive stages of *Plasmodium* – the merozoite, the ookinete and the sporozoite – share a large number of structures and organelles as well as their organization. Additionally, the phylum of Apicomplexa that *Plasmodium spp.* belong to, includes other protist parasites like for example *Toxoplasma gondii* that share a significant number of features.

Apicomplexan parasites in general and *Plasmodia* in particular have both organelles in common with mammalian cells and unique organelles that are not seen in other organisms or even in any other stage. Organelles *Plasmodia* share with other higher eukaryotes are the plasma membrane, the nucleus, the ER, a Golgi (although only consisting of a minimal number – possibly only one or two – of cisternae (Schrevel *et al.*, 2008) and an endosome-like compartment.

An organelle that is not commonly found in higher eukaryotic cells but is typical for Apicomplexans is a plastid-like organelle called the apicoplast, a red algae secondary endosymbiont. This resulted in the apicoplast being surrounded by four membranes (Lemgruber *et al.*, 2013). The apicoplast harbors several essential metabolic pathways like fatty acid and isoprenoid synthesis of the parasite (McFadden, 2011). Additionally, Apicomplexa contain a number of organelles that secrete their content in a concerted fashion in order to facilitate invasion. These are called micronemes, rhoptries and dense granules (Blackman & Bannister, 2001). Micronemes are small, elongated vesicles, that are concentrated at the apical end of the cells. They contain for example integrin-like transmembrane proteins that facilitate adhesion of the cell to a variety of substrates or the GPI-anchored major surface protein of sporozoites called circumsporozoite protein (CSP). Rhoptries are pear-shaped organelles that taper at the apical end of the parasite. They too, are secreted upon contact with a host cell and

help facilitate invasion. Dense granules are round vesicles that release their content once the vacuole has closed to help maintain the PV although very little is know about their role in *Plasmodium* and they have not been described in sporozoites.

Another defining feature of Apicomplexa is the so-called inner membrane complex (IMC). The IMC is best described as flattened vesicles called alveoli, whose two double membranes are in close proximity to one another. In *T. gondii* and *Plasmodium* gametocytes several flattened vesicles are connected to each other through sutures, while in all other stages of *Plasmodium* it is a single continuous flattened vesicle (Harding & Meissner, 2014). The outer double membrane of the IMC facing the plasma membrane creates a space between itself and the PM that is called the supra-alveolar space. A very peculiar organelle unique to ookinetes and early oocysts is the crystalloid body (Lemgruber & Lupetti, 2012), which is thought to store proteins and/or lipids. Impairing the integrity of this organelle prevented sporulation or salivary gland invasion, implying an essential role of this organelle in sporozoite development (Saeed *et al.*, 2015, Santos *et al.*, 2016).

On a smaller scale, microtubules are also found in *Plasmodium*. But in contrast to typical eukaryotic cells where microtubules are used for internal stability, the invasive stages of *Plasmodium* have a microtubular cage beneath their pellicle that – together with the IMC and the SPN – gives these cells a high degree of rigidity (Morrissette & Sibley, 2002).

1.6 The sporozoite

The sporozoite is a thin, highly polarized, crescent-shaped cell (Figure 5); on average 1 µm wide and 10-12 µm long (Muthinja *et al.*, 2017). In mature sporozoites the inner double membrane of the IMC is connected to an intermediate-filament network, called subpellicular network (Khater *et al.*, 2004, Mann & Beckers, 2001). This in turn is connected to a cage of microtubules (MT) that originates from the larger apical polar ring (APR) and runs along half to two thirds of the length of the sporozoite. The majority of microtubules are tightly packed on the ventral side, while a single one runs down the dorsal side (Kudryashev *et al.*, 2010b). The apical polar rings that lie at the front end of the cell are tilted toward the substrate and the single microtubule originates from the highest point of the large APR (Kudryashev *et al.*, 2012). The mitochondrion, apicoplast and Golgi are located perinuclear (Kudryashev *et al.*, 2010b). The sporozoite is the only stage of the parasite that resides in and invades both mosquito and vertebrate cells. Thus, the parasite needs to be able to replicate and spread in the

environment presented by two very different hosts. This forces the parasite to retain diverse capacities to adapt to two different species at different stages of the life cycle.

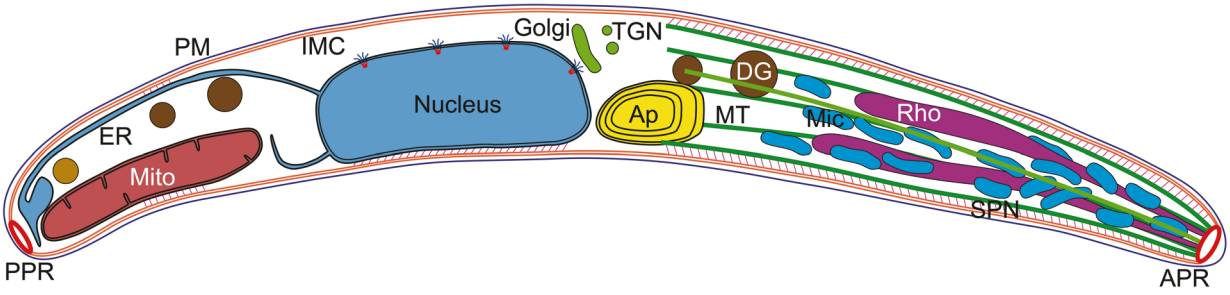

Figure 5: Cartoon of a sporozoite. This extremely polarized cell (top view) consists of several outer layers to create the specific shape of the sporozoite: The plasma membrane (PM, black) is underlined by the inner membrane complex (IMC, red lines) that consists of two additional membranes and is connected to the subpellicular network (SPN, magenta angled lines) that is anchored at the microtubules (MT, green cables). The microtubules originate from the large apical polar ring (APR) and build a cage around the apical half of the cell. The apical end of the sporozoite also contains a series of secretory organelles called micronemes (Mic, cyan) and rhoptries (Rho, magenta) that can secrete their content at the apical end to help facilitate adhesion and motility as well as invasion and formation of the parasitophorous vacuole (PV). Dense granules (DG) are secreted to maintain the PV formed during invasion. The nucleus is located behind the middle of the cell where it is closely associated to the IMC. The apicoplast (Ap), Golgi and *trans* Golgi network (TGN) are located in front of the nucleus, whilst the mitochondrion (Mito) can be located either in front of or behind the nucleus. The endoplasmic reticulum (ER, light blue) extends from the nucleus towards the rear of the cell where the posterior polar ring (PPR) is situated. The cartoon was modified from Kudryashev *et al.* (Kudryashev *et al.*, 2010b).

1.7 Sporozoite motility

Sporozoites have an uncommon way of moving that is remarkably different from all classical movement types discussed before. In the skin of vertebrate hosts, sporozoites are highly motile displaying complex movement patterns (Amino *et al.*, 2006). The most peculiar thing about sporozoite motility is that they move without any apparent changes in cell shape. This has given this form of movement the name ‘gliding motility’. Remarkably they move, with an average speed of 1-2 µm/s in 2D (Vanderberg, 1974) as well as in 3D (Amino *et al.*, 2006, Hellmann *et al.*, 2011, Hopp *et al.*, 2015), but displaying peak speeds of at least 6 µm/s (Munter *et al.*, 2009, Quadt *et al.*, 2016). These speeds are at least ten times higher than cells that move by crawling e.g. neutrophils of the mammalian immune system that would be responsible for chasing and eliminating pathogens in the skin (Lammermann *et al.*, 2013).

The curved shape of the sporozoite that is not changed during motility in 2D has consequences for the way it moves forward. On a flat substrate the result is almost perfectly circular gliding that was already described in 1974 (Vanderberg, 1974). Intriguingly, the sporozoite is a chiral cell that has a ventral side and prefers to circle in a clockwise manner (Kudryashev *et al.*,

2012). The resulting movement in 3D resembles a corkscrew pattern or helical gliding (right-handed) that appears as curved meandering behavior when the cell switches direction, for example to avoid obstacles.

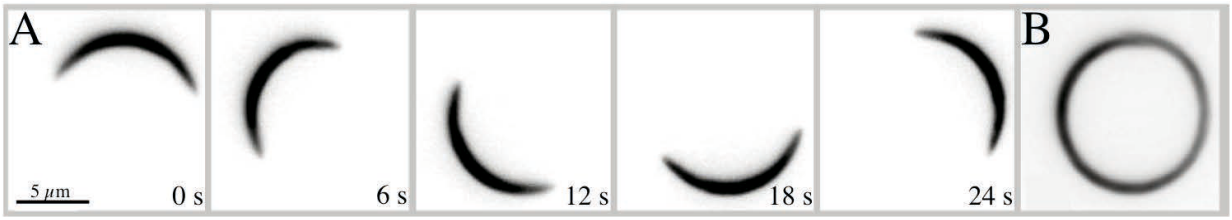

Figure 6: Exemplary sporozoite moving in a perfect circle on a 2D surface. (A) Inverted fluorescence images of a moving sporozoite expressing cytoplasmic mCherry. The clock-wise movement was imaged from below with an inverted microscope, generating the appearance of counter-clockwise motility. Images are shown every 6 seconds and the scale bar is 5 µm. (B) Projection of sporozoite from A.

Interestingly, the quality of motility is influenced by the composition of the tissues the sporozoites encounter, as they tend to meander less in the tail of a mouse than in the ear (Hellmann *et al.*, 2011). Intriguingly, the sporozoite has been found to circle around blood capillaries *in vivo* before invading them (Amino *et al.*, 2006). This behavior could be partially reconstituted *in vitro,* using micro-pillar arrays where sporozoites were shown to prefer a diameter of 10 µm that is the same as the diameter of peripheral capillaries (Muthinja *et al.*, 2017).

Indications that this peculiar way of cell movement also relies on actin have been around for a long time (Dobrowolski & Sibley, 1996, King, 1988). The speed of sporozoite gliding motility could be reduced by applying Cytochalasin D (CytoD) or Jasplakinolide (Jas) (Munter *et al.*, 2009), which are drugs that influence actin dynamics (Bubb *et al.*, 1994, Forscher & Smith, 1988). Interestingly, CytoD increased and Jas reduced adhesion in sporozoites (Munter *et al.*, 2009).

1.7.1 Plasmodium actin

Usually actins show a very high degree of conservation among their isoforms and across different species (~95 %) and have the ability to form very long filaments. The *Plasmodium* genome encodes for two actin isoforms that are only about 80 % conserved compared to canonical actins and each other (Vahokoski *et al*., 2014).

Actin 1 is expressed in all stages and is presumed to be essential in blood stages (*Plasmo*GEM phenotype: relative growth rate of 0.17 out of 1; http://plasmogem.sanger.ac.uk/phenotypes). Actin 1 was shown to form very short filaments *in vitro*, but could be forced to make longer filaments by adding jasplakinolide (Schmitz *et al*., 2010, Vahokoski *et al*., 2014). The same

properties have been described for the single copy of actin from *Toxoplasma gondii*. *Plasmodium* actin 1 filaments have the peculiar property of having a higher crossover distance (40.65 nm) than any other actin filament investigated so far (36 – 37 nm) (Schmitz *et al*., 2010, Vahokoski *et al*., 2014). This difference in crossover distance is thought to result from changes at the monomer-level (Ross Douglas, unpublished data).

In contrast to this, *Plasmodium* actin 2 is able to form long filaments *in vitro* with a crossover distance of 36-37 nm just as in classical actin filaments (Vahokoski *et al*., 2014). Actin 2 is dispensable for the blood stage according to the *Plasmo*GEM phenotype analysis (relative growth rate of 0.97 out of 1) and only present in male gametocytes, both male and female gametes, ookinetes and early oocysts. There it is essential for exflagellation of male gametes and early sporogony (Andreadaki *et al*., 2014, Deligianni *et al*., 2011). There is conflicting evidence on whether the actin 2 protein is present in sporozoites (Le Roch *et al*., 2004, Lindner *et al*., 2013), but the transcript seems to be absent (Andreadaki *et al*., 2014). Even though cryo-EM was used to investigate sporozoites in great detail, actin filaments could not be identified with certainty (Kudryashev *et al*., 2010a). However, addition of Jas led to visible actin filaments at the tip of the sporozoite, sometimes even breaking through the membrane at the front of the cell (Dissertation Misha Kudryashev, 2009). This means that under normal conditions, actin filaments are not very long indicating that the actin 2 protein is not present in large quantities at the sporozoite stage as actin 2 tends to form long filaments that should then be visible. Thus, most likely actin 1 is the only functionally required actin isoform present at the sporozoite stage.

One of the main difficulties of working with apicomplexan actin is that its filaments cannot be stained by phalloidin dyes, LifeAct fused to fluorescent proteins or SiR-actin that is based on jasplakinolide (Ross Douglas, unpublished data). Thus, we are left with antibody-stainings that are not necessarily filament-specific and the results from *Plasmodium* actin-antibodies are difficult to interpret. They often appear as rather amorphous stainings that do not look like filaments formed by classical actin (Angrisano *et al*., 2012, Whitelaw *et al*., 2017). This could be due to the very short filaments that are in close proximity to each other or actin monomer aggregates, as the majority of apicomplexan actin is likely present in the monomeric form (Dobrowolski *et al*., 1997, Skillman *et al*., 2011).

A hint towards actin filament localization in the sporozoite has come from tagging the only known F-actin binding protein in the parasite: coronin. Interestingly, the protein is localized along the periphery of the cell that upon activation of gliding motility localizes to the rear end

of the cell (Bane *et al*., 2016). Recently, a study in *Toxoplasma gondii* employed commercial F-actin-specific chromobodies that also yielded promising results concerning F-actin-specificity (Periz *et al*., 2017). These chromobodies are currently being adapted for the use in *Plasmodium* in our group and preliminary results also look promising. Stainings of sporozoites reproduced the results from the coronin-localization, meaning that F-actin predominantly accumulates at the back of the sporozoites (Julia Sattler, unpublished data). What is consistent, even in staining attempts with antibodies, is that upon treatment of parasites with jasplakinolide, actin and or actin filaments accumulate at the apical and basal end of the parasites.

1.7.2 The motor model

As mentioned before, actin and myosin were known to be involved in *Plasmodium* gliding motility. The classical motor model that has been developed from this and other studies is however debated. It is clear that the model is incomplete, but it is the only palpable one that currently exists.

Apicomplexa have a unique type of myosin (class XIV) that contains only a single head and no dimerization domain (Heintzelman & Schwartzman, 1997). Six different types of myosins (MyoA-MyoF) have been identified in *Plasmodium* (Chaparro-Olaya *et al.*, 2005). A proteomics study reported only MyoA, MyoC and MyoD to be expressed at the sporozoite stage (Le Roch *et al.*, 2004). However, a recent publication investigated MyoB further and revealed expression in all observed stages, including sporozoites. The study found MyoB to be located at the apical tip of all stages. In sporozoites, the protein was additionally found throughout the cell (Yusuf *et al.*, 2015).

In *T. gondii*, MyoA and MyoC have both been shown to use the same myosin light chain. Additionally, MyoC that is localized at the rear of the cell in normal tachyzoites redistributes to the cell periphery upon MyoA deletion, indicating a complementary role of MyoC (Egarter *et al.*, 2014, Frenal *et al.*, 2014). So far, MyoC function has not been studied intensively in *Plasmodium*.

Due to the abundance of the protein (Le Roch *et al.*, 2004), its distribution in wild type parasites and its indispensability for gliding motility (Meissner *et al.*, 2002, Siden-Kiamos *et al.*, 2011), MyoA is generally assumed to be the main motor during gliding motility (Figure 7).

Myosin light chain binds to MyoA (Bergman *et al.*, 2003, Green *et al.*, 2006) and is associated with the IMC (Margos *et al.*, 2000, Matuschewski *et al.*, 2001, Pinder *et al.*, 1998). Evidence of

anchoring of the myosin-MLC complex in the IMC through glideosome-associated proteins 45 and 50 (GAPs) first came from *T. gondii* (Gaskins *et al.*, 2004) and was later confirmed for *Plasmodium* (Sanders *et al.*, 2007).

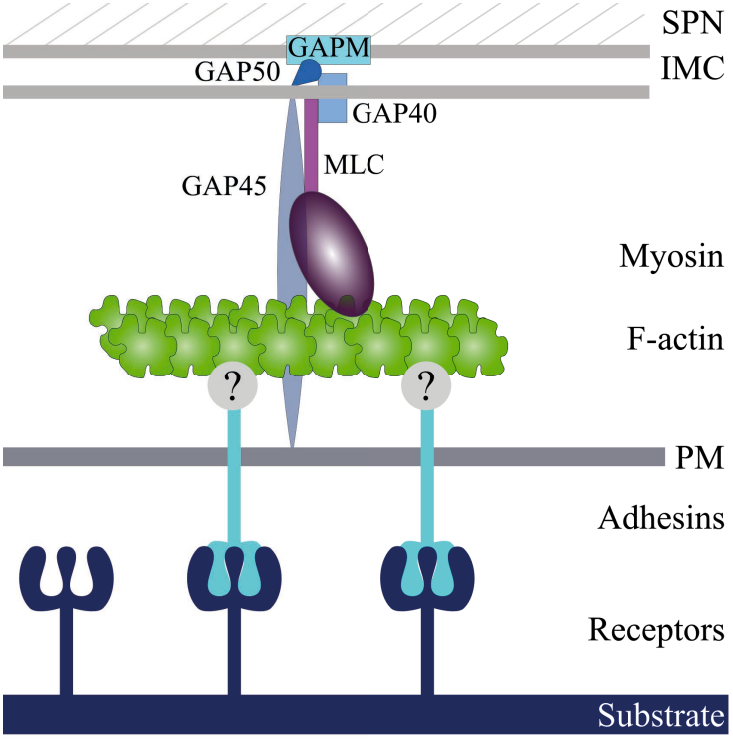

Figure 7: Working model of the *Plasmodium* motor. Short actin filaments are located in the supra-alveolar space. They are connected to adhesins via an unknown adaptor (grey with question mark). The adhesins span the membrane and are attached to the substrate on the extracellular side. The myosin – myosin light chain (MLC) complex is anchored to the IMC via a number of different adaptor proteins (GAPs). The complex is probably stabilized by anchoring it in the subpellicular network (SPN) by GAPMs. Through the power stroke of myosin, a rearward directed force is generated that results in a forward movement.

The tethering of myosin was reported to also extend to the subpellicular network enabling the exertion of force necessary to propel the parasite forward (Bullen *et al.*, 2009). GAP40, an additional anchoring protein and a more detailed localization of GAP45 were described in *T. gondii* (Frenal *et al.*, 2010).

In contrast to classical cell motility, actin is thought to be arranged parallel to the plasma membrane. On the other side of the supra-alveolar space, adhesins span the plasma membrane (Figure 7). It is assumed that the actin filament is connected to the substrate via transmembrane adhesins. Through the action of myosin, this generates a rearward-directed force that results in a forward movement (Baum *et al.*, 2006).

In 1988, a parasite surface protein called thrombospondin related anonymous protein (TRAP) was identified (Robson *et al.*, 1988) and later shown to be necessary for sporozoite motility and salivary gland invasion (Sultan *et al.*, 1997). Additionally, TRAP has been shown to bind to heparan sulphate (Tossavainen *et al.*, 2006) on the surface of liver cells and saglin on the surface of the mosquito salivary glands (Ghosh *et al.*, 2009), hinting towards a role in host cell recognition.

Beside TRAP, homologues like TRAP-like protein (TLP) and S6 in sporozoites, merozoite TRAP (MTRAP) and circumsporozoite and TRAP-related protein (CTRP) in ookinetes have been identified. In contrast to TRAP, TLP can be knocked out without affecting salivary gland invasion of sporozoites. However, there is a possible slight decrease in cell traversal in the TLP knockout sporozoites (Heiss *et al.*, 2008, Moreira *et al.*, 2008). Similar to the TRAP knockout, S6 knockout sporozoites have a greatly reduced ability to invade salivary glands and move in 2D (Combe *et al.*, 2009, Steinbuechel & Matuschewski, 2009). It has been shown, that adhesins are secrete to the PM from micronemes at the front of the sporozoite like protein (TLP) can also be found in micronemes, from where they are secreted to the PM (Morahan *et al.*, 2009).
The mechanism and protein that connects TRAP with actin filaments have been under heavy debate: TRAP was originally shown to be connected to actin through aldolase (Jewett & Sibley, 2003), results that were later proven to be false (Shen & Sibley, 2014). Recently, another protein has been suggested to connect adhesins with actin filaments (Jacot *et al.*, 2016). However, the protein is localized apically, which does not fit well with the above-described motor model (Figure 7) that would hint toward a peripheral localization along the whole cell. That probably means that the search for the connector is still ongoing.
It is evident, that regulation of actin and actin filament formation and turnover has a significant influence on gliding motility. Strikingly, the genome of *Plasmodium* only encodes a very limited number of ABPs (Schuler & Matuschewski, 2006). Many of the key ABPs, like for example the Arp2/3 complex that plays such a central role in other eukaryotic cells are absent. The few ABP that exist in *Plasmodium* and are conserved in yeast or mammalian cells often have non-conserved or only partially-conserved functions (Schuler *et al.*, 2005). Interestingly, even though three genes coding for formins exist in *Plasmodium*, they contain only rudimentary FH1 domains. In contrast to classical cell motility, profilin in combination with formin did not enhance actin polymerization significantly (Ignatev *et al.*, 2012). Thus, it might be possible that profilin fulfills slightly different functions in *Plasmodium*.

1.7.3 Apicomplexan profilin

One isoform of profilin has been found in each *Plasmodium* and *Toxoplasma* (Baum *et al.*, 2006). *Toxoplasma gondii* profilin (*Tg* Pfn) was shown to be involved in immune responses in mice. *Tg* Pfn, especially the acidic loop region, is recognized by toll-like receptor 11 (TLR11) and TLR12 homodimers as well as TLR11/12 heterodimers (Koblansky *et al.*, 2013, Kucera *et al.*, 2010, Yarovinsky *et al.*, 2005). As TLR11 is a pseudogene and TLR12 is not even present

in the human genome, this is presumably not relevant for human infections (Gazzinelli *et al.*, 2014).

Biochemically, *Tg* Pfn primarily acts to sequester actin (Skillman *et al.*, 2012) but in contrast to mammalian actin it slows down nucleotide exchange (Kucera *et al.*, 2010). *In vivo*, *Tg* Pfn is required for motility as well as egress and invasion from and into host cells (Plattner *et al.*, 2008) and has recently been reported to be involved in apicoplast division (Jacot *et al.*, 2013). In *P. berghei*, strong overexpression of profilin was reported to lead to an inability of sporozoites to invade salivary glands and a reduced capacity of hemolymph sporozoites to glide (Sato *et al.*, 2016) whereas conditional knock-down of the protein led to a defect in merozoite invasion (Pino *et al.*, 2012). Due to its important functions, profilin was thought to be essential and indeed attempts to knock out profilin in *P. berghei* remained unsuccessful (Kursula *et al.*, 2008a).

In 2008 Kursula *et al.* solved the crystal structure of *Plasmodium falciparum* profilin (Kursula *et al.*, 2008a). This revealed three secondary structure elements that had not been seen in any other solved profilin crystal structure before: an acidic loop, a small α-helix and a β-hairpin adding to and protruding from the conserved profilin core fold (Figure 9). These three motifs correspond to a 35-amino acid long insertion in the protein at position 40 (Figure 8). Similarly, *Toxoplasma gondii* also contains these additional structural motifs in profilin, albeit with a shorter acidic loop (Kucera *et al.*, 2010). The sequence insertion is also present in other sequenced apicomplexan species (Figure 8). Interestingly, the insertion can also be found in profilin of two free-living algae related to the ancestor of Apicomplexa (Janouskovec *et al.*, 2013).

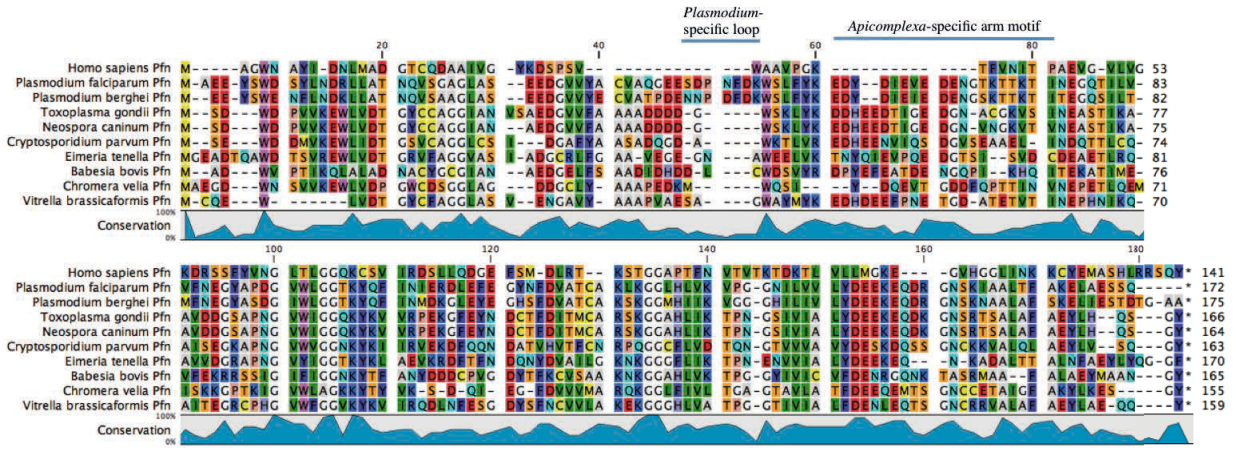

Figure 8: Amino acid sequence alignment of human profilin (top) with several apicomplexan profilins (middle) and profilin from the two ancestral chromerids (bottom). The *Plasmodium*-specific acidic loop and the β-hairpin extension (arm motif) are indicated above their respective sequences. The level of sequence conservation is show below in blue. Note the labeled unique features and the corresponding gaps in the human sequence. A larger version of this figure can be found in the appendix. Alignment was created using the CLC Main Workbench software version 5.1 (CLC bio).

Work by Bhargav et al. revealed that *Plasmodium falciparum* profilin spontaneously assembles from two independently expressed pre-folded halves (Bhargav *et al.*, 2015). This hints at a gene fusion event in the evolution of profilin, combining two smaller proteins - one with the actin-binding face and one containing the proline-rich repeat binding face - into one single-domain protein (Bhargav *et al.*, 2015).

The function of these additional motifs has not been investigated yet. However, the turn at the tip of the additional β-hairpin is acidic in nature and in close proximity to a basic patch in actin. It was already speculated that this might be an apicomplexa-specific additional actin-binding site (Kursula *et al.*, 2008a).

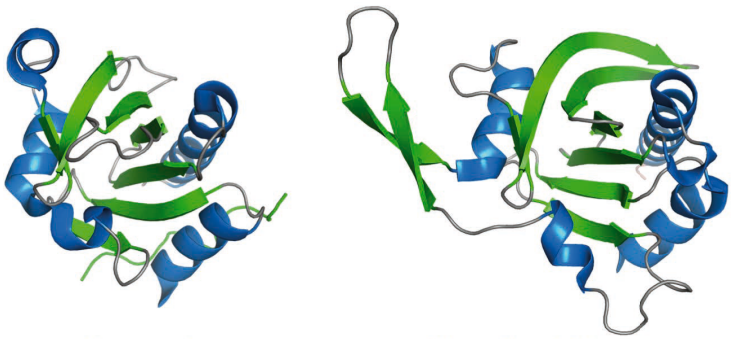

Mus musculus *Plasmodium falciparum*

Figure 9: Crystal structures of mouse (left) and parasite profilin (right). Mouse profilin is globular whereas parasite profilin contains three unique structures that protrude from the left and at the bottom of the core. β-sheets are colored green and α-helices blue. Images are from Kursula *et al.* (Kursula *et al.*, 2008a).

1.8 Aim of this work

Profilin is a key actin monomer binding protein and plays a major role in cellular motility. *Plasmodium* profilin contains unique structural features that have not been observed in profilin from plants, yeast or animals (Kursula *et al.*, 2008a). One feature is the β-hairpin arm motif and the other is an unstructured acidic loop (Figure 9). The role of the acidic loop remains elusive whereas the arm motif was suggested to be involved in actin binding (Kursula *et al.*, 2008a). Thus, *Plasmodium* profilin is thought to bind to actin in a slightly different way than in classical cell motility to help regulate the actin-myosin motor of gliding motility

During this work, I wanted to test this hypothesis and study the role of profilin in *Plasmodium*. It had not been possible to knock out profilin (Kursula *et al.*, 2008a) so we first aimed at specifically altering the tip of the arm motif. Thus, I created several profilin mutants with an altered arm motif. Additionally, I investigated possible differences between *P. falciparum* and *P. berghei* profilin that involved mutations of the acidic loop. Eventually, I managed to generate a profilin knockout. These mutants were analyzed using *in vitro*, *in vivo* and *in silico* approaches.

2 Materials and Methods

2.1 Devices, tools and chemical reagents

1kb DNA Ladder	New England Biolabs.
5-FC	5-Fluorocytosine, nucleoside analog, Sigma-Aldrich.
24-well plate	Greiner CELLSTAR® 24-well cell culture plates, Sigma-Aldrich.
96-well plate for microscopy	Corning® 96-well plate, clear bottom polystyrene, TC-treated, clear flat bottom wells, black, Sigma-Aldrich.
96-well plate for actin polymerization assays	Greiner 96-well plate, polystyrene, flat-bottom (chimney well), µclear®, black, cellstar®, TC, sterile, Greiner Bio-one.
α−mCherry antibody	Polyclonal rabbit IgG antibody ab167453, Abcam.
α−mouse	Goat anti-Mouse IgG (H+L) Highly Cross-Adsorbed Secondary Antibody, Alexa Fluor 488, Thermo Fisher Scientific.
α−rabbit	Goat anti-Rabbit IgG (H+L) Cross-Adsorbed Secondary Antibody, Alexa Fluor 546, Thermo Fisher Scientific.
Acetic acid	glacial, Carl Roth.
Agar	Bacto™ Agar, BD.
Agarose	UltraPure™ Agarose, Invitrogen, Thermo Fisher Scientific.
Alsever's solution	Sigma Aldrich.
Ampicillin	Ampicillin sodium salt, Sigma Aldrich.
Antibiotic-Antimycotic	100x concentrate, containing 10,000 units/ml penicillin, 10.000 µg/ml streptomycin and 25 µg/ml Fungizone® Gibco™, Thermo Fisher Scientific.
Axiovert 200M	Widefield microscope containing an XBO 75 xenon lamp, Zeiss.
Bromophenol blue	AppliChem.
BSA	Bovine serum albumin, Fraction V, Carl Roth.
Cannulas	BD Microlance™ 3, 27G" Nr. 20 0.4 x 19 mm, BD.
CIAP	Calf intestine alkaline phosphatase, Thermo Fisher Scientific.
Chirascan Plus CD spectropolarimeter	Chirascan Plus (V100) CD spectropolarimeter, Applied Photophysics.
Chloramphenicol	Sigma-Aldrich.
CoolSnap HQ2	high resolution charged coupled device (CCD), Photometrics.
Cover slip round	diameter 12 mm, 0.13-0.16 mm thickness (No. 1), Marienfeld.
Cover slip square	24 x 24 mm, 0.13-0.16 mm thickness (No. 1), Marienfeld.
Cover slip rectangular	24 x 60 mm, 0.13-0.16 mm thickness (No. 1), Marienfeld.
DMSO	Dimethylsulfoxide, Rotipuran, Carl Roth.
DMEM	Dulbecco's Eagle modified medium containing 4,5mM glucose, Gibco™, Thermo Fisher Scientific.
dmH_2O	Demineralized water.
EDTA	EDTA disodium salt dihydrate crystalline, Acros organics, Thermo Fisher Scientific.

FBS US	Fetal bovine serum, certified, US origin, Gibco™, Thermo Fisher Scientific.
FBS	Fetal bovine serum, qualified, E.U.-approved, South America origin, Gibco™, Thermo Fisher Scientific.
Freund's adjuvants	complete & incomplete, Sigma-Aldrich.
Gentamicin	10 mg/ml PAA (now part of GE Healthcare).
Giemsa stain	Giemsa's azur eosin methylene blue solution, Merck.
Glass slide	76 x 26 mm, 1 mm thickness, Marienfeld.
Glycerol	98 %, water free, Sigma-Aldrich.
IPTG	Isopropyl-β-D-thiogalactopyranosid, Carl Roth.
Kanamycin	Kanamycin sulfate, Sigma Aldrich.
Ketamin	Ketamin hydrochlorid 10 %, Bremer Pharma.
Mercurochrome	Mercury dibromofluorescein disodium salt, Sigma-Aldrich.
Midori green advance	DNA/RNA dye, Nippon Genetics Europe.
NP40	Nonidet™ P-40, Nonylphenylpolyethylene Glycol, AppliChem.
Nucleofector™ kit	Nucleofector™ kit for human T cells, Amaxa™ technology, Lonza.
Nycodenz®	Gradient medium, Axis-Shield.
PCR product gel-extraction kit	High Pure PCR Product Purification Kit, Roche.
Penicillin/Streptomycin	100x solution, PAA (now part of GE Healthcare).
Pestle	Compatible with 1.5 ml tubes for smashing salivary glands, Bel-Art™ SP Scienceware™.
Phenylhydrazine	97 %, Sigma-Aldrich.
Plasmid Mini extraction kit	AccuPrep Plasmid Mini Extraction kit, Bioneer
Platinum® *Taq* DNA Polymerase	High Fidelity, Thermo Fisher Scientific.
ProLong® Gold	ProLong® Gold Antifade Mountant, Thermo Fisher Scientific.
Protease inhibitors	cOmplete™, Mini, EDTA-free Protease Inhibitor Cocktail, Roche.
Pyrimethamine	Sigma-Aldrich.
Restriction enzymes	Supplied with recommended buffers, New England Biolabs.
RPMI 1640	Culture medium containing 25mM HEPES, L-Glutamine and Phenol red, Gibco™, Thermo Fisher Scientific.
Saponin	Quillaja bark extract, 20-35 % sapogenin content, Sigma-Aldrich.
SDS	Sodium dodecyl sulfate (sodium lauryl sulfate), Omni Life Science.
Sodium deoxycholate	Sodium Deoxycholate BioChemica, AppliChem.
Supercompetent *E. coli* XL1-Blue	Genotype: *recA1 endA1 gyrA96 thi-1 hsdR17 supE44 relA1 lac* [F′ *proAB lacIqZ*Δ*M15* Tn*10* (Tetr)] Agilent Technologies.
Syringe	BD Plastipak™ 1 ml, BD.
T4 DNA Ligase	Promega.
***Taq* DNA polymerase**	Thermo Fischer Scientific.
Tris	Carl Roth.

Triton	Triton X-100, Merck.
Tryptone	Bacto™ Tryptone, BD.
Trypsin	10x Trypsin EDTA 0.5 %/0.2 % in 10x PBS, PAA (now part of GE Healthcare).
Tween 20	Carl Roth.
Xanthurenic acid	4, 8-Dihydroxyquinoline-2-carboxylic acid, Sigma Aldrich.
Xylazin	20 mg/ml Xylazinhydrochlorid, Xylariem ®, Ecuphar.
Yeast Extract	Bacto™ Yeast extract, BD.

2.2 Buffers and solutions

5-FC solution	Dissolved 1 mg/ml 5-FC in warm tap water.
DNA loading buffer (6x stock solution)	125 mg bromophenol blue 35 ml dmH_2O 15 ml glycerol
Freezing medium for mammalian cells (2x stock solution)	25 ml FBS 15 ml DMEM 10 ml DMSO A confluent 75 cm^2 flask was treated with 3 ml trypsin until cells detached, mixed with 3 ml freezing media and frozen as 1 ml aliquots at -80°C.
Freezing solution	5 ml Glycerol in 45 ml Alsever's solution
F-buffer	10 mM Tris pH 7.5 0.2 mM $CaCl_2$ 0.2 mM ATP 1 mM DTT 0.1 mM $MgCl_2$ 100 mM KCl
F-buffer (high salt)	10 mM Tris pH 7.5 0.2 mM $CaCl_2$ 0.5 mM ATP 1 mM DTT 2 mM $MgCl_2$ 700 mM KCl
G-buffer	10 mM Tris pH 7.5 0.2 mM $CaCl_2$ 0.5 mM ATP 1 mM DTT
Giemsa working solution	7,5 ml Giemsa stain in 50 ml of tap water
Ketamine / Xylazine	25 mg/ml Ketamine 2.5 mg/ml Xylazine in PBS.
Lysogeny broth (LB)	10 g NaCl (Sigma-Aldrich) 10 g Bacto™ Tryptone (BD) 5 g Bacto™ Yeast extract (BD) Dissolved in 1 l of dmH_2O and autoclaved at 121°C for 20 min.
LB agar	15 g of Bacto™ agar was added to the recipe above. After autoclaving, the mixture had to cool to 50°C before the

	respective antibiotics were added and the plates cast.
Nycodenz solution	Stock solution (100 %): 138 g Nycodenz® 394 mg Tris-HCl 112 mg KCl 56 mg Na_2EDTA This was filled up to 500 ml with Millipore water and stirred for 2-3 h at RT until dissolved completely, adjusted pH to 7,5 using 5 M KOH or HCl. The solution was autoclaved for 20 min at 121°C and stored at 4°C. Working solution (55 %): Mix 27,5 ml Nycodenz® solution with 22,5 ml PBS (+ Ca & Mg).
Ookinete medium	250 ml RPMI with HEPES and Glutamine 12.5 mg Hypoxanthine 2.5 ml Pen/Strep 0.5 g $NaHCO_3$ 5.12 mg Xanthurenic acid pH was adjusted to 7,8 and 20 % of FBS added just before starting a culture. The mixture was equilibrated for 30 min @ 19°C (Shaker cold room). Blood from a mouse was added and incubated for 20 h @ 19°C (Shaker cold room).
PBS	8.0 g NaCl 0.2 g KCl 1.42 g Na_2HPO_4 Dissolved in 1 l dmH_2O and adjusted pH to 7.4.
PBS-T	1 l PBS 1 ml Tween™ 20
Permeabilization & blocking solution	0.2 % Triton X-100 3 % BSA Dissolved in PBS (not stable more than 6 months!)
Protein dialysis buffer	10 mM Tris 50 mM NaCl
Protein elution buffer	10 mM Tris pH 7.5 300 mM NaCl 5 % glycerol 300 mM Imidazole
Protein expression lysis buffer	10 mM Tris pH 7.5 300 mM NaCl 5 % glycerol
Pyrimethamine	Stock solution (7mg/ml): 350 mg Pyrimethamine were dissolved in 50 ml of DMSO. Working solution (0.07 mg/ml): Stock solution was diluted 1:100 with tap water and adjusted to pH 4.8 with HCl.
RIPA buffer	50 mM Tris pH 8.0 150 mM NaCl

	2 mM EDTA 1 % NP-40 0.5 % sodium deoxycholate 0.1 % SDS in dmH_2O
TAE buffer	<u>50x stock solution</u> 242 g Tris base in water 57.1 ml glacial acetic acid (Sigma-Aldrich) 100 ml of 500 mM EDTA (pH 8.0) Filled up to 1 l and diluted 1:50 for a 1xTAE working solution.
Transfection medium (T-medium)	15 ml FCS (US) 60 ml RPMI containing 25 mM HEPES 22.5 µl Gentamicin Mixed and sterile-filtered and kept at 4°C

2.3 Bacteria work

2.3.1 Transformation

For amplification of plasmids, bacteria were transformed using a heat shock. An aliquot of 35 µl of supercompetent *E. coli* XL-1 Blue were thawed and kept on ice and 0.68 µl (27.6 mM) of β-mercaptoethanol added. After 10 min, 1 µg of DNA (or 3 µl ligation reaction) was added to the bacteria. They were kept of ice for 30 min, heated to 42°C for 50 s and afterwards cooled on ice for 2 min.

If the vector contained an ampicillin resistance gene, the bacteria were directly plated on LB-agar containing 0.1 mg/ml ampicillin and incubated at 37°C over night.

If the vector contained the kanamycin resistance gene, the tube was filled with LB and incubated in a shaker at 37°C for 90 min. Then, the bacteria were centrifuged for 2 min at 3,000 g and 900 µl of the supernatant were discarded. The remaining bacteria with 100 µl supernatant were re-suspended, plated on LB-agar plates containing 0.1 mg/ml kanamycin and incubated at 37°C over night.

2.3.2 Liquid culture

Liquid overnight cultures were prepared by inoculating 4 ml of LB media containing the respective antibiotic with a colony from an LB agar plate or directly from re-transformed bacteria. The culture was placed in a 37°C shaking incubator over night.

2.3.3 Production of recombinant profilin using E. coli

For expression of recombinant profilin, the EMBL vector pETM-11 (Figure 10) was used. BL21 (DE3) RIPL cells were transformed with pETM-11 carrying different versions of profilin and grown for 12 h at 37°C in 25 ml LB medium containing 100 µg/ml kanamycin and 24 µg/ml chloramphenicol. The next day, 10 ml of the culture were used to inoculate 1 l of medium and grown until an OD_{600} of 0.6. The culture was cooled to 20°C and induced with 0.8 mM IPTG. Profilin expression was driven by a T7 promoter that - without IPTG - was blocked by the lac repressor. Upon induction with IPTG the T7 promoter was freed from the lac repressor and profilin expression was initiated. The cells were pelleted at 4°C, resuspended in 10 ml of lysis buffer and sonicated.

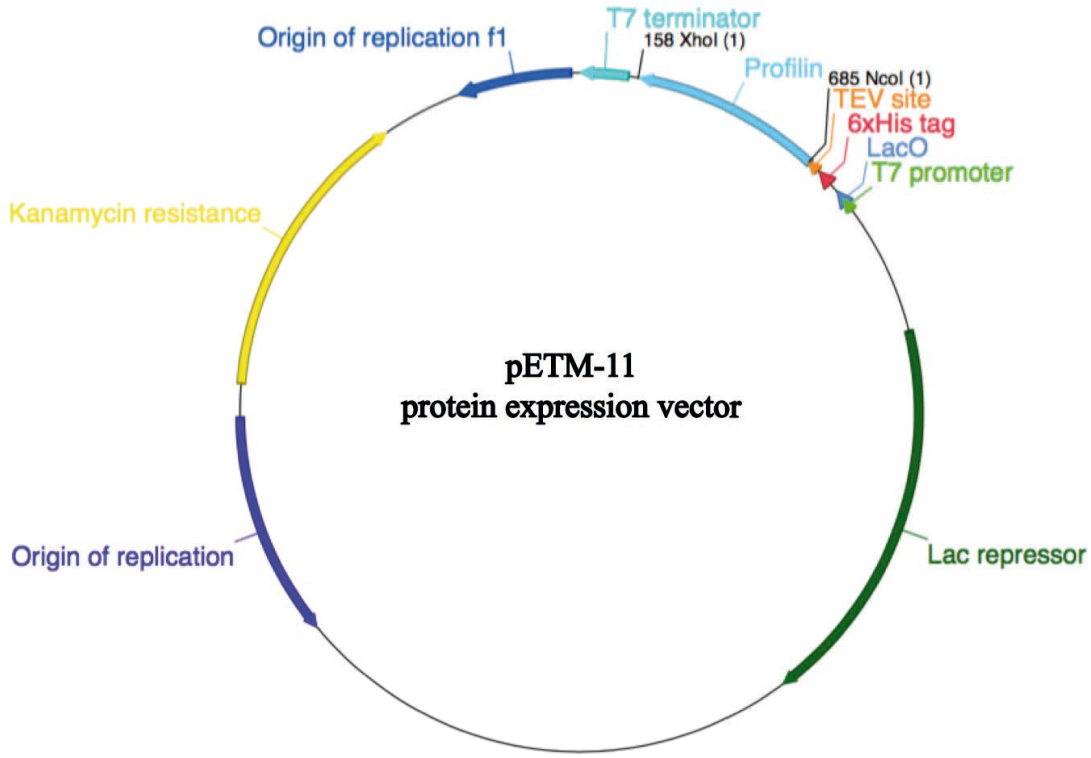

Figure 10: Layout of the pETM-11 inducible protein expression vector containing the *P. berghei* profilin gene. Genes and regulatory elements are shown as arrows. Restriction sites from cloning are depicted and labeled in black.

2.4 *In vitro* protein work

2.4.1 Isolation of recombinant profilin

After pelleting the sonicated bacterial debris from 2.3.3, the supernatant was loaded onto Ni-NTA columns and washed three times. The protein was eluted from the column with elution buffer and the eluate dialyzed over night at 4°C. This was performed in dialysis buffer containing TEV protease to remove the 6x His-tag. The next day, the protein was concentrated, subjected to size exclusion chromatography. If necessary, the purified protein was concentrated to reach a concentration of 10 mg/ml to be used in other assays.

2.4.2 Circular dichroism

The folding state of profilin and its mutants was examined using circular dichroism spectroscopy. This was done using a Chiracan Plus CD spectropolarimeter. Spectra were measured between 180 and 280 nm in a quartz cuvette at room temperature.

2.4.3 Isolation of pig muscle actin

Acetone extracted pig muscle powder (Pardee & Spudich, 1982) was rehydrated in G-buffer, filtered and centrifuged. The supernatant containing globular actin (G-actin) was allowed to

polymerize into filamentous actin (F-actin). This was done by adding $MgCl_2$ and KCl to the buffer (generating high salt F-buffer) and slowly stirring the mixture at room temperature for 40 min. Afterwards the solution was cooled down again and ultra centrifuged (235000 g for 3 h) to pellet the filaments. After removing the supernatant, the pellet was mechanically removed from the tube, homogenized and resuspended in a small volume of G-buffer. The mixture was dialyzed in G-buffer overnight allowing actin to depolymerize. The next day, the solution was ultra centrifuged again (186,000 g for 2 h). The supernatant containing G-actin was run over a gel filtration column and either used directly or stored in a dialysis bag in G-buffer.

2.4.4 Pyrene labeling of actin

Monomeric actin was polymerized in F-buffer for 15 min. Then, a sevenfold excess of pyrene was added and stirred over night. To preserve the integrity of pyrene, the following steps were carried out in the dark. The next day, the solution was ultra centrifuged (186,000 g for 2 h), the pellet homogenized and dialyzed in G-buffer for 36 h. The solution was ultra centrifuged (100,000 g for 2 h) again and the supernatant subjected to size exclusion chromatography.

2.4.5 Actin polymerization assays

The effect of profilin and its mutants on actin polymerization was investigated using *in vitro* polymerization assays. 4 µM purified G-actin (with 5 % pyrene-labeled G-actin) was allowed to polymerize in F-buffer with different concentrations of profilin (0-20 µM). Polymerization was measured as the increase in fluorescence as more pyrene-labeled molecules are incorporated into the filaments. This was measured using a Tecan M1000 pro plate reader with an excitation of 365 nm and an emission wavelength of 407 nm in black, clear flat-bottom 96-well plates. Polymerization assays were performed in triplicates and repeated three times if not indicated otherwise. Polymerization curves were set to start at zero fluorescence. Experiments described in 2.4.2 - 2.4.5 were performed by Bhargav Saligram Prabhakar at the University of Oulu, Finland.

2.5 DNA work

2.5.1 Polymerase chain reaction (PCR)

PCR was used to amplify specific DNA fragments. For analytic integration PCRs, normal *Taq* polymerase was used to analyze the gDNA of transgenic parasites. For preparative PCRs intended for cloning, Platinum® *Taq* DNA Polymerase High Fidelity was used for amplification of genomic DNA (gDNA) or plasmid DNA to reduce errors in the amplified sequences. Reaction mix conditions can be found in Table 1 and PCR cycling temperatures used for standard PCR reactions are shown in Table 2.

Table 1: Components of PCR reactions using different polymerases

Ingredient	***Taq* polymerase**		**Hifi *Taq* polymerase**	
	Concentration	Volume	Concentration	Volume
Primer fw	500 nM	0.25 µl	500 nM	0.5 µl
Primer rv	500 nM	0.25 µl	500 nM	0.5 µl
10 x buffer	1x	2.5 µl	1x	5 µl
$MgCl_2$	1.5 mM	1.5 µl	-	-
$MgSO_4$	-	-	1.5 mM	1.5 µl
dNTPs	200 µM	2.5 µl	200 µM	5 µl
***Taq* polymerase**	1.25 U	0.25 µl	1 U	0.2 µl
Plasmid or gDNA	10-200 ng	2 µl	10-200 ng	2 µl
dmH_2O	ad 25 µl	15.75 µl	ad 50 µl	35.3 µl
Total	-	25 µl	-	50 µl

Table 2: Timeline of standard incubation temperatures of PCR reactions

PCR cycler program		
Temperature	Time	Cycles
94°C	5'	
94°C	30"	⎫
T_{anneal} Primer	30"	⎬ x 25
60°C	1'/1kbp + 30"	⎭
60°C	10'	
4°C	∞	

2.5.2 Overlap extension PCR

In contrast to traditional cloning techniques that use restriction digest and thus introduction of cutting sites into the DNA, overlap extension PCR can be used to fuse two gene sequences together without introduction of restriction enzyme cutting sites. Two separate PCRs (1a & b) were set up to amplify the genes that should be fused together (see Figure 11).

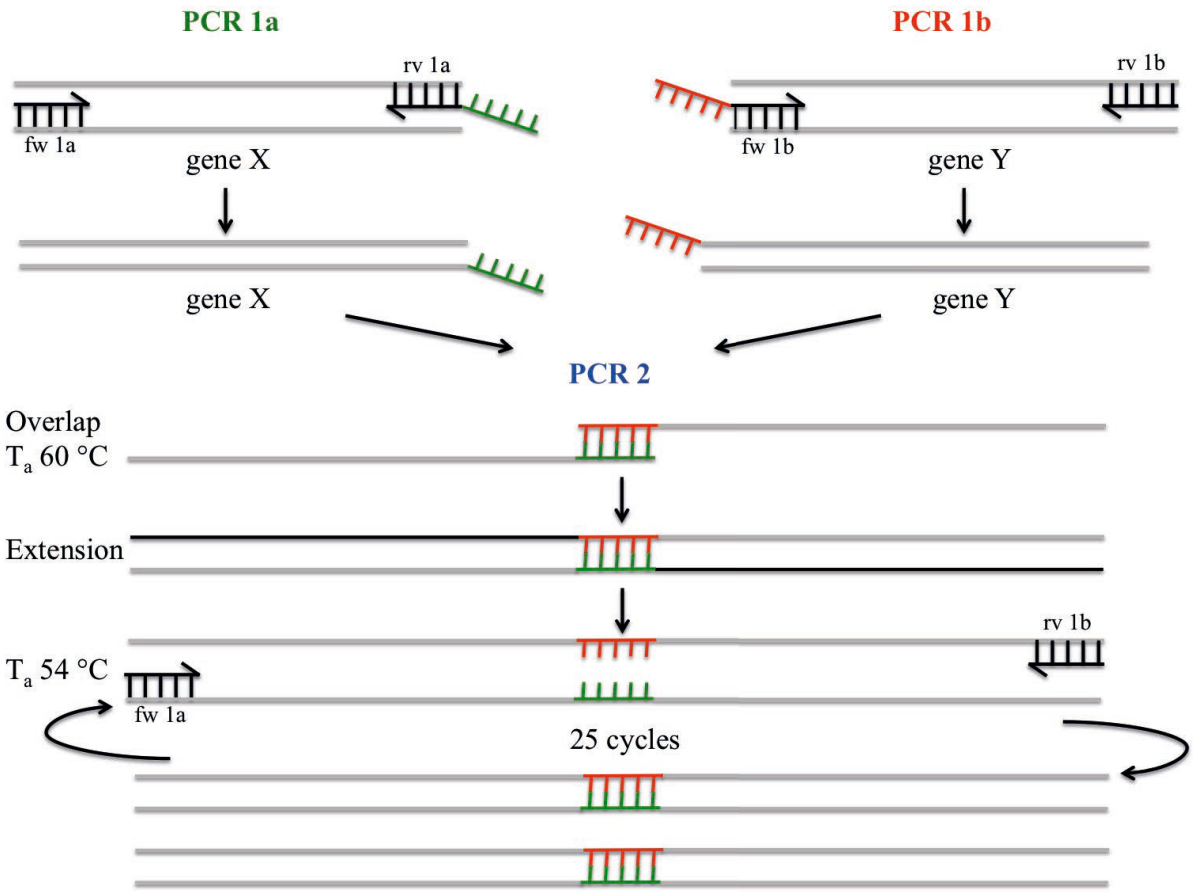

Figure 11: Fusing two genes through overlap extension PCR. Two primer pairs complementary to the two genes that should be fused were used to generate overhangs at the end of the first (green overhang) and the beginning of the second gene (red overhang). Both products were used as templates in the second PCR to fuse the genes at the overhang (annealing temperature: 60°C). After extension of the fusion product (5 cycles), the longer template was amplified with the outer primers (annealing temperature 54°C).

Primers were designed accordingly to include overlaps and the end of the first (rv 1a) and the beginning of the second gene (fw 1b). The amplification was done with standard cycler temperatures (Table 2) and 1 µl of each reaction were then used as templates for PCR 2. In the second PCR, the two products from PCR 1a and 1b were combined and annealed at 60°C i.e. at a higher temperature than the regular primers. The ends of the overlap were extended by the polymerase and the fused sequences amplified with the outer primers (T_a 54°C). The reaction conditions can be seen in Table 3. This method was employed to create mCherry tagged profilins (Pfn$^{+/-i}$ mCh, see 3.1) and the profilin loop chimeras (*Pb* Pfn$^{Pf\,loop}$, *Pf* Pfn$^{Pb\,loop}$ and *Pf* Pfn$^{Tg\,loop}$, see 3.3).

Table 3: Timeline of incubation temperatures of overlap extension PCR reactions

Overlap extension PCR cycler program		
Temperature	Time	Cycles
94°C	5'	
94°C	30"	
T_{anneal} Overlap	30"	x 5
60°C	1'/1kbp + 30"	
94°C	30"	
T_{anneal} Primer	30"	x 25
60°C	1'/1kbp + 30"	
60°C	10'	
4°C	∞	

2.5.3 Primer

All primers were designed with the help of the software ApE ('A plasmid Editor'; http://biologylabs.utah.edu/jorgensen/wayned/ape/). Primers were ordered lyophilized and desalted from Life Technologies (now Thermo Fisher Scientific). Primer sequences used during this work can be found in the appendix (8.2).

2.5.4 Agarose gel electrophoresis

0.8 – 1 % agarose gels were prepared by heating UltraPure™ Agarose in 1xTAE buffer until the agarose was dissolved completely. At around 55°C the solution was poured into a mold to cast analytical or preparative gels. As soon as the gel solidified it was covered with 1xTAE buffer. DNA was mixed with 5x loading dye containing midori green and loaded onto the gel. For size estimation of the DNA fragments 4 µl of the molecular weight marker 1kb DNA ladder was included. The electrophoretic separation was conducted at 80-120 V.

2.5.5 Extraction of DNA fragments from agarose gels

After electrophoretic separation, the desired fragments were extracted from preparative gels using a PCR Product Purification Kit according to the manufacturer's protocol. Respective DNA fragments were cut out of the gel, melted and purified using silica membrane columns followed by elution in 35 µl of dmH_2O.

2.5.6 DNA preparation

Preparation of plasmid DNA from liquid overnight cultures was performed using a plasmid extraction kit according to the manufacturer's instructions. The DNA was eluted in 35 µl of autoclaved dmH_2O.

2.5.7 Restriction enzyme digestion

Restriction enzymes for specifically cutting certain palindromic DNA sequences were used with recommended buffers. Preparative or analytical digests were performed with 2.5 – 15 U of the desired enzyme(s) in a total volume of 50 or 10 µl, respectively. Digests were incubated at designated temperatures for either 1 or 3 h.

2.5.8 DNA dephosphorylation with calf intestine alkaline phosphatase (CIAP)

After the restriction digests, the vectors were dephosphorylated in order to prevent re-ligation without insert. This was done by addition of 1 µl (10 U) of CIAP to the restriction digest and incubation at 37°C for one hour.

2.5.9 DNA Ligation

For the ligation of at least 1 µg of DNA fragments, three-fold excess (molarity) of insert to vector was mixed together with 10x ligation buffer and 5 units of T4-DNA-Ligase in a total volume of 10 µl. The ligation was performed at room temperature for 3 hours or over night at 16°C respectively.

2.5.10 DNA sequencing

Integrity of amplified sequences was monitored by sequence analysis. Sequencing was performed by GATC or Eurofins. 2-3 µg DNA were analyzed with corresponding primers. Resulting sequences were validated by alignment with expected sequences using ApE.

2.6 Genetic manipulation of *Plasmodium berghei* parasites

2.6.1 Transfection vectors

Integration of manipulated DNA into the *P. berghei* (ANKA strain) genome was accomplished via double homologous recombination. To achieve replacement of the endogenous profilin gene with a mutant version, the DNA used for transfection needed to be flanked by two homology regions (Figure 12) that – upon double strand breaks, the parasite can recognize and initiate recombination. The nB3D+ based vectors (Dissertation Natalia Lüsebrink, 2011) contain an origin of replication (blue) as well as resistance against ampicillin (yellow) for bacteria and a selection marker conveying resistance to successfully transfected parasites against the drug pyrimethamine inhibiting the parasites' folate synthesis pathway. I introduced the profilin 5' and 3' UTRs (green) as well as different versions of profilin genes. Before electroporation, the vectors were linearized by double restriction enzyme digestion (NaeI & KpnI or SacII & KpnI) adjacent to the homology regions.

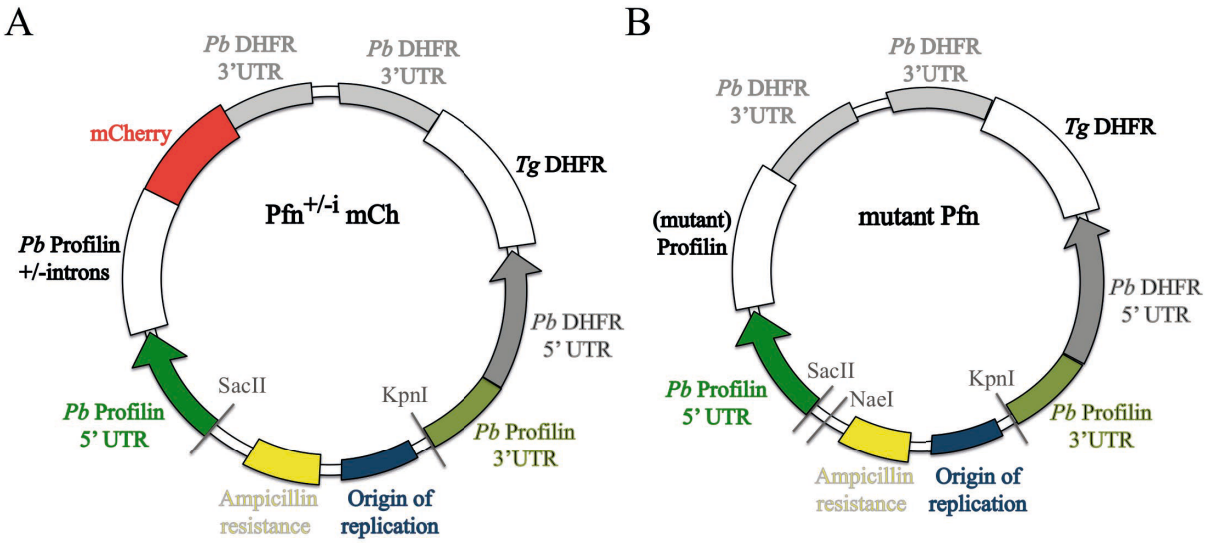

Figure 12: Layout of profilin transfection vectors. Open reading frames are shown in white, red and yellow. Arrows indicate promoter activity of the respective 5'UTRs. Thin, grey and olive green bars depict 3'UTRs. Light grey lines with labels inside the vector show restriction enzyme cutting sites. Maps are not to scale. (A) Vector for replacing profilin with an mCherry-tagged version of profilin either containing or lacking its introns under the expression of the endogenous promoter. (B) Vector map for replacement of profilin with a mutant version under the expression of the endogenous promoter.

2.6.2 *Plasmo*GEM vectors

The *Plasmo*GEM project developed by the Wellcome Trust Sanger Institute produces and distributes free tools for the genetic manipulation of malaria parasites (Pfander *et al.*, 2011). They provide transfection vectors containing very long homology regions (2 kb on the one and 10 kb on the other side of coding genes) that greatly enhance transfection efficiency. To generate a profilin knockout we employed vector *Pb*GEM-286426 (http://plasmogem.sanger.ac.uk). The *Plasmo*GEM vectors were prepared as described in 2.3.1 and 2.3.2 but digested using NotI and contain the hDHFR/yFCU selection marker flanked by identical *Pb*DHFR 3'UTRs. Detailed protocols are available online. This means that parasites that integrated the transfection vectors can be positively selected using pyrimethamine and negatively selected using 5-fluorocytosine. The latter is turned into the lethal 5FCTG and kills parasites containing the hDHFR/yFCU. Thus, 5-FC selects for parasites that looped out the selection marker using the *Pb*DHFR 3'UTRs.

2.6.3 Isolation of schizonts

Blood from an infected mouse with at least 2 % parasitemia was mixed with 250 µl of heparin, washed and incubated at 37°C for 20-22 h in 30 ml of T-medium.

The culture was subjected to a density gradient centrifugation step using 55 % Nycodenz solution. The resulting purified schizonts on top of the Nycodenz phase were isolated with a Pasteur pipette, washed and used for electroporation.

2.6.4 Electroporation

Linearized DNA and isolated schizonts were mixed together with Nucleofector™ solution from an amaxa™ human T cell Nucleofector™ Kit and electroporated using the amaxa™ Nucleofector™ II device (program U-33). Immediately after electroporation, the transfected parasites were injected into the tail vein of a naïve NMRI mouse.

2.6.5 Parasite selection

Positive selection: 24 h after transfection, the drinking water of the mice was replaced with working solution of pyrimethamine (0.07 mg/ml). Parasites containing the *Tg*DHFR were selected for as this protein confers resistance against pyrimethamine.
Negative selection: At a parasitemia of ≥0.1 % after transfection, the mice's drinking water was replaced with of 5-FC (1 mg/ml). Parasites containing the hDHFR/yFCU were killed as these parasites were able to turn the 5-FC pro-drug into the lethal 5' fluorocytosine triphosphate (FCTP).
At a parasitaemia of at least 1.5 % the blood of the mouse was harvested and parasite gDNA isolated. Two stabilates (100 µl infected blood mixed with 200 µl freezing solution) were snap-frozen in liquid nitrogen for later use.

2.6.6 Parasite genomic DNA isolation

Parasites were freed from red blood cells using 0.03 % saponin in PBS. After washing the parasites in PBS, their gDNA was isolated using a Qiagen Blood and tissue spin column as described by the manufacturer.

2.6.7 Limiting dilution

If correct integration after transfection could be verified via PCR, a stabilate was thawed and injected intraperitoneally into a naïve mouse. Once a parasitemia between 0.2 and 1 % was reached, the blood was harvested and diluted to 9 parasites in 1 ml PBS. Ten naïve mice were then injected with 100 µl of the parasite dilution. If mice developed parasitemia, their blood was harvested and the parasites' gDNA checked for presence of desired mutations and absence of the wildtype gene.

2.7 Parasite work

2.7.1 Generation of *Plasmodium berghei* ookinetes

A stabilate was injected IP into a naïve mouse. At a parasitemia of at least 1.5 % a fresh blood transfer (FBT) into one mouse was performed. Three days later, 10 ml of ookinete medium

was supplemented with 2 ml FBS (US) and the mixture equilibrated in a T75 cell culture flask for 30 min at 19°C. Blood from the mouse was isolated, added to the medium and incubated for 20 h at 19°C.

2.7.2 Infection of mosquitos

A stabilate was injected IP into a naïve mouse. At a parasitemia of at least 1.5 % we performed a fresh blood transfer (FBT) into three naïve mice. Three days later, the mosquitoes were starved from their sugar solution for at least four hours. The mice were then anesthetized with 120 µl of ketamine / xylazine and laid on top of the mosquito cage for 35 – 45 minutes. Every five minutes, the mice were flipped to allow different mosquitoes to feed. During this work we used *Anopheles stephensi* mosquitoes from the FDA500 strain.

2.7.3 Oocyst counting

On day 12 after infection, mosquito midguts were isolated, permeabilized with 1 % NP40 in PBS for 20 min and stained with 0.1 % Mercurochrome solution in PBS (Moll K, 2008). After washing the midguts in PBS, they were applied to a glass slide, covered with a coverslip and sealed for imaging.

2.7.4 Isolation of sporozoites

Between day 17 and 25 after infection, mosquito midguts and salivary glands were isolated and collected in PBS or RPMI containing 3 % BSA. Sporozoites were released from the respective tissues by grinding them with a small pestle. The midgut sporozoites were diluted 1:10 in PBS and counted in a Neubauer chamber. Salivary gland sporozoites were counted undiluted and/or used for other assays.

2.7.5 *In vitro* infection of liver cells

$5x10^4$ HepG2 cells per well were seeded into a 24-well plate. The next day (or at 80-95 % confluence) sporozoites were isolated (2.7.4) and $5x10^4$ sporozoites per well were added on top of the HepG2 cells in a volume of 200 µl. The cells were incubated at 37°C for 2 h. Afterwards the cells were washed with PBS and the cells trypsinized. The cells were then distributed into three new wells containing glass cover slips. One well (24 h sample) received half of the cells and the other two wells (48 h and 65 h) received a quarter of the cells each. To avoid contamination the cells were kept in DMEM containing 'Antibiotic-Antimycotic' and washed daily. At 24, 48 and 65 h, the corresponding cells were fixed in 4 % paraformaldehyde for 20 min. The cells were then permeabilized, blocked and antibodies

against HSP70 (Tsuji *et al.*, 1994) and mCherry allowed to bind. DNA was stained with Hoechst, α–HSP70 stained with an α–mouse alexa488 antibody and α–mCherry stained with an α–rabbit alexa546 antibody. Cover slips were mounted using ProLong® Gold Antifade Mountant and imaged with an inverted Axiovert 200M (Zeiss).

2.8 Mouse work

During this work, we used NMRI mice for general maintenance of parasites and infection of mosquitoes. C57BL/6 mice were used for standard growth monitoring of parasite lines. When indicated, we used BALB/c mice for additional growth assessments. Mice were supplied by Charles River and Janvier. Animal experiments were approved by the Regierungspräsidium Karlsruhe.

2.8.1 Infections of mice with *Plasmodium berghei* by injections

Intraperitoneal (IP): Mice were infected using frozen stabilates or fresh blood. Either solution was injected into the abdominal cavity of a naïve mouse using a 0.4 x 19 mm cannula and a 1 ml syringe.

Intravenous (IV): Blood stage growth rates and prepatent periods were assessed through daily blood smears after injecting either iRBCs or sporozoites. The injection volume was 100 µl containing either 100 or 5000 parasites. The mice were restrained in a holding chamber and their tails dipped into warm water to dilate the veins for better visibility. The respective solution was injected into one of the lateral tail veins using a 0.5 ml insulin syringe.

Injection of defined numbers of blood stage parasites enabled us to calculate the multiplication or growth rate (Equation 1). Parasitemia was counted and values between 0.2 and 1.2 % were used to calculate growth rates. This range minimizes counting errors but still represents the linear growth phase where reticulocyte numbers are not a restricting factor (Russell *et al.*, 1951).

Equation 1: Calculation of blood stage multiplication rates.

$$growth\ rate = \left(\frac{number\ of\ parasites}{number\ of\ injected\ parasites} \right)^{1/day}$$

2.8.2 Infection of mice with *Plasmodium berghei* by mosquito bite

Mosquitoes infected with the respective parasite line were starved off their sugar solution for at least 4h or over night. Next, mice were injected IP with 50 µl of ketamine / xylazine working solution. Once they were anesthetized sufficiently they were laid either directly on

top of a mosquito cage or a paper cup covered with a net containing ten (selected) mosquitoes. Mosquitoes were allowed to bite for 5-10 minutes.

2.8.3 Blood smears

Parasitemia of mice was monitored by daily blood smears from the tip of the tail. The tails were nicked at the very end using a 0.4 x 19 mm cannula. If necessary, the resulting drop of blood was enlarged by pushing more blood from the tail. The blood was transferred onto a glass microscopy slide and dispersed into a thin layer using a second glass slide. The smear was air-dried, fixed with 100 % methanol for 10 seconds and stained in Giemsa working solution for 10 - 20 minutes. The slide was rinsed with tap water, dried and analyzed under a Zeiss microscope with a 100x Apoplan objective (NA 1.25, oil).

2.8.4 Treatment with phenylhydrazine

To achieve higher levels of parasitemia in mice, they were treated with a drug called phenylhydrazine to kill off a proportion of RBCs in order to boost reticulocyte production using (Magnani *et al.*, 1986). As *P. berghei* prefers to invade reticulocytes, increasing their numbers can improve and accelerate parasite growth. To that end mice were injected IP with 1.2 mg of phenylhydrazine in PBS 1-3 days prior to infection.

2.8.5 Antibody production

Recombinant *Plasmodium berghei* profilin was used to immunize mice to generate polyclonal antibodies against *P. berghei* profilin. The time schedule and volumes of injections are shown in Figure 13. Injections were performed subcutaneously (SC) at the hind leg.

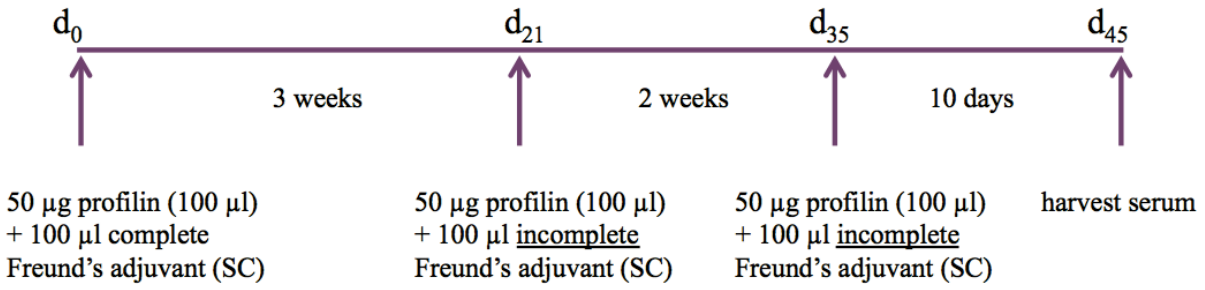

Figure 13: Time course for antibody generation. Immunization of mice using recombinant *P. berghei* profilin and Freund's adjuvant for generating profilin-specific antibodies was performed by injecting two mice three times according to the depicted schedule and harvesting their serum on day 45.

2.9 Western blot

Protein expression of parasite blood stages was monitored through western blots. Samples were prepared as follows: a naïve mouse was infected with the respective parasite line (IP)

and the blood isolated at a parasitemia of at least 5 %. The blood was subjected to an overnight culture and schizonts were isolated (see section 2.6.2). After washing the schizonts in PBS they were pelleted and lysed for 60-90 min on ice in 100-200 µl of RIPA buffer containing protease inhibitors. The sample was frozen in 20 µl aliquots at -20°C as repetitive freeze and thaw cycles severely diminished protein detection.

2.10 Microscopy and image analysis

2.10.1 Fluorescence quantification and volume approximation

Analysis of fluorescence images was performed using an automated ImageJ macro (written by Mirko Singer, see appendix) that yielded the parameters 'fluorescent area' and 'total intensity' in pixel units. Volume calculation of blood stages was performed as follows: we assumed spheres for the shape of ring stages and trophozoites. Their volumes were calculated using their radius deduced from the measured fluorescent area 'A' (Figure 14A). We used the pixel factor (1 pixel = 0.102 µm) to convert the values for r into µm and used these values to calculate the volume of a sphere.

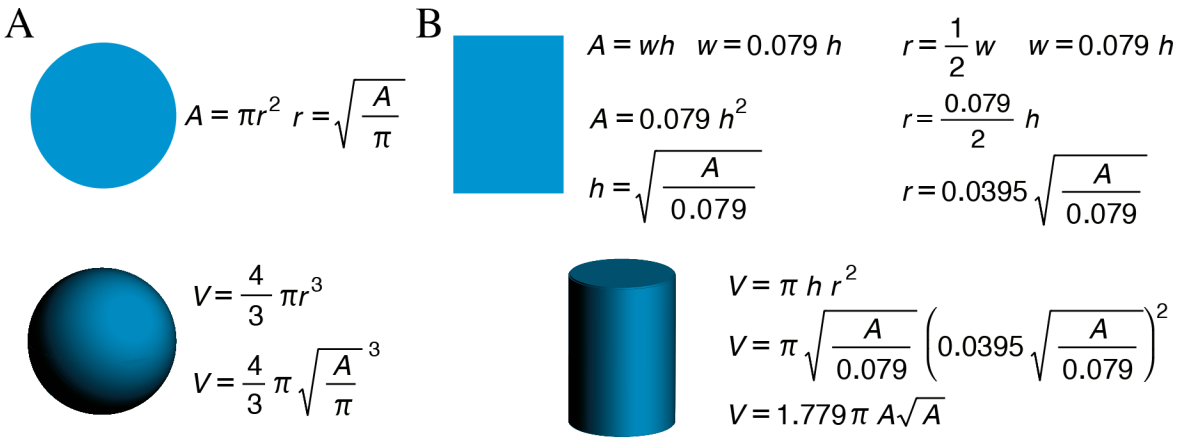

Figure 14: Formula for approximation of fluorescence volumes of blood stages and sporozoites. Formulas are depicted next to their relating geometrical shape. (A) Ring stages and trophozoite shape approximation - circle area to sphere volume: The formula for the area of a circle is solved for the radius 'r' that is then substituted to calculate the volume of the corresponding sphere. (B) Sporozoites - rectangle area to cylinder volume: The average width 'w' to height 'h' ratio of sporozoites is used to substitute 'w' in the formula for the area. The resulting formula is then solved for 'h'. In the formula for the radius 'r' 'w' and 'h' are also substituted. Both 'h' and 'r' are now expressed using 'A' and substituted in the formula for the volume of a cylinder.

Volume calculation of sporozoites was performed as follows: We measured 30 sporozoites to obtain an average of their width to length ratio (0.079). This was used to substitute the variable w in solving for h and r. The values were converted into µm using the pixel factor and used to calculate the volume of the respective cylinders (Figure 14B).

For both shapes the measured total intensities given by the macro were divided by the approximated volumes to obtain the fluorescence of each μm^3.

2.10.2 Sporozoite gliding assay

Infected mosquitoes were dissected using a SMZ 1500 binocular microscope (Nikon). Mosquitoes were washed with 70 % ethanol and kept in PBS until dissection. Using two cannulas attached to 1 ml syringes as knifes I dissected mosquitoes by pulling the head off the thorax and then detached the salivary glands. The salivary glands were kept in 50 µl of RPMI containing 3 % BSA. Sporozoites were freed from the salivary glands by smashing them with a pestle. Sporozoites were transferred onto a 96 well plate with an optical bottom and centrifuged (170 *g*, 5 min).

Images were acquired using the Axiovision 4.7.2 software and either the 63x objective (NA 1.4, oil) or the 25x objective (NA 0.8, water). Imaging of parasites was performed with an inverted Axiovert 200M (Zeiss) for up to 70 min. For tracking the speed of sporozoites, images were acquired every three seconds for 5 min with an exposure time of 400 ms.

Tracking of sporozoite speed was performed utilizing the open source software ImageJ and the according plugin "manual tracking". For analysis, sporozoites that were not attached to the surface were excluded.

2.10.3 Laser tweezer experiments

We employed a self-built setup (Martin Streichfuss, AG Spatz) of holographic optical tweezers for analyzing sporozoites carrying different versions of profilin. These experiments were developed by Katharina Quadt and Martin Streichfuss and performed by Katharina Quadt and myself, as the setup required two people to operate.

Sporozoites were isolated as described in 2.7.4 and applied into a self-assembled flow chamber where they were allowed to adhere to 5 min (for more details, see Quadt *et al.* (Quadt *et al.*, 2016)). Streptavidin-coated polystyrene beads were washed in dmH_2O and equilibrated in RPMI with 3 % BSA. The bead solution was applied to the flow chamber and pulled into the chamber using a paper towel.

Two kinds of experiments were performed: 1. A bead was captured in the laser trap with minimal laser power (and thus minimal force) and positioned on top of a moving sporozoite. Immediately when the sporozoite obtained contact to the bead it was transported rearwards by the parasite. These events were recorded with a frame rate of 100 fps. Afterwards the speed at which the beads were transported to the back of the cell was determined using an automated particle tracking routine in MATLAB. 2. Beads were held with defined trap forces (70 pN,

130 pN and 190 pN) and again deposited on top of moving sporozoites. It was then observed whether the sporozoites were able to overcome these forces and actively pulled the beads from the trap completely or not. Events where sporozoites pushed the bead out of the trap in x/y or z-direction were excluded from the analysis, as this did not involve active pulling.

2.10.4 Generation and imaging of *Plasmodium berghei* ookinetes

Infection and FBT of mice were done as described in 2.7.1. 10 ml ookinete medium was supplemented with 2 ml FBS (US) and the mixtures temperature adjusted in a T75 flask for 30 min at 19°C. Three days after the FBT, the blood was isolated from the mouse, added to the medium and incubated for 20 h at 19°C. The next day, 500 µl of the culture were pelleted and 350 µl of the supernatant were discarded. 3 µl of the concentrated culture were applied to a glass slide, covered with a cover slip and the rims sealed with wax. Ookinetes were imaged with a 25 x objective and a frame rate of 0.05 Hz (1 image every 20 s) for 15 min.

3 Results

3.1 Tagging of profilin with mCherry

As a first step to characterize the role of profilin (Pfn) in *P. berghei* we created a parasite line containing a C-terminally mCherry-tagged profilin to investigate its subcellular localization. N-terminal tagging had been done before (Dissertation Simone Lepper, 2011) but we chose to tag the C-terminus of profilin, as it is more flexible and accessible than the N-terminus (Kursula *et al.*, 2008a). N-terminal tagging had resulted in a uniform distribution throughout the cell and the nucleus (Dissertation Simone Lepper, 2011). During my Master thesis I had already introduced a C-terminal mCherry-tag of profilin as an additional copy under the control of a strong sporozoite-specific promoter (UIS3). Just as with N-terminal tagging, profilin-mCherry localized throughout the sporozoites uniformly (Master thesis, 2012). To check whether C-terminal tagging of endogenous profilin would lead to the same result or possibly be concentrated in the supra-alveolar space where the motor of the gliding machinery is located or at the membranes of other organelles through PIP binding, we replaced the parasite's endogenous profilin with an mCherry-tagged version. For that we modified an nb3D+ vector backbone by inserting profilins 5' and 3' homology regions as well as the cDNA of profilin fused to mCherry (see Figure 12 and section 2.6.1).

3.1.1 Profilin is expressed in all stages of the life cycle and is distributed throughout the cell

All stages of this parasite line (designated Pfn^{-i} // mCh) had a strong mCherry signal throughout the whole cell similar to sporozoite-specific overexpression of mCherry-tagged additional copies of profilin (Master thesis 2012). However, western blot analysis of lysed mixed blood stages showed that the majority of mCherry was cleaved off (Figure 15A). Closer investigation of the vector sequence for Pfn^{-i} // mCh revealed that the 4 x alanine linker connecting profilin with mCherry was duplicated. This, in addition to the multiple cloning sites in between the two linkers, rendered the resulting linker sequence twelve amino acids long (AAAASRTSAAAA). Bioinformatical searches for canonical peptidase motifs did not find any cleavage sites within this sequence. However, many of the parasites' proteases and their cleaved motifs are still not known. Thus, the link between profilin and mCherry could have been cleaved by an unknown protease or mechanism.

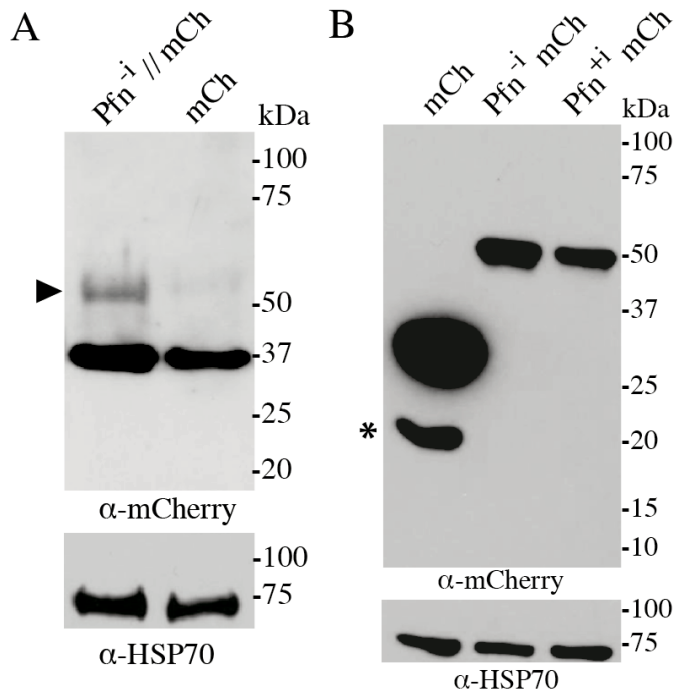

Figure 15: Western blot of parasites expressing different version of mCherry-tagged *P. berghei* profilin. (A) Mixed blood stages from an infected mouse were lysed in RIPA buffer and probed with an mCherry antibody as well as HSP70 antibodies as loading control. As a control for mCherry presence, a parasite line from AG Heussler expressing mCherry under the ef1a promoter was treated accordingly. Note the faint band for mCherry-tagged profilin (~50 kDa, arrowhead) and the majority of mCherry (~37 kDa) not attached to profilin. (B) Schizont lysates from two parasite lines (with or without introns, Pfn$^{+/-i}$ mCh) where profilin is directly connected to its mCherry tag via a linker of 4 glycines. Note the unspecific band or degradation product (~20 kDa, asterisk) in the mCherry control sample.

To achieve consistent tagging of profilin, profilin was fused to mCherry with a 4 x glycine linker in between. To avoid undesired effects of multiple cloning sites, the two genes were connected seamlessly by overlap extension PCR (see Material and Methods section 2.5.2). I used both gDNA (containing introns, 1210 bases) and cDNA (lacking introns, 525 bases) of *P. berghei* profilin, to investigate whether the lack of introns influenced protein expression as we planned on using profilin mutants based on *P. falciparum* cDNA. The resulting parasite lines (Figure 16) were designated Pfn^{+i} mCh and Pfn^{-i} mCh respectively.

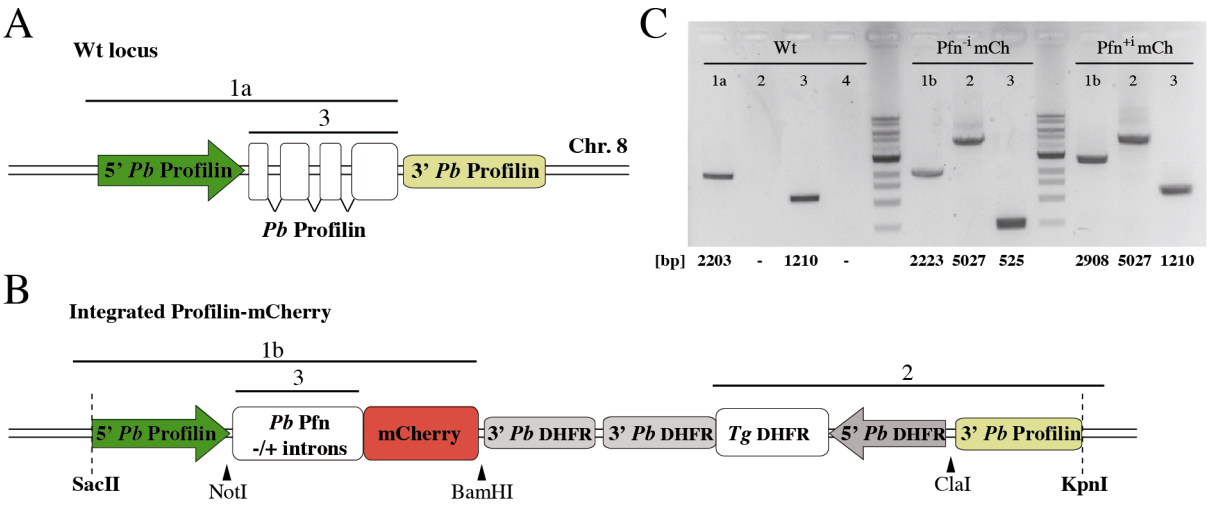

Figure 16: Genomic integration of mCherry-tagged profilin. (A) Locus of wild type profilin containing 4 exons and 3 introns. (B) Profilin locus after integration. Restriction enzymes for cloning and their cutting sites are indicated with black arrowheads. Enzymes for and locations of vector linearization are indicated by vertical dashed lines. (C) Integration PCR as indicated with black bars and numbers in A and B. Expected fragment sizes are shown below their corresponding lane. Wild type control 4 is equivalent to fragment 3 with *Pf* profilin-specific primers. Wild type controls also correspond to Figure 23. Note that fragments 1b and 3 differ by 685 bases between parasites with or without introns in profilin.

Western blot showed the proper fusion proteins with mCherry clearly tagged to profilin (Figure 15B). Localization in both Pfn^{+i} mCh and Pfn^{-i} mCh parasites remained throughout the whole cell in all stages (Figure 17) as seen in Pfn // mCh parasites. In ookinetes and gametocytes profilin-mCherry strongly accumulated in the nucleus (Figure 17).

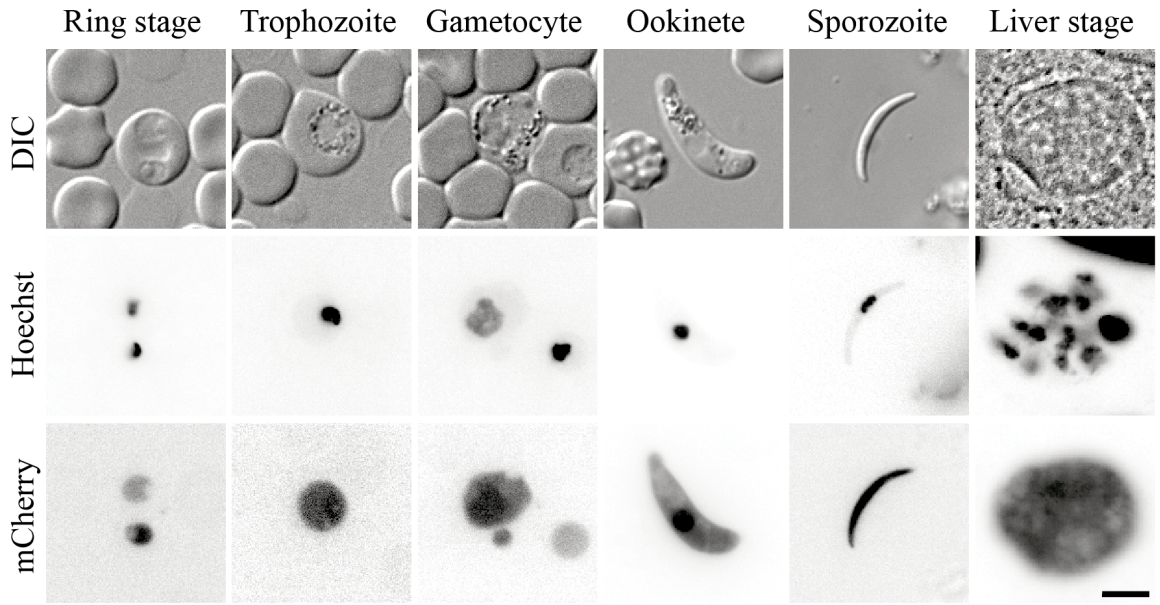

Figure 17: Localization of mCherry-tagged profilin in different stages of the life cycle. Representative images of a double infected erythrocyte with two ring stages, trophozoite, gametocyte with a ring stage on its right, ookinete with an echinocyte on its left, sporozoite and liver stage from the Pfn^{+i} mCh line. The first row shows the parasites in differential interference contrast (DIC). The two bottom rows are inverted fluorescence images with the middle row showing Hoechst, staining the nucleus and the bottom row showing profilin-mCherry expression.

3.1.2 Presence or absence of profilin's introns influences protein expression slightly but does not affect life cycle progression

The two parasite lines Pfn^{-i} mCh and Pfn^{+i} mCh allowed me to investigate the effect of the introns on profilin expression through measuring mCherry fluorescence intensity. To that end, I performed quantitative fluorescence microscopy: ring stages and trophozoites in the blood as well as salivary gland sporozoites and ookinetes were imaged with the same exposure times and microscope settings. I quantified fluorescence intensities as well as cell sizes (fluorescent area) automatically and compared Pfn^{+i} mCh with Pfn^{-i} mCh parasites (Figure 18). Initially, I compared total fluorescence intensities of each of the stages analyzed (Figure 18A-D). The fluorescence in ring stages was significantly less in the absence of introns. However, fluorescence in trophozoites was not different whether introns were present or not. As the blood stages were not synchronized, I wanted to compare the cells independent of cell size. Thus, I approximated the shapes of rings and trophozoites as spheres and the shape of

sporozoites as a cylinder (see Figure 14). From this, we calculated the fluorescence intensities per µm^3 (see 2.10.1, analysis done together with Léanne Strauß). This allowed us to compare fluorescence levels across the different stages (Figure 18E).

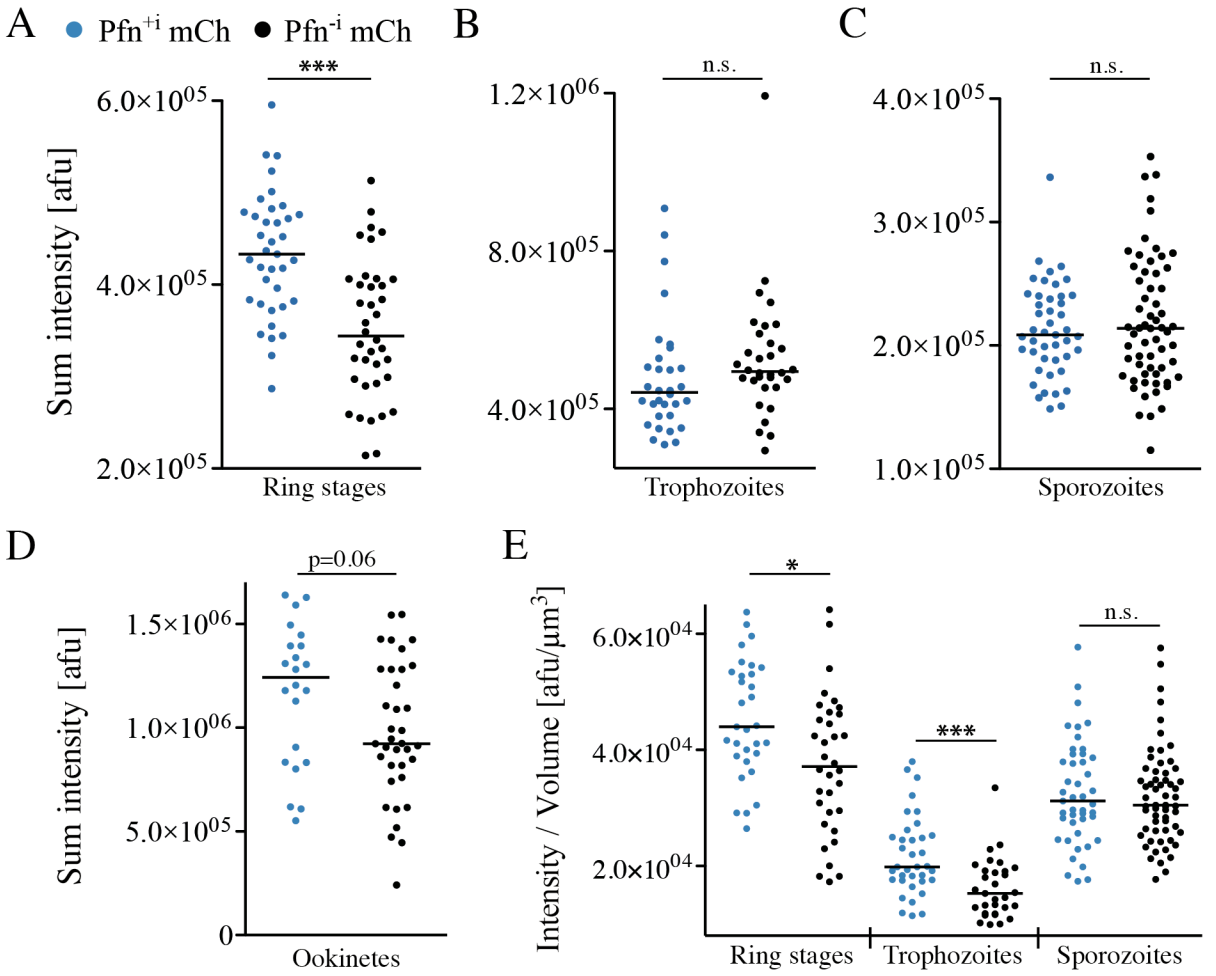

Figure 18: Fluorescence analysis of parasites expressing mCherry-tagged profilin. Expression of profilin with introns (blue) and without introns (black) was compared by tagging both version with mCherry. Significances were tested using a Mann-Whitney test. (A) Comparison of total intesity of ring stages. (B) Comparison of total intesity of trophozoites. (C) Comparison of total intesity of sporozoites. (D) Comparison of total intesity of ookinetes. (E) Comparison of the parasite lines in ring stage, trophozoite and sporozoite stages. The intensity determined using an ImageJ macro was divided by the approximated volume (2.10.1, Figure 14). This allowed a direct comparison across different stages and thus cell shapes.

Ookinetes were excluded from this type of analysis and we just compared total intensities of ookinetes from Pfn^{-i} mCh and Pfn^{+i} mCh (Figure 18D), as their distribution of fluorescence intensities was not uniform throughout the cell, but accumulated in the nucleus. This additional way to analyze the data revealed that in parasites containing introns in the profilin gene both ring stages and trophozoites fluorescence levels were higher than if profilin lacked introns (Figure 18E). In general, fluorescence was higher in ring stages than in trophozoites. This is in good agreement with transcriptional data (Bozdech *et al.*, 2003) that shows that

profilin transcription peaks at the schizont stage. In good agreement with this, we found that profilin concentrations peaked in schizont during western blot analysis of blood stages. So the level of protein is still high in ring stages and reduces during the trophozoite stage as transcription in ring stages decreases. In-depth analysis of blood stages showed, that the smaller the cells were (ring stages) the higher the intensity per µm^3 (Figure 19). This indicates that the amount of profilin that is translated is the same regardless of the cell size and thus smaller cells contain a higher concentration of profilin. In the total intensities of ookinetes (Figure 18D) we found that the presence of introns led to a slight increase in fluorescence intensity (p=0.06). However, at the sporozoite stage, introns did not influence the total or relative fluorescence intensity and thus profilin levels at all (Figure 18C, E).

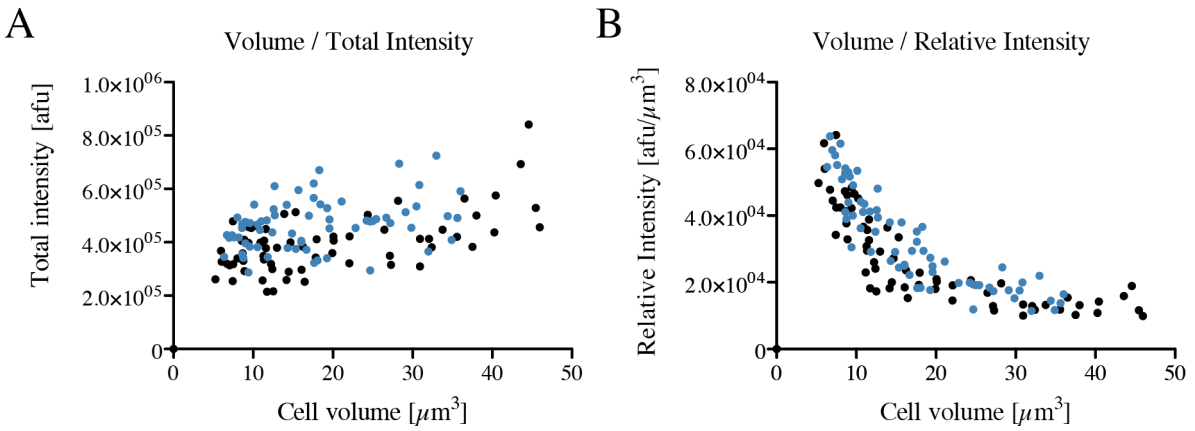

Figure 19: In depth analysis of blood stages (ring stages and trophozoites). Blood stage parasites expressing profilin with introns (blue) or without introns (black). (A) Correlation of cell size and total fluorescence intensity. (B) Correlation of cell size and relative fluorescence intensity.

Given the importance and sensitivity of actin dynamics, even a standard alteration like an mCherry tag has to be monitored very carefully. The mCherry tag (~37 kDa) is almost twice the size of *Plasmodium* profilin (19 kDa) so it was necessary to investigate possible effects *in vivo*. Thus, we compared blood stage growth of the two mCherry tagged lines (Pfn$^{-/+i}$ mCh) with the wild type. Mice infected with either 100 or 5000 blood stage parasites were monitored daily through blood smears from the tail vein. Their parasitemia was counted and used to calculate growth rates (Equation 1, Table 4). This revealed that both the Pfn^{+i} mCh and Pfn^{-i} mCh lines have similar growth rates as the wild type, however, the parasites containing introns in profilin (Pfn^{+i} mCh) grew slightly faster than the parasites without introns in profilin (Pfn^{-i} mCh). Also, I infected mosquitoes with the respective lines and assessed oocyst, midgut sporozoites and salivary gland sporozoites numbers (Table 4). All three parameters were very similar and within the natural variation. In addition infected

mosquitoes were allowed to bite naïve mice (see 2.8.2) and determined their prepatency as well as parasitemia on day 6 (Table 4). The prepatency did not differ much, considering that only 4 mice were used. These differences might be even smaller if more mice would have been used. The parasitemia on day 6 was higher in wild type parasites but also Pfn^{+i} mCh and Pfn^{-i} mCh parasites were within the normal range. These parameters also vary in clonal lines compared to polyclonal lines that have been in culture for years instead of months.

Table 4: Development of parasites expressing mCherry-tagged profilin in mice and mosquitoes.

Parasite line	Blood stage growth rate (median)	Mosquito infection rate [%]	Oocysts / iMG (mean)	MG spz / mosquito (mean)	SG spz / mosquito (mean)	Prepatency [days] (mean)	Parasitemia d6 [%] (mean)
Pb Wt	8.9	50	105	39 000	9 400	3.75	2.3 ± 0.4
Pfn^{+i} mCh	9.8	50	90	38 000	7 600	3.5	1.7 ± 0.6
Pfn^{-i} mCh	8.5	50	75	37 000	6 400	4	1.4 ± 0.1

Analysis of parasite lines expressing mCherry-tagged profilin with or without introns. Blood-stage growth rates were determined after injecting either 100 or 5000 iRBCs IV into four C57BL/6 mice respectively (see 2.8.1). Infection rates of mosquitoes were established by checking mosquito midguts for oocysts between day 17 and 25. Oocyst numbers were obtained by counting the cysts of at least 50 infected mosquito midguts (MG) on day 12 (see 2.7.3). MG and salivary gland (SG) sporozoite (spz) numbers were assessed between days 17 and 25 (2.7.4). At least three different cages of each parasite line were assessed. Parasitemia on day 6 and prepatency (first day of detectable blood-stage infection) were determined for each line after four C57BL/6 mice were bitten by 5-10 infected mosquitoes (see 2.8.2).

3.1.3 Tagging of profilin with mCherry impairs sporozoite gliding motility

I performed 2D gliding assays (see 2.7.1 and 2.10.2), recorded time-lapse images and tracked both ookinetes (Figure 20A) and sporozoites (Figure 20B).

I did not observe a difference in ookinete gliding speeds between wild type and Pfn-mCh expressing parasites (Figure 20A). However, sporozoites gliding speeds in both parasite lines expressing mCherry-tagged profilin (Pfn^{+i} mCh and Pfn^{-i} mCh) were significantly reduced, indicating an impairment of profilin function due to the mCherry tag. It did not matter whether profilin contained introns, as these two lines did not show a difference in speeds. This is in good agreement with the previous results of sporozoites from both the Pfn^{+i} mCh and Pfn^{-i} mCh line having equal fluorescence intensities and thus equal amounts of profilin (Figure 18C, E). It is important to note that sporozoites from the Pfn^{-i} // mCh line, in which the mCherry tag was cleaved off, were gliding just as fast as wild type sporozoites. This substantiates that the mCherry tag caused the reduced gliding speed of Pfn^{+i} mCh and Pfn^{-i} mCh sporozoites. In hindsight, this also makes the Pfn^{-i} // mCh line the perfect control that

helped to exclude artifacts due to integration or the presence of a different 3' UTR (DHFR). It also suggests that mCherry is cleaved off in vivo and not during western blot sample preparation.

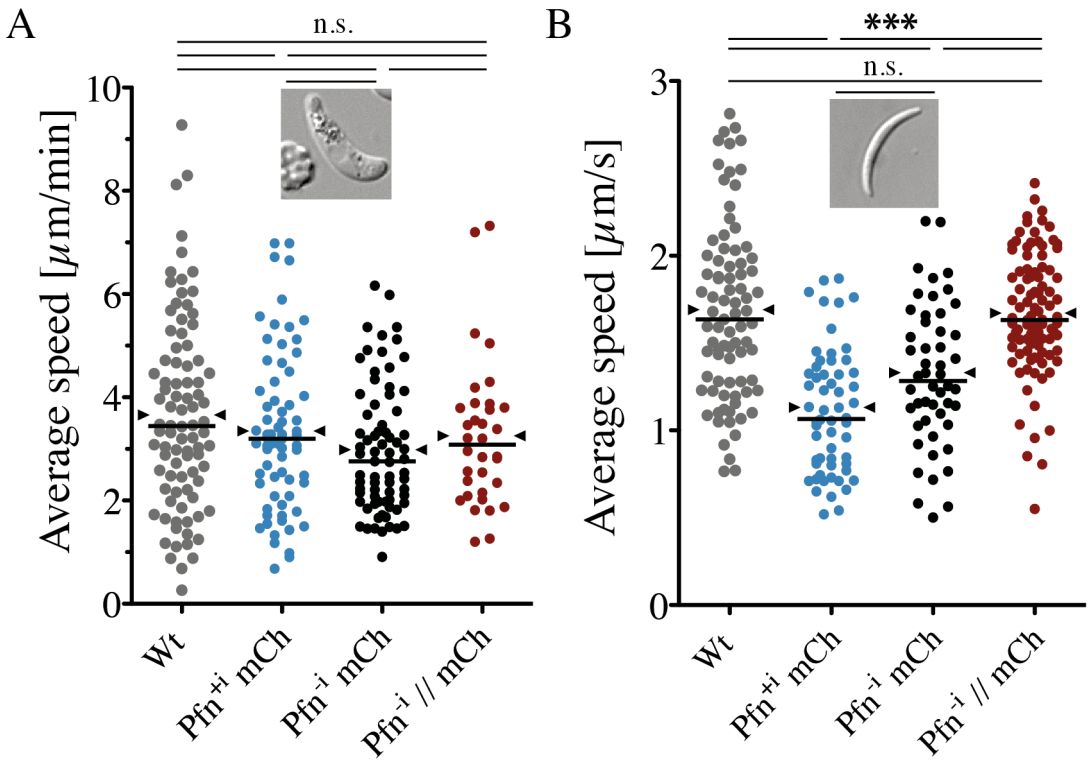

Figure 20: Tagging of profilin with mCherry impairs sporozoite but not ookinete gliding. Insets show representative DIC images. Black bars indicate the median and arrowheads show the mean. (A) Average ookinete speed of wild type and Pfn-mCh lines in µm/min. (B) Average sporozoite speed of wild type and Pfn-mCh lines in µm/s. Significances were tested using a Kruskal-Wallis and Dunn's post test. In general I indicated the median for the data as not all groups were normally distributed. I included the mean to show that it is not strikingly different from the median, indicating a symmetric distribution of data sets.

These data show that it is essential to control for effects that occur when tagging a protein with mCherry or GFP. As we wanted to introduce subtle mutations into profilin and analyze the effects these mutation might have on sporozoite motility, we did not tag these profilin versions with mCherry.

3.2 Tip mutants and arm deletion

We collaborated with the group of Inari Kursula at the University of Oulu in Finland who had solved the crystal structure of *Plasmodium falciparum* profilin (Kursula *et al.*, 2008a). As they had already proposed a role for the β-hairpin (referred to as arm-motif) in actin binding, our goal was to test this hypothesis. Therefore, we used several mutant versions of profilin (Figure 21) that the Kursula group investigated biochemically in parallel. The tip of the arm-motif is acidic in nature, consisting of the three amino acids EDE that were proposed to interact with a basic patch in actin. In the first mutant 'QNQ Pfn' these amino acids were turned into their corresponding amino acids with opposite polarity. In the second mutant 'AAA Pfn' the EDE residues were changed to three uncharged and non-polar alanines (AAA). These mutants are summarized under 'tip mutants'. In addition to these specific substitutions, we also included an arm motif deletion lacking ten amino acids ('Δ arm Pfn'). As all of these mutations were based on *P. falciparum* profilin, we included *Pf* wild type profilin ('*Pf* Pfn') as a control.

```
                                        20                  40                  60
P. falciparum Profilin  MAEEYSWDSY LNDRLLATNQ VSGAGLASEE DGVVYACVAQ GEESDPNFDK WSLFYKEDYD
QNQ Profilin            MAEEYSWDSY LNDRLLATNQ VSGAGLASEE DGVVYACVAQ GEESDPNFDK WSLFYKEDYD
AAA Profilin            MAEEYSWDSY LNDRLLATNQ VSGAGLASEE DGVVYACVAQ GEESDPNFDK WSLFYKEDYD
Δ arm Profilin          MAEEYSWDSY LNDRLLATNQ VSGAGLASEE DGVVYACVAQ GEESDPNFDK WSLFYKEDYD
P. berghei Profilin     M-EEYSWENF LNDKLLATNQ VSAAGLASEE DGVVYECVAT PDENNPDFDK WSLFYKEDYD

                                        80                  100                 120
P. falciparum Profilin  IEVEDENGTK TTKTINEGQT ILVVFNEGYA PDGVWLGGTK YQFINIERDL EFEGYNFDVA
QNQ Profilin            IEVQNQNGTK TTKTINEGQT ILVVFNEGYA PDGVWLGGTK YQFINIERDL EFEGYNFDVA
AAA Profilin            IEVAAANGTK TTKTINEGQT ILVVFNEGYA PDGVWLGGTK YQFINIERDL EFEGYNFDVA
Δ arm Profilin          I---------TKTINEGQT ILVVFNEGYA PDGVWLGGTK YQFINIERDL EFEGYNFDVA
P. berghei Profilin     IEIEDENGSK TTKTITEGQS ILTMFNEGYA SDGIWLGGTK YQFINMDKGL EYEGHSFDVA

                                        140                 160
P. falciparum Profilin  TCAKLKGGLH LVKVPGGNIL VVLYDEEKEQ DRGNSKIAAL TFAKELAESS Q*----  172
QNQ Profilin            TCAKLKGGLH LVKVPGGNIL VVLYDEEKEQ DRGNSKIAAL TFAKELAESS Q*----  172
AAA Profilin            TCAKLKGGLH LVKVPGGNIL VVLYDEEKEQ DRGNSKIAAL TFAKELAESS Q*----  172
Δ arm Profilin          TCAKLKGGLH LVKVPGGNIL VVLYDEEKEQ DRGNSKIAAL TFAKELAESS Q*----  162
P. berghei Profilin     TCAKSKGGMH IIKVGGGHIL IVLYDEEKEQ DRGNSKNAAL AFSKELIEST DTGAA*  175
```

Figure 21: Amino acid sequences alignment of *Plasmodium* profilins, tip mutants and arm deletion. Mutations (QNQ, AAA) and the deletion (Δ arm) are highlighted with red boxes. *Plasmodium falciparum*-based sequences have a white background, *Plasmodium berghei* profilin a grey background. The lengths of the different sequences are indicated behind the last row. Sequences were aligned using CLC Main Workbench software version 5.1 (CLC bio).

The sequences of *P. falciparum* and *P. berghei* profilin are very similar. It includes stretches of perfect conservation as well as more diverse regions. The acidic loop (amino acid 40-50) is one of the more diverse stretches whereas the arm domain is very well conserved.

3.2.1 *Plasmodium falciparum* profilin sequesters actin monomers better than its tip mutants and arm deletion

Bhargav Saligram Prabhakar from the Kursula lab performed *in vitro* polymerization assays (Figure 22) with the same profilin mutants (2.3.3 - 2.4.5). These experiments revealed that α-actin polymerizes best in the absence of profilin (light blue curves). *Pf* Pfn strongly reduced fluorescence intensity and thus the amount and/or length of actin filaments in a concentration-dependent manner (Figure 22A). This means that *P. falciparum* profilin has the ability to bind and sequester α-actin monomers, thereby reducing their incorporation into filaments. This ability was retained, but notably reduced with QNQ and AAA profilin (Figure 22B,C).

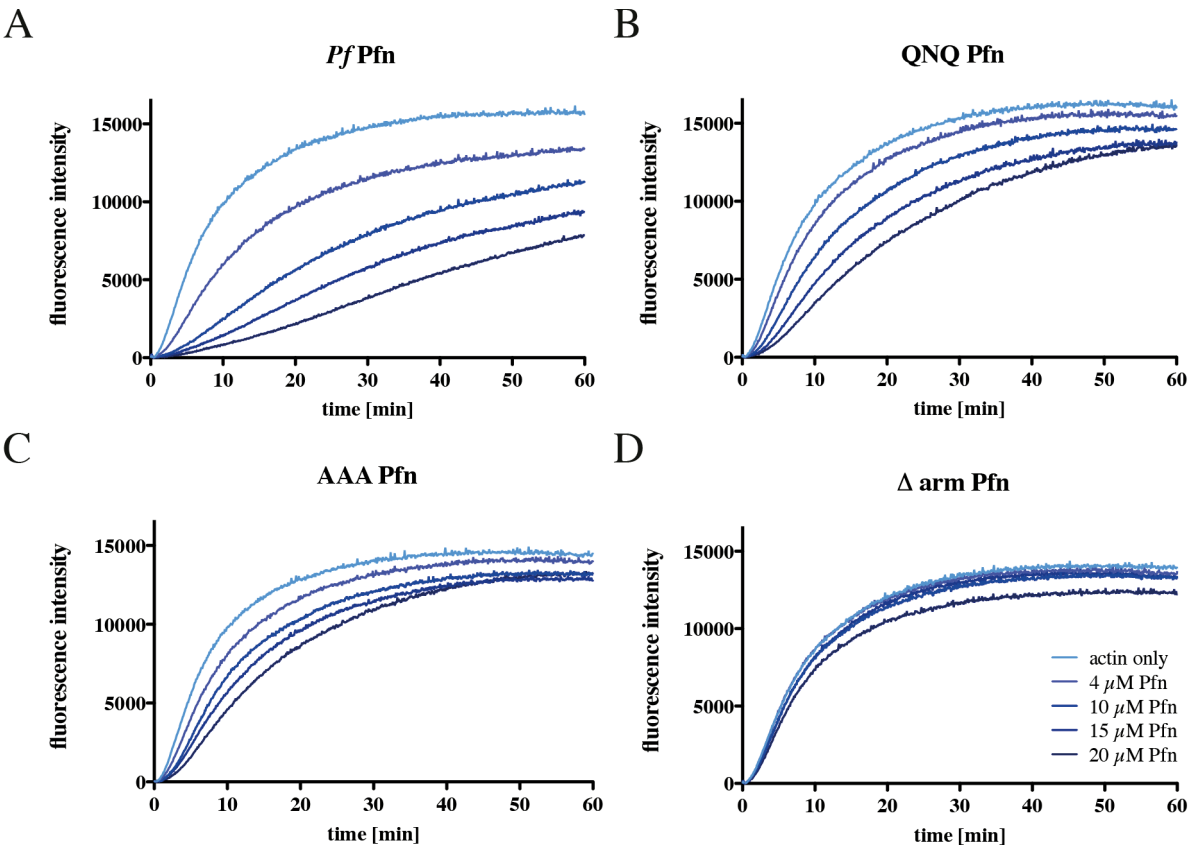

Figure 22: *In vitro* α-actin polymerization is strongly reduced by *Pf* Pfn, but less by its mutants. (A-D) α-actin isolated from pig muscle acetone powder containing 4 % of the α-actin labeled with pyrene was allowed to polymerize without or with increasing concentrations of *Pf* profilin (A) or one of its mutants QNQ Pfn (B), AAA Pfn (C) and Δ arm Pfn (D). This data was acquired by Bhargav Saligram Prabhakar in the group of Inari Kursula.

Even at the highest profilin concentration (20 µM) Δ arm Pfn did not affect actin polymerization (Figure 22D). This suggests that the arm-motif is required for actin sequestration and thus most likely for proper actin binding.

3.2.2 Parasites carrying profilin tip mutants or the arm deletion are able to complete the life cycle

Given the pronounced differences of these profilin mutants on actin biochemistry, I investigated the *in vivo* effects of these profilin mutations in *P. berghei*. I replaced the endogenous single profilin gene of *P. berghei* parasites (Figure 23A) with the above-described mutant versions of profilin using the methods and vectors described in 2.6. After creating clonal lines I checked their DNA for integration. The 5' integration was verified using *Pf* profilin or mutant profilin-specific primers (Figure 23C, fragment 1c). In addition I showed the absence of the wild type profilin gene (Figure 23C, fragment 3), confirming successful replacement of endogenous profilin.

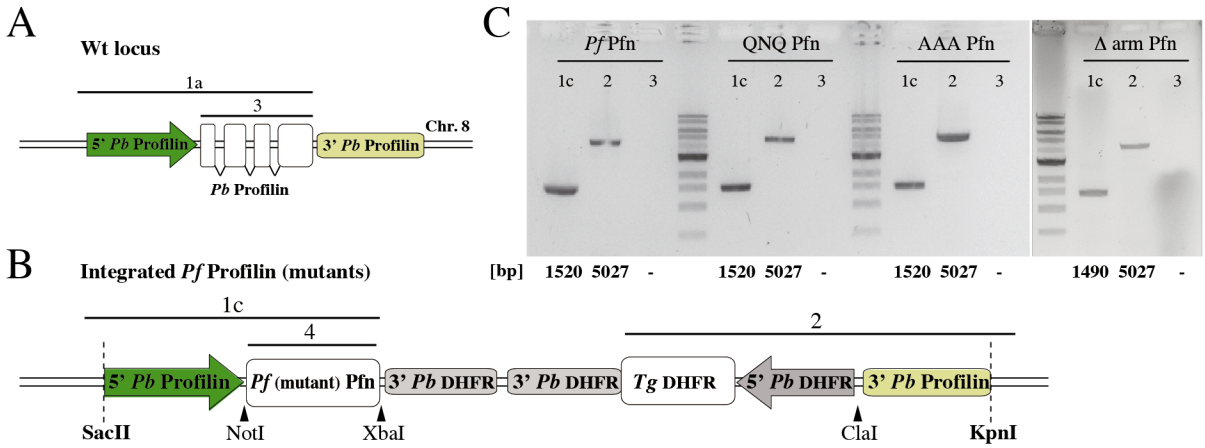

Figure 23: Genomic locus after integration of *P. falciparum* profilin, tip mutants and arm deletion. (A) Wild type profilin locus before integration. (B) Profilin locus after integration. Key restriction enzymes for cloning and their cutting sites are indicated with black arrowheads. Enzymes for and locations of vector linearization are indicated by vertical dashed lines. (C) Integration PCR of indicated parasite lines. The corresponding sequences of the amplified fragments are shown with black bars and numbers in A and B. Expected fragment sizes are shown below their corresponding lane. Note the reduced length of fragment 1c in Δ arm Pfn due to the deletion of 30 bases. Wild type controls are shown in Figure 16.

We subsequently analyzed the ability of the above-described mutant to progress through the life cycle. The blood stage multiplication rate of *Pf* Pfn parasites was slightly higher than wild type (Table 5). QNQ Pfn and AAA Pfn growth rates were very similar to the *Pf* Pfn wildtype. However, the multiplication rate of Δ arm Pfn was significantly lower than wild type or *Pf* Pfn parasites indicating a more pronounced defect in this particular mutant. Oocyst numbers of infected midguts in *Pf* Pfn, QNQ Pfn and AAA Pfn were similar, just as MG and SG sporozoite numbers. Oocysts numbers in Δ arm Pfn were actually higher than wild type, however only 17 % of mosquitoes were infected. The infected mosquitoes however, had a high number of oocysts. Δ arm Pfn MG and SG sporozoite numbers both were reduced

around 90 % compared to wild type. In addition to this reduced number of sporozoites, prepatency was much longer and parasitemia on day 6 was once again reduced by ~ 90 %.

Table 5: Development of parasites expressing profilin tip mutants or arm deletion in mice and mosquitoes.

Parasite line	Growth rate (BS) (median)	Mosquito infection rate [%]	Oocysts / iMG (mean)	MG spz / mosquito (mean)	SG spz / mosquito (mean)	Prepatency [days] (mean)	Parasitemia d6 [%] (mean)
Pb Wt	8.9	50	105	39 000	9 400	3.75	2.3 ± 0.4
Pf Pfn	10.5	33	75	36 000	4 300	4	1.7 ± 0.8
QNQ Pfn	9.2	33	80	37 000	7 400	4.5	1.7 ± 0.7
AAA Pfn	9.5	33	90	50 000	7 300	4.25	1.5 ± 0.3
Δ arm Pfn	6.5	17	130	3 400	1 100	6	0.3 ± 0.1

Analysis of parasite lines expressing different mutant profilins. Blood stage (BS) growth rates were determined after injecting either 100 or 5000 iRBCs IV into four C57BL/6 mice respectively (see 2.8.1). Infection rates of mosquitoes were established by checking mosquito midguts for oocysts between day 17 and 25. Oocyst numbers were obtained by counting the cysts of at least 50 infected (i) mosquito midguts (MG) on day 12 (see 2.7.3). MG and salivary gland (SG) sporozoite (spz) numbers were counted between days 17 and 25 (2.7.4). At least three different cages of each parasite line were assessed. Parasitemia on day 6 and prepatency (first day of detectable blood-stage infection) were determined for each line after four C57BL/6 mice were bitten by five to ten infected mosquitoes (see 2.8.2).

3.2.3 Ookinetes carrying Δ arm Pfn are drastically reduced in speed

To pinpoint the cause of the reduced infection rate of mosquitoes with Δ arm Pfn we investigated ookinete motility. Wild type ookinetes moved with a speed of 3.9 µm/min. Both *Pf* Pfn and QNQ Pfn ookinetes moved faster than that with 5.4 and 5.7 µm/min respectively. Compared to the *Pf* Pfn control, AAA ookinetes were significantly reduced in speed (4.1 µm/min). Interestingly, the speed of Δ arm Pfn ookinetes was reduced even more drastically to only 1.4 µm/min, a reduction of 75 % compared to *Pf* Pfn. This could possibly lead to problems in crossing the mosquito midgut, which might explain the low mosquito infection rates of this mutant (Table 5).

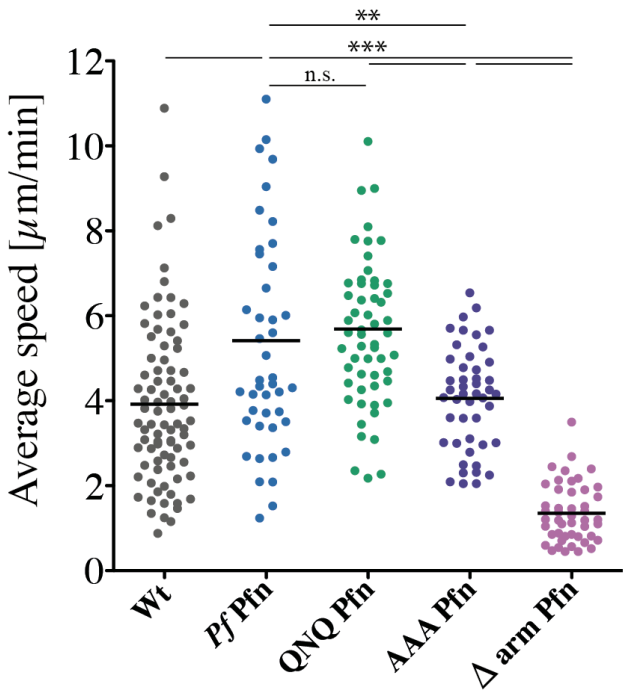

Figure 24: Ookinetes carrying Δ arm Pfn are drastically reduced in speed. Average speeds of at least 45 wild type and tip mutant ookinetes in µm/min are shown. Black bars indicate the mean. Differences were assessed using a one-way ANOVA.

3.2.4 Sporozoites carrying AAA Pfn or Δ arm Pfn show defects in gliding motility

Afterwards, I investigated sporozoite motility of the *Pf* Pfn, QNQ Pfn, AAA Pfn and Δ arm Pfn transgenic lines. I grouped the sporozoites according to their motility patterns (Figure 25A). Sporozoites that were not motile while being attached to the surface with at least one end were grouped as 'attached/waving' (Hegge *et al.*, 2009). Sporozoites that exhibited gliding motility were grouped into 'partially moving' (moving less than 150 s) and 'consistently moving' (moving for more that 150 s). Approximately 20 % of *Pf* Pfn and QNQ Pfn sporozoites were moving consistently. This represents a cut in half compared to wild type sporozoites. However, only 5 % of AAA Pfn and Δ arm Pfn sporozoites were able to glide consistently, representing a 90 % reduction compared to wild type. Yet, as the mutants are based on *Plasmodium falciparum* profilin, the mutants should be compared to *Pf* Pfn as control. This means QNQ Pfn does not show any difference to *Pf* Pfn but the percentages of consistently gliding sporozoites of AAA Pfn and Δ arm Pfn are still reduced 80 %. Together with Samantha Ebersoll, I tracked the consistently moving sporozoites and assembled 40 trajectories of each parasite line to visualize their motile behavior (Figure 25B-E).

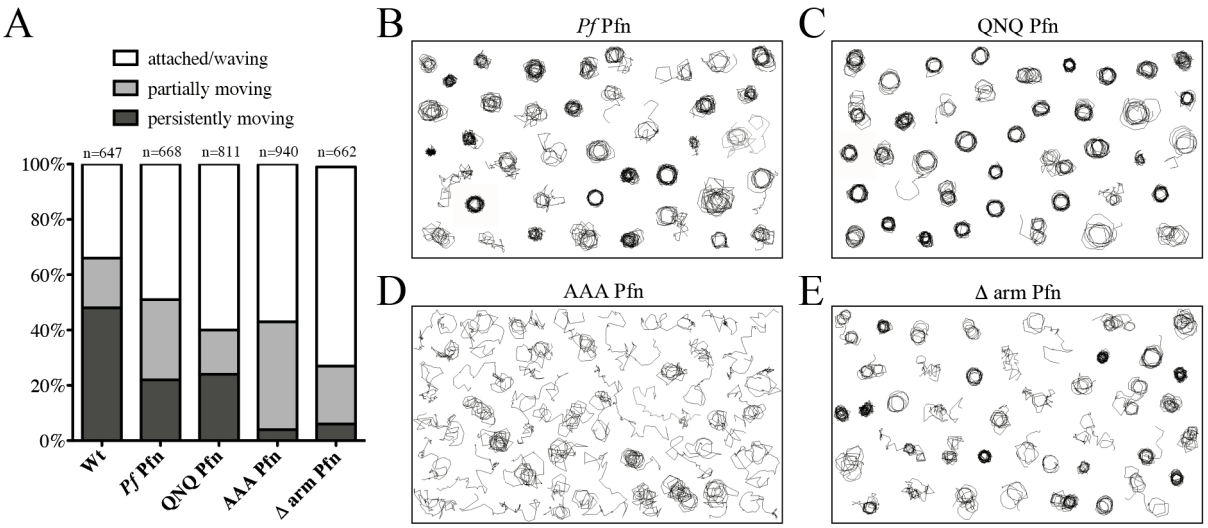

Figure 25: Mutations in the profilin arm motif affect sporozoite motility. (A) Percentages of sporozoites exhibiting specific motility patterns. Sporozoites were either attached at one ('waving') or both ends ('attached', white) or persistently moving over at least 150 s (dark grey). Sporozoites that were moving less than 150 s were grouped as 'partially moving' (light grey). Numbers of sporozoites analyzed for each line are indicated above each column. (B-E) Trajectories of 40 persistently moving sporozoites of each indicated parasite line.

This clearly demonstrated that *Pf* Pfn and QNQ Pfn are capable of performing regular, consistent circular gliding motility. AAA Pfn and Δ arm Pfn had more difficulties to accomplish smooth regular trajectories. Sporozoites were still able to move in circles, but

their trajectories were more edgy and sporozoites changed direction more frequently. This is in line with the motility pattern data also showing that *Pf* Pfn & QNQ Pfn as well as AAA Pfn & Δ arm Pfn group together in pairs. Δ arm Pfn sporozoites moved better than AAA Pfn sporozoites, as their motile behavior was less erratic.

Tracking of the consistently moving sporozoites also allowed us to analyze their speed. Interestingly, the average speed of *Pf* Pfn sporozoites was around 2.3 µm/s, faster than wild type sporozoites that move with approximately 1.6 µm/s (Figure 26A). Again, there was no significant difference between *Pf* Pfn and QNQ Pfn sporozoites that moved with 2.1 µm/s. However, the average speeds of AAA Pfn that moved with 1.2 µm/s and Δ arm Pfn that moved with 1.4 µm/s were notably reduced. As seen before with the motility patterns, the AAA Pfn and Δ arm Pfn sporozoite show similar behavior.

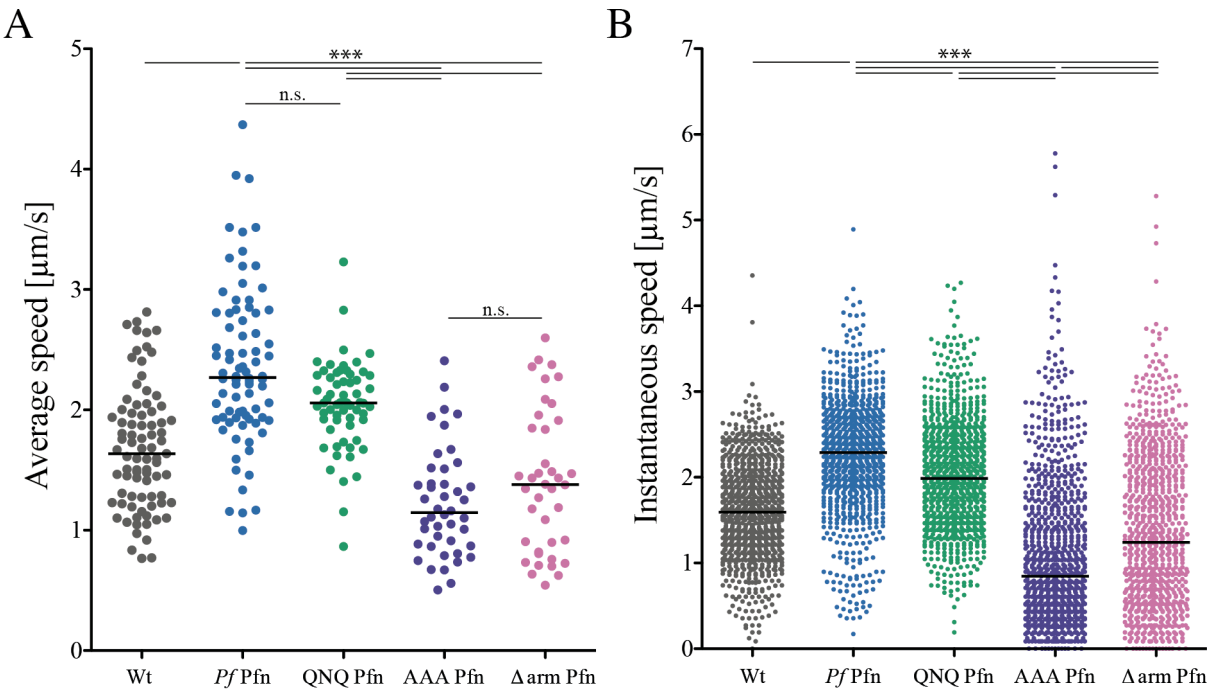

Figure 26: Mutations in profilin's arm region can reduce sporozoite speed. Statistics were analyzed using a Kruskal-Wallis test. The black lines indicate the median. (A) Average speeds of at least 40 sporozoites persistently moving (see Figure 25) between 150-300 s. Data was acquired using the ImageJ plug-in 'manual tracking' that provided the instantaneous speeds (from one frame to the next = 3 s). From these values the average speeds were calculated. (B) Instantaneous speeds from 50-100 frames of 10 sporozoites closest to their respective median in A.

For a closer look at the sporozoites' speed distributions, we analyzed the instantaneous speeds (Figure 26B) of 10 sporozoites of each parasite line, whose average speed was closest to their respective median (Figure 26A). In general, the median instantaneous speeds of wild type, *Pf* Pfn and QNQ Pfn sporozoites were very similar in their median average speeds (Figure 26B). However statistical analysis differed from that in the average speeds (Figure 26A) as each of the 10 sporozoites analyzed, delivered 100 values, whereas only one value per sporozoites

was obtained for the average speeds. For wild type, *Pf* Pfn, and QNQ Pfn sporozoites, the instantaneous speeds cluster around the median. Due to the high amount of values, they create the appearance of columns that taper on both ends (Figure 26B). Wild type sporozoite instantaneous speeds had a median of 1.6 µm/s, *Pf* Pfn sporozoites of 2.3 µm/s and QNQ Pfn of 2.0 µm/s. However, for AAA Pfn and Δ arm Pfn, smaller values were much more abundant so that the columns for these two lines taper only at the top end, but reach all the way down to zero at the lower end (Figure 26B). As a result, the median instantaneous speed of AAA Pfn and Δ arm Pfn were lower than their median average speed with 0.9 µm/s (average median: 1.2 µm/s) and 1.2 µm/s (average median: 1.4 µm/s) respectively. However, AAA Pfn especially and Δ arm Pfn also showed a larger range of instantaneous speeds with higher values than the other mutants in general and bars that stretched farther than in wild type, *Pf* Pfn, and QNQ Pfn sporozoites. These higher values probably somewhat counteract the lower speeds, and thus produce higher median average speeds.

3.2.5 Molecular dynamics simulations reveal loss of interaction between the profilin arm-motif and actin in the AAA Pfn mutant

In the *in vitro* data QNQ Pfn and AAA Pfn show similar behavior – an observation that did not fit with the motility data where *Pf* Pfn and QNQ Pfn cluster together. To further investigate, I collaborated with Hirdesh Kumar who did molecular dynamics simulations in the group of Rebecca Wade at the Heidelberg Institute for Theoretical Studies (HITS). For these experiments, we excluded Δ arm Pfn because of its dimer formation (Bhargav *et al.*, 2015).

Hirdesh ran 150 ns simulations for *Plasmodium* actin in complex with *Pf* Pfn, QNQ Pfn as well as AAA Pfn (Figure 27A) and analyzed the overall conformation of the complexes (Figure 27B) as well as hydrogen bonds that were formed (Figure 27C, D). The arm-motif of *Pf* Pfn and QNQ Pfn was bound to actin and thus the arm did not move a lot. However, in AAA Pfn the arm-motif was flipping away from actin (Figure 27B, yellow arrow). Closer examination revealed a salt bridge with two hydrogen bonds between E_{66} of *Pf* wild type profilin's arm-motif and R_{291} of actin's subdomain 3 (Figure 27C, D). This salt bridge is lost in the QNQ Pfn mutant, however a single hydrogen bond is retained between Q_{66} of profilin and R_{291} of actin. All interactions (hydrogen bonds and salt bridge) at the arm-motif (A_{66}) are abolished in the AAA mutant (red residues and bars).

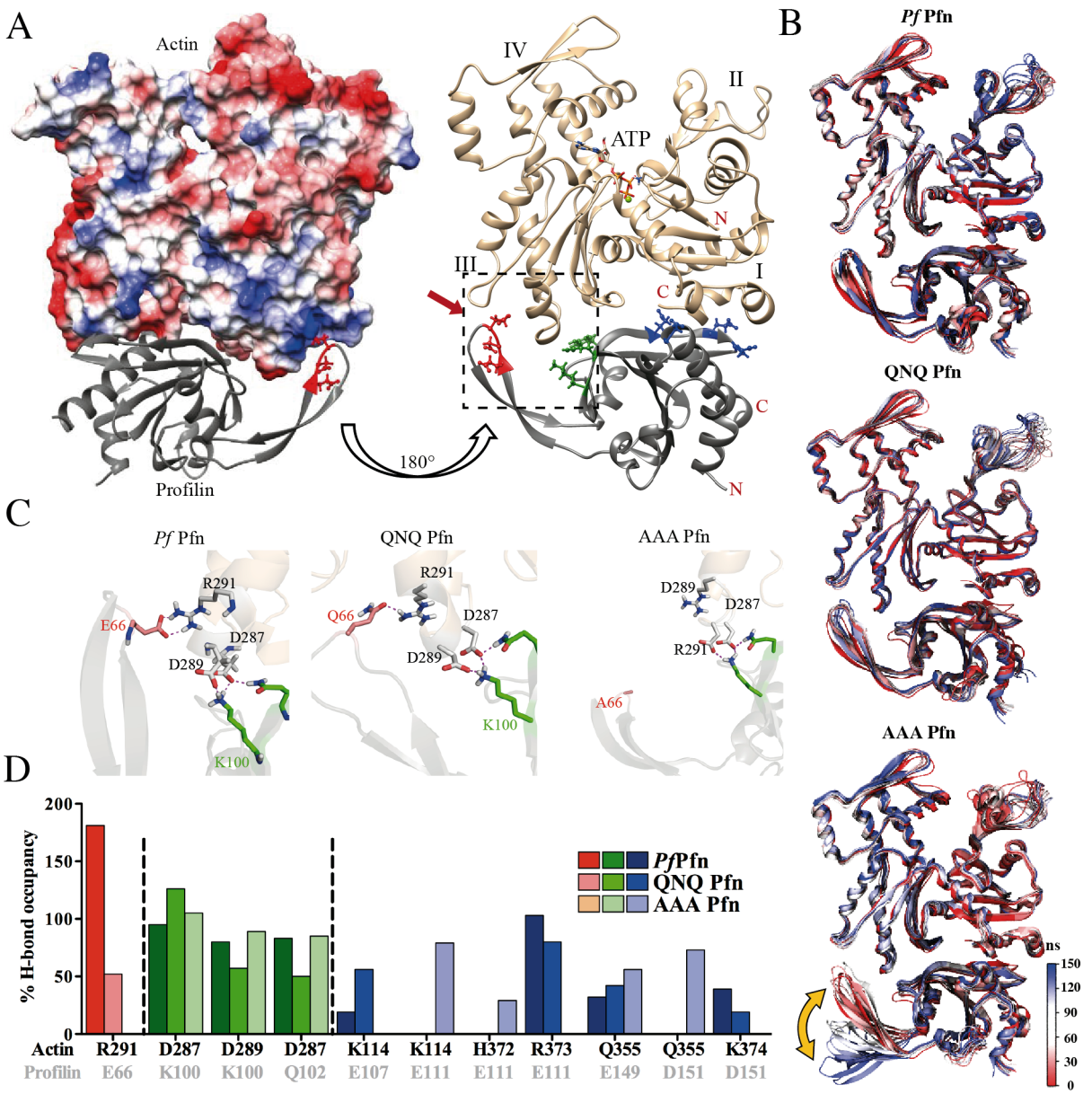

Figure 27 Analysis of hydrogen bonds formed during molecular dynamics simulations of *Plasmodium* actin-profilin binding. (A) *P. falciparum* actin and profilin in complex. Left: The actin surface shows its electrostatic potential (acidic - red; basic - blue) and profilins acidic residues (EDE) are displayed as red sticks. Note the blue basic patch on actin opposite E_{66} of profilin's arm-motif. Right: Actin (gold) with its subdomains labeled (roman numbers). Residues of profilin that form hydrogen bonds with actin are displayed as sticks and coloured either in red (arm-motif interactions, red arrow), green (arm-neighboring interactions) or blue (classical actin-profilin interactions). Dashed box illustrates area shown in C. (B) Molecular dynamics simulations of ensemble structures of *Pf* Pfn, QNQ Pfn or AAA Pfn in complex with *Plasmodium* actin during 150 ns. The starting structure is colored red and the final structure blue (see legend). Note the great flexibility of the arm motif due to loss of hydrogen bonds in the AAA mutant (yellow arrow). (C) Zoom-in into the hydrogen bonds at the tip of the arm-motif (dashed box in A). Note that E_{66} can form two hydrogen bonds at the same time. Oxygen atoms are colored bright red and nitrogen atoms blue. A Close-up can be found in Figure 47. (D) Hydrogen bond occupancy of indicated residues in actin (black numbers) and profilin (grey) for *Pf* Pfn and the QNQ Pfn and AAA Pfn mutants. The occupancy is a maximum of 200 % as E_{66} can form two hydrogen bonds. Colors for interactions as described and displayed in A.

In addition to the interactions at the acidic tip of the arm-motif, the simulations also revealed arm-neighboring hydrogen bonds (green residues and bars). In stark contrast to the arm-motif, these arm-neighboring hydrogen bonds remain almost unchanged in the two mutants QNQ Pfn and AAA Pfn (Figure 27C, D). Interestingly, the simulations revealed differences at the classical profilin-actin interface. While *Pf* Pfn and QNQ Pfn displayed very similar hydrogen bonding patterns, the AAA Pfn mutant clearly diverged. Three of the four hydrogen bonds ($E_{107}^{Pfn} - K_{114}^{Act}$, $E_{111}^{Pfn} - R_{373}^{Act}$ and $D_{151}^{Pfn} - K_{374}^{Act}$) were completely abolished in AAA Pfn mutant (Figure 27D). However, most likely as compensation, two of the residues in AAA Pfn formed hydrogen bonds with different, previously unused residues in actin ($E_{111}^{Pfn} - K_{114}^{Act}$ /$E_{111}^{Pfn} - H_{372}^{Act}$ and $D_{151}^{Pfn} - Q_{355}^{Act}$).

In addition, Hirdesh also calculated binding free energies of the complexes. *Pf* Pfn – actin had a free binding energy of -61.8 ± 9.2 kcal/mol, QNQ Pfn – actin -50.7 ± 10.8 kcal/mol and AAA Pfn – actin had a free binding energy of -45.6 ± 9.2 kcal/mol (Hou *et al.*, 2011). As we were comparing QNQ Pfn and AAA Pfn with the wild type *Pf* Pfn, this additional information also indicated that AAA Pfn is less capable in binding actin than QNQ Pfn.

3.3 Loop chimeras

As seen in Figure 26, the mean average and instantaneous speeds of *Pf* Pfn sporozoites were higher than the speeds of wild type sporozoites carrying *Pb* profilin. To find out more about the differences between these two proteins and to investigate the reason for this difference in speeds, we created a homology model of *Pb* profilin on the basis of the *Pf* profilin crystal structure (Kursula *et al.*, 2008a) and aligned them (Figure 28).

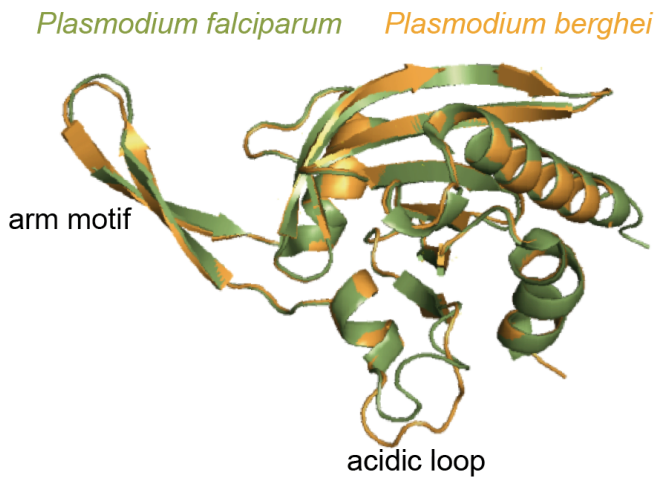

Figure 28: Alignment of the *P. falciparum* profilin crystal structure (green) with a *P. berghei* profilin homology model (yellow). The homology model was generated using the Phyre2 server (Protein Homology/AnalogY Recognition Engine). The β-hairpin (arm motif) on the left shows a high degree of structural conservation with only a slightly different orientation in the tip of the motif. Note the most divergent region: the acidic loop at the bottom of the overlaid structures.

This revealed that the orientation of the arm motif was the same but the most divergent region between the two proteins was the *Plasmodium*-specific acidic loop. The rest of the structures aligned almost perfectly. To probe the function of the loop, I created two chimeras using overlap extension PCR (2.5.2) where I changed the acidic loops in *Pf* and *Pb* profilin into their counterpart (*Pb* Pfn$^{Pf\ loop}$ and *Pf* Pfn$^{Pb\ loop}$). In addition, I generated a chimera based on *Pf* profilin containing the *Toxoplasma gondii* acidic loop (*Pf* Pfn$^{Tg\ loop}$). The acidic loop of *T. gondii* is very short (Figure 29B) and thus this mutant was thought to serve as a loop deletion control (Kucera *et al.*, 2010).

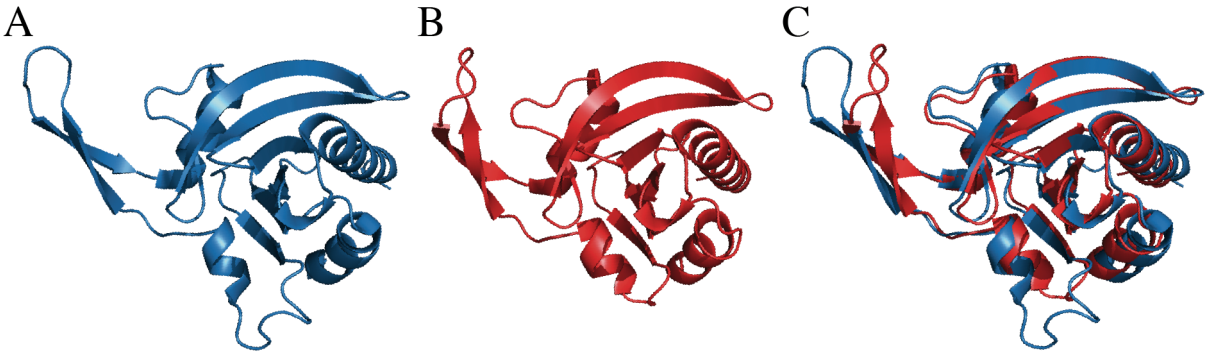

Figure 29: Crystal structures and alignment of *Plasmodium falciparum* and *Toxoplasma gondii* profilin. (A) Crystal structure of *Plasmodium falciparum* profilin (PDB: 2JKF, (Kursula *et al.*, 2008a). (B) Crystal structure of *Toxoplasma gondii* profilin (PDB: 3NEC, (Kucera *et al.*, 2010). (C) Alignment of the two structures from A and B.

To minimize problems with protein folding, the length of the exchanged sequence was chosen according to the next conserved amino acid in the backbone (Figure 30). Thus, the exchanged sequence in *Pf* Pfn $^{Tg\ loop}$ is longer than for the other two loop chimeras.

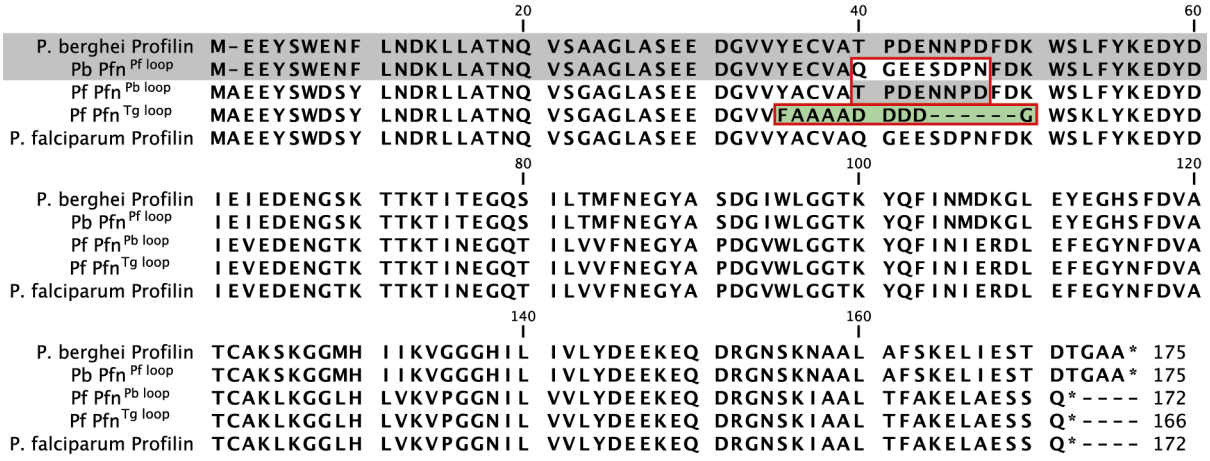

Figure 30: Alignment of *Plasmodium* profilins and chimeric mutants' amino acid sequences. Background colors indicate the species that the profilin sequence originates from: white – *P. falciparum*, grey – *P. berghei*, green – *T. gondii*. Mutations are highlighted with red boxes. *Plasmodium falciparum*-based sequences have a white background, *Plasmodium berghei* profilin a grey background. The lengths of the different sequences are indicated behind the last row. Sequences were aligned using CLC Main Workbench software version 5.1 (CLC bio).

3.3.1 Profilin loop chimeras behave similarly to their respective backgrounds in actin polymerization assays

I joined the lab of our collaboration partners in Oulu as a visiting scientist to perform polymerization assays for the loop chimeras. I inserted the loop chimeras into the pETM-11 vector for *in-vitro* protein expression (2.3.3) and performed these assays together with Bhargav Saligram Prabhakar.

Interestingly, *Pb* Pfn showed a different behavior than *Pf* Pfn (Figure 31A, B). In contrast to the polymerization assays of the tip mutants (Figure 22), due to time constrains the assays of the loop chimeras were only performed once. *Pf* Pfn behaved similarly as before (Figure 22) inhibiting polymerization in a concentration-dependent manner (Figure 31A). Strangely, there was a lag phase of 5 – 10 minutes before actin started to polymerize that had not been observed before (Figure 22). The same lag phase could be observed in the polymerization assay with *Pb* Pfn (Figure 31B). However, *Pb* Pfn had a much weaker effect on actin polymerization even at the highest concentration of 20 µM. Its monomer-sequestration ability was rather comparable with the QNQ Pfn or AAA Pfn (Figure 22B, C). Interestingly, the loop chimeras behaved similarly to the Pfn of their respective backbone (Figure 31C-E). The two chimeras based on *Pf* Pfn (*Pf* Pfn$^{Pb\ loop}$ and *Pf* Pfn$^{Tg\ loop}$) were weaker in sequestering actin

than *Pf* Pfn itself, indicating that the acidic loop somehow has an influence on actin binding even though it is located on the opposite side of the profilin-actin interface.

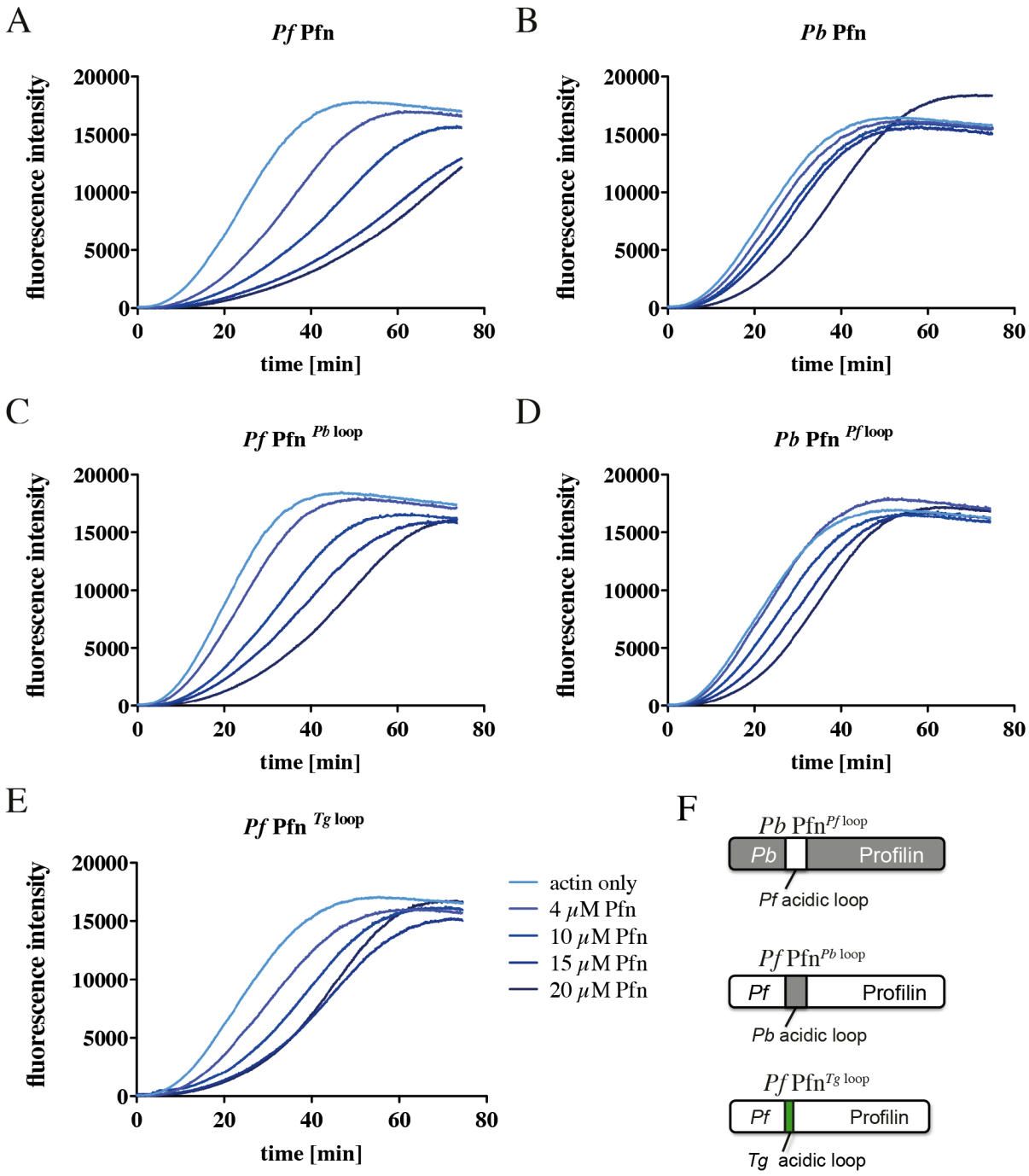

Figure 31: *In vitro* α-actin polymerization is influenced more strongly by *Pf* Pfn than by *Pb* Pfn and depends on the backbone of profilin. (A-E) α-actin isolated from pig muscle acetone powder containing 4 % of the α-actin labeled with pyrene was allowed to polymerize without or with increasing concentrations of *Pf* Pfn (A), *Pb* Pfn (B) or one of the loop chimeras *Pf* Pfn$^{Pb\ loop}$ (C), *Pb* Pfn$^{Pf\ loop}$ (D) and *Pf* Pfn$^{Tg\ loop}$ (E). The graphs of the mutants are displayed below their respective backgrounds. Legend with profilin concentrations is shown in panel E. This data was acquired together with Bhargav Saligram Prabhakar in the group of Inari Kursula. (F) Layout cartoon of loop chimeras. Colors represent the origin of the sequences: grey – *P. berghei*; white – *P. falciparum*; green – *T. gondii*.

3.3.2 Parasites carrying loop chimeras are able to complete the life cycle

As before, I replaced profilin in *P. berghei* parasites (Figure 32A) with the above-described profilin chimeras (see 2.6 for methods and vectors). I checked the 5' integration using *Pf* profilin or *Pb* profilin-specific primers (Figure 32B, C; fragment 1c) and 3' integration amplifying the *Toxoplasma gondii* DHFR (fragment 2). In addition we showed the absence of the wild type profilin gene or its introns (Figure 32C, fragment 3). As a result, the profilin gene was replaced with the respective mutant versions resulting in the desired transgenic parasite lines.

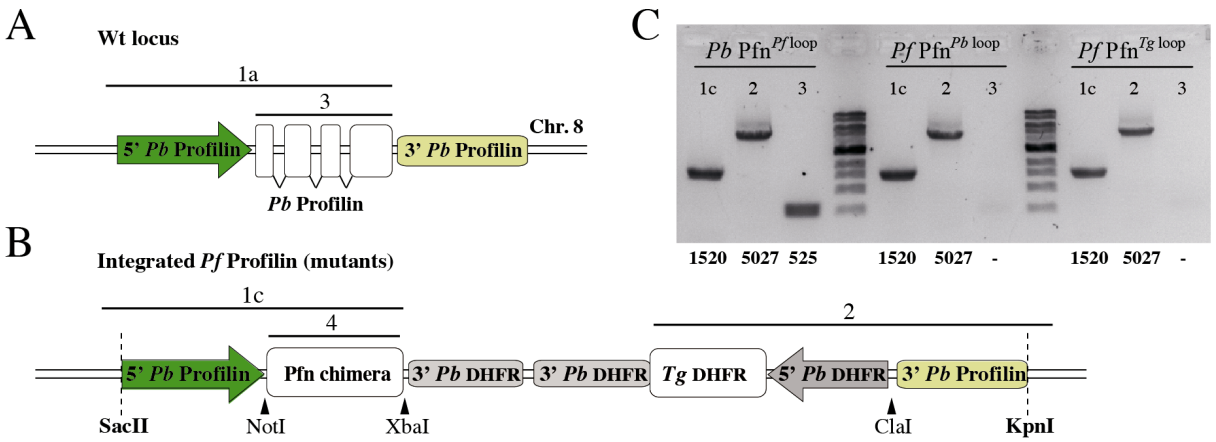

Figure 32: Genomic layout after integration of profilin chimeras. (A) Wild type profilin locus. (B) Profilin locus after integration. Key restriction enzymes for cloning and their cutting sites are indicated with black arrowheads. Enzymes for and locations of vector linearization are indicated by vertical dashed lines. (C) Integration PCR fragments as indicated with black bars and numbers in A and B. As *Pb* Pfn$^{Pf\,loop}$ is based on the wild type backbone it is amplified as fragment three, but lacks introns and is thus smaller (525 bases) than wild type profilin (1210), showing successful replacement. Expected fragment sizes are shown below their corresponding lane. Wild type controls for *Pb* Pfn and *Pf* Pfn can be found in Figure 16.

In contrast to the tip mutants, life cycle progression in the loop chimeras differed more from each other and from their respective controls (Table 6). Especially, the 'loop deletion' *Pf* Pfn $^{Tg\,loop}$ differed a lot with respect to its multiplication rate. The other two loop chimeras seemed to behave very similarly to their respective backbone profilins. *Pb* Pfn $^{Pf\,loop}$ had a multiplication rate of 8.4, very similar to the *Pb* Pfn with a growth rate of 8.9. On the other hand, *Pf* Pfn $^{Pb\,loop}$ with a growth rate of 10.8 behaved almost like its control *Pf* Pfn with a rate of 10.5. However, *Pf* Pfn $^{Tg\,loop}$ parasites multiplied far slower with a rate of only 7.7. The infection rates and oocyst numbers of the loop chimeras were comparable, within the normal range of biological variation and only slightly different from their respective controls. The number of salivary gland sporozoites of all three loop chimeras were comparable and as expected from clonal lines.

Table 6: Development of parasites expressing profilin chimeras in mice and mosquitoes.

Parasite line	Blood stage growth rate (median)	Mosquito infection rate	Oocysts / iMG (mean)	MG spz / mosquito (mean)	SG spz / mosquito (mean)	Prepatency [d] (mean)	Parasitemia d6 [%] (mean)	C57BL/6 mice
Pb Wt	8.9	50	105	39 000	9 400	3.75	2.3 ± 0.4	4
Pb Pfn $^{Pf\,loop}$	8.4	33	90	23 000	5 000	3.75	1.9 ± 0.5	4
Pf Pfn $^{Pb\,loop}$	10.8	25	75	19 000	4 600	4.5	0.8 ± 0.3	4
Pf Pfn $^{Tg\,loop}$	7.7	25	100	22 000	3 800	4.83	0.7 ± 0.1	6
Pf Pfn	10.5	33	75	36 000	4 300	4	1.7 ± 0.8	4

Analysis of parasite lines expressing different mutant profilins. Blood stage growth rates were determined after injecting either 100 or 5000 iRBCs IV into four C57BL/6 mice respectively (see 2.8.1). Infection rates of mosquitoes were established by checking mosquito midguts for oocysts between day 17 and 25. Oocyst numbers were obtained by counting the cysts of at least 50 infected mosquito midguts (MG) on day 12 (see 2.7.3). MG and salivary gland (SG) sporozoite (spz) numbers were counted between days 17 and 25 (2.7.4). At least three different cages of each parasite line were assessed. Parasitemia on day 6 and prepatency (first day of detectable blood-stage infection) were determined for each line. Either four or six C57BL/6 mice were bitten by five to ten infected mosquitoes (see 2.8.2).

The number of midgut sporozoites was lower compared to controls but still within a normal range. Also, salivary gland sporozoite numbers were lower than wild type but not drastically reduced within the replacements. The prepatency and parasitemia on day 6 was normal for the *Pb* Pfn$^{Pf\,loop}$ but not for the two chimeras based on the *Pf* Pfn backbone. In *Pf* Pfn$^{Pb\,loop}$ and *Pf* Pfn$^{Tg\,loop}$ parasites, prepatency was delayed and parasitemia reduced to below 1 %.

3.3.3 Loop chimeras display slower sporozoite speeds

I then investigated sporozoites expressing the profilin chimeras in terms of gliding motility. I compared these chimeras to sporozoites expressing the profilin version of their respective backbone (Figure 30). All three chimeric sporozoite lines had lower average speeds than their respective controls (Figure 33A). Wild type sporozoites that moved with 1.6 µm/s served as a control for *Pb* Pfn$^{Pf\,loop}$ sporozoites that moved with an average of 1.0 µm/s. *Pf* Pfn sporozoites that moved with a speed of 2.3 µm/s, served as a control for both *Pf* Pfn$^{Pb\,loop}$ and *Pf* Pfn$^{Tg\,loop}$ that moved with 1.4 µm/s and 1.3 µm/s respectively. Interestingly, the two lines based on the *Pf* Pfn backbone, *Pf* Pfn$^{Pb\,loop}$ and *Pf* Pfn$^{Tg\,loop}$ displayed very similar speeds, suggesting a backbone-determined behavior of profilin. However, all three chimeras moved significantly slower than their controls, implicating a role for the acidic loop in gliding motility. As for the tip mutants, single speeds of the chimeric sporozoites had similar medians as the average speeds (Figure 33B).

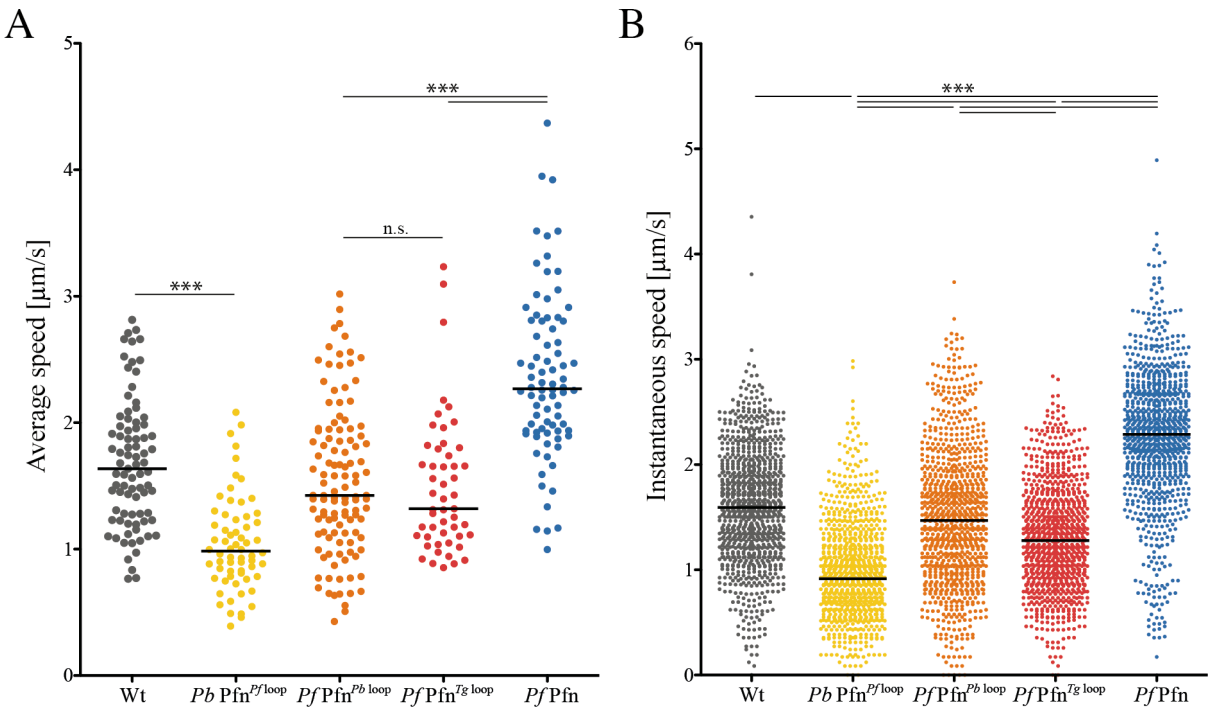

Figure 33 Profilin loop chimeras reduce sporozoite speed. Differences were analyzed using a Kruskal-Wallis test. The black lines indicate the median. (A) Average speeds of at least 40 sporozoites persistently moving between 150-300 s. Data was acquired using the ImageJ plug-in 'manual tracking' that provided the instantaneous speeds (from one frame to the next = 3 s). From these values the average speeds were calculated. (B) Instantaneous speeds from 10 sporozoites closest to their respective median in A.

Even though *Pb* Pfn$^{Pf\,loop}$ sporozoites displayed very similar average speeds as AAA Pfn or Δ arm Pfn sporozoites their instantaneous speeds differed. In contrast to AAA Pfn and Δ arm Pfn the instantaneous speeds of *Pb* Pfn$^{Pf\,loop}$ tapered at both ends. *Pb* Pfn$^{Pf\,loop}$ sporozoites did also not display the small number of high speeds (up to 6 µm/s) that were observed in AAA Pfn and Δ arm Pfn sporozoites. The median instantaneous speed of *Pb* Pfn$^{Pf\,loop}$ sporozoites was 0.9 µm/s. Also for *Pf* Pfn$^{Pb\,loop}$ and *Pf* Pfn$^{Tg\,loop}$ instantaneous speeds – their medians were 1.5 µm/s and 1.3 µm/s respectively – tapered at both ends of the bar generated by 900-1000 values.

3.4 Sporozoites carrying mutant profilins are weaker than wild type but show enhanced retrograde flow speed

In addition to motility, we also measured the sporozoites' capability to overcome forces during gliding motility. We employed a self-built setup of holographic optical tweezers in order to further characterize the profilin mutants (Quadt *et al.*, 2016). Optical tweezers are a tool to capture and move microscopic objects like microspheres through a highly focused laser beam.

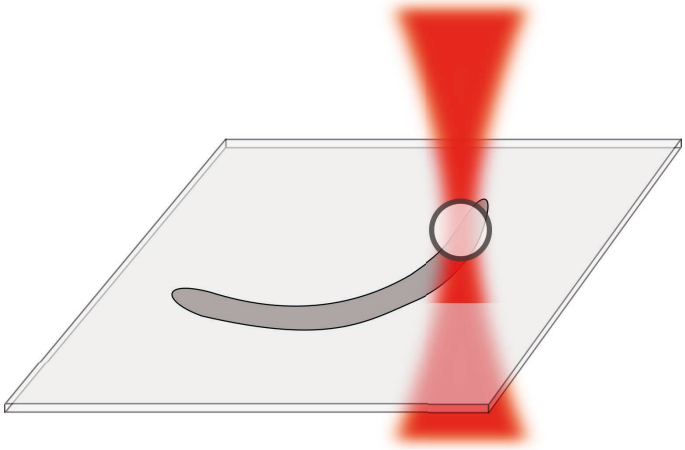

Figure 34: Cartoon of a bead caught in the focus of the laser trap. The bead is being deposited onto the front end of a sporozoite moving on glass.

We used the setup to conduct two types of experiments: First, beads were positioned on top of moving sporozoites that were consequently transported rearwards by the parasite. Transport speed profiles of representative sporozoites from wild type, *Pf* Pfn, QNQ Pfn and AAA Pfn are displayed in Figure 35A. The speed of this retrograde flow was tracked automatically and the speed peaks compared between parasite lines (Figure 35B). In the second assay, beads were held with defined forces and deposited on top of moving sporozoites. We observed and recorded whether the sporozoites could actively pull the bead out of the trap at the tested forces (Figure 35C). For more details on these experiments see section 2.10.3.

In both laser tweezer experiments, wild type sporozoites and *Pf* Pfn sporozoites showed almost identical behavior, similarly as in gliding motility. The speed of retrograde flow in wild type sporozoites was between 5.9 and 7.4 μm/s (Figure 35B). *Pf* Pfn sporozoites showed very similar retrograde flow speeds between 5.4 and 6.7 μm/s (Figure 35B). As a reference, I included the values of wild type sporozoites in the presence of 50 nM Jasplakinolide (black dashed line) or Cytochalasin D (white dashed line) for both types of experiments (Figure 35B, C) (Quadt *et al.*, 2016). In the second type of experiments at 70 pN, 74 % of wild type and 71 % of *Pf* Pfn sporozoites managed to pull the bead from the trap. At 130 pN, 38 % of wild type and 32 % of *Pf* Pfn sporozoites were able to displace the bead from the optical trap (Figure 35C).

Sporozoites carrying tip mutants or the arm deletion clearly behaved differently: QNQ Pfn sporozoites displayed peak transport speeds between 7.2 and 10.9 μm/s, AAA Pfn sporozoites between 6.4 and 9.8 μm/s and Δ arm Pfn between 7.6 and 10.9 μm/s (Figure 35B). At 70 pN, 26 % of QNQ Pfn, 32 % of AAA Pfn and 39 % of Δ arm Pfn sporozoites were able to pull beads from the trap. At 130 pN, this was reduced to 5 %, 12 % and 16 % respectively (Figure 35C).

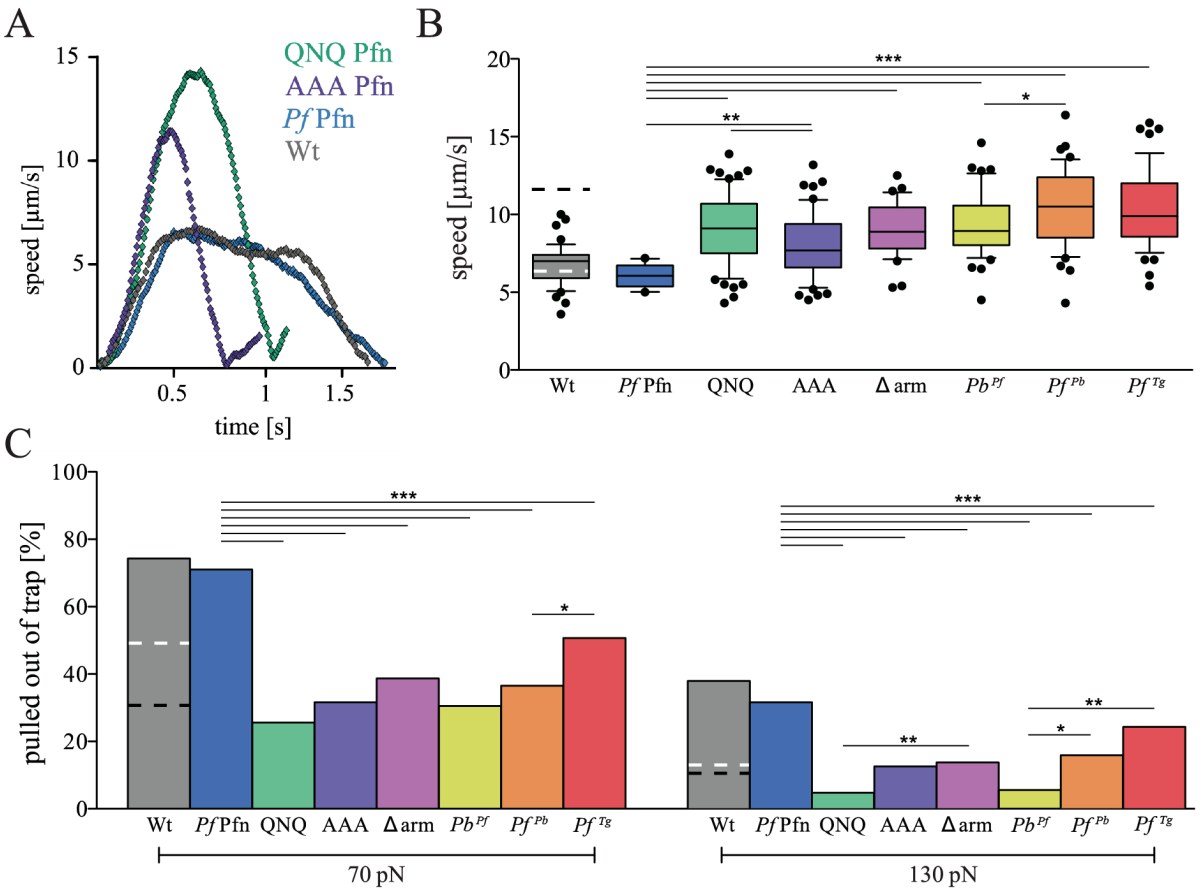

Figure 35: Sporozoites carrying mutations in the profilin gene are weaker than wild type sporozoites and show increased retrograde flow rates. (A) Exemplary speed progression plots of beads being translocated by sporozoites. Colors of the curves correspond to the indicated parasite line (top right). (B) Peak speeds of beads being translocated rearwards by sporozoites carrying different profilin mutations. The boxes contain 50 % of the values, 15 % are displayed on each whisker and another 10 % on each side are depicted as dots. The black lines indicate the median. Dashed lines in the grey bars represent wild type sporozoites with 50 nM of either Cytochalasin D (white) or Jasplakinolide (black). (C) Percentages of sporozoites carrying different profilin mutations that were able to actively pull beads from laser traps 70 or 130 pN strong. Statistics were determined with Fischer's exact test. Dashed lines in the grey bars represent wild type sporozoites with 50 nM of either Cytochalasin D (white) or Jasplakinolide (black) (Quadt *et al.*, 2016). Numbers of sporozoites probed in B and C are shown in Table 7.

Sporozoites carrying profilin loop chimeras behaved similarly to the tip mutants: the peak transport speeds of beads being moved to the rear of sporozoites from *Pb* Pfn$^{Pf\,\mathrm{loop}}$, *Pf* Pfn$^{Pb\,\mathrm{loop}}$ and *Pf* Pfn$^{Tg\,\mathrm{loop}}$ were also elevated compared to wild type and *Pf* Pfn: *Pb* Pfn$^{Pf\,\mathrm{loop}}$ transport speeds were between 7.8 and 11.2 µm/s, *Pf* Pfn$^{Pb\,\mathrm{loop}}$ transport speeds between 8.0

and 12.6 µm/s and *Pf* Pfn$^{Tg\ loop}$ transport speeds between 8.2 and 12.5 µm/s (Figure 35B). At 70 pN, 31 % of *Pb* Pfn$^{Pf\ loop}$ sporozoites, 37 % of *Pf* Pfn$^{Pb\ loop}$ sporozoites and 51 % of *Pf* Pfn$^{Tg\ loop}$ sporozoites displaced the bead from the trap. This was reduced to 13 %, 16 % and 24 % respectively, when the force of the trap was set to 130 pN (Figure 35C). Intriguingly, the behavior of all sporozoites carrying mutant versions of profilin was rather similar: Faster retrograde flow and lower forces, no matter the exact nature of the mutation. Moreover, this seemed to mimic the behavior of wild type sporozoites in the presence of Jas (Quadt *et al*., 2016).

The numbers of sporozoites that were investigated in the two different experiments are listed in Table 7.

Table 7: Number of parasites probed in different experiments with laser tweezer setup

Parasite line **Experiment**	**Wild type**	***Pf* Pfn**	**QNQ Pfn**	**AAA Pfn**	**Δ arm Pfn**	***Pb* Pfn *Pf* loop**	***Pf* Pfn *Pb* loop**	***Pf* Pfn *Tg* loop**
Retrograde flow	47	10	63	51	33	44	47	48
Force 70 pN	214	59	112	79	79	89	74	69
Force 130 pN	208	67	98	72	88	54	86	76

3.5 Δ arm Pfn sporozoite infections can convey protective immunity in mice

3.5.1 Outcome of Δ arm Pfn infections differs depending on the infection route

During assessment of parasite blood stage growth rates (2.8.1, Table 5), all parasite lines behaved very similarly. The only apparent difference was the lower multiplication rate of Δ arm Pfn (6.5) compared to the QNQ and AAA Pfn mutants (~9.3, Table 5). All C57BL/6 mice that were infected with 100 or 5000 infected red blood cells (iRBCs) of Δ arm Pfn died of ECM (experimental cerebral malaria) around day 8 or 6 respectively. Mice that had been infected with 100 Δ arm Pfn iRBCs died at unusually low parasitemias below 2 %.

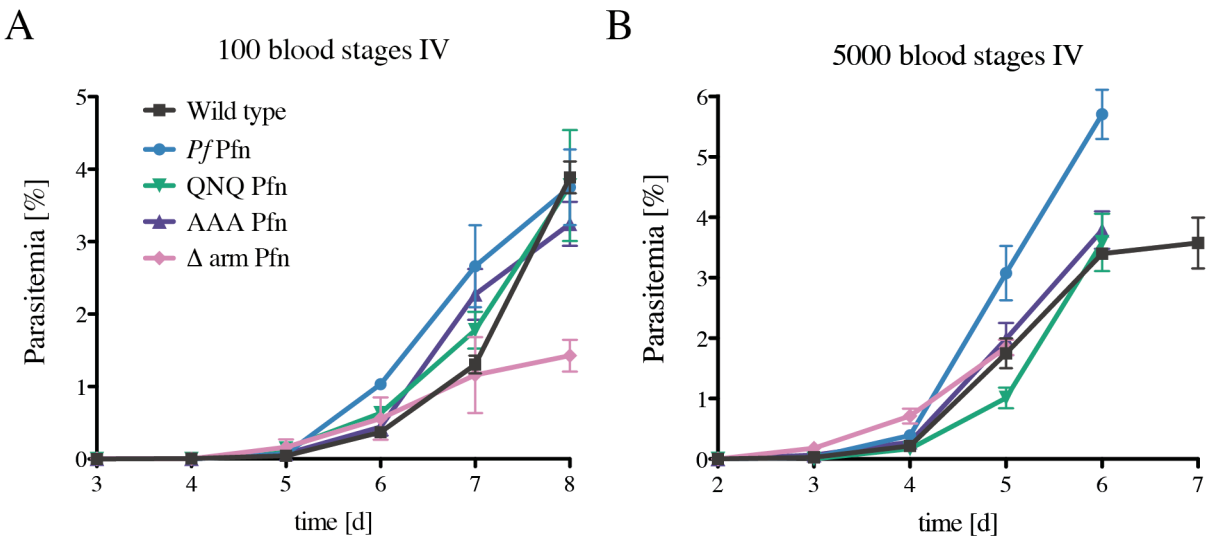

Figure 36: Progression of parasitemia of iRBC-induced infection is similar in all parasites carrying the different tip mutants or the arm deletion. For each parasite line, four C57BL/6 mice were injected intravenously with (A) 100 or (B) 5000 iRBCs and monitored for their parasitemia by daily blood smears. All of these mice died around day 8 (100 iRBCs) or day 6 (5000 iRBCs).

Similarly, all C57BL/6 mice infected with sporozoites through bites of wild type-, *Pf* Pfn-, QNQ Pfn- or AAA Pfn-infected mosquitoes died around day 9 (Figure 37A, B). In contrast to this, only 50 % of C57BL/6 mice infected with Δ arm Pfn sporozoites died due to ECM, while the other 50 % survived the infection. They reached parasitemias of up to 35 % but were able to permanently clear parasites from their blood (Figure 37C). The experiment was repeated three times, with similar results. Due to the low infection rate of only 1 in 6 mosquitoes being infected with Δ arm Pfn (Table 5), the bite back experiments were rather unreliable to infect all mice properly (although this was exploited for challenging the mice later as mice that had remained negative provided naïve controls that were of the same age (Figure 40)). Thus, I changed from infections by bite to IV injections of 100 Δ arm Pfn sporozoites, which also yielded the same result of 50 % of mice being able to clear the infection. To investigate

whether the parasites being cleared were still viable or incapable of establishing infections, I transferred iRBCs from mice that were close to clearing their sporozoite-induced Δ arm Pfn infection into three naïve C57BL/6 mice. One mouse received 5000 iRBCs and two mice received 100 iRBCs IV. All three mice that had received the transfer of almost-cleared iRBCs died of ECM on day 7 and day 10 respectively, showing that these parasites were generally viable, able to replicate and induce pathology (Figure 37D). It also suggested that immune factors are present in the sporozoite-infected mice that were not transferred.

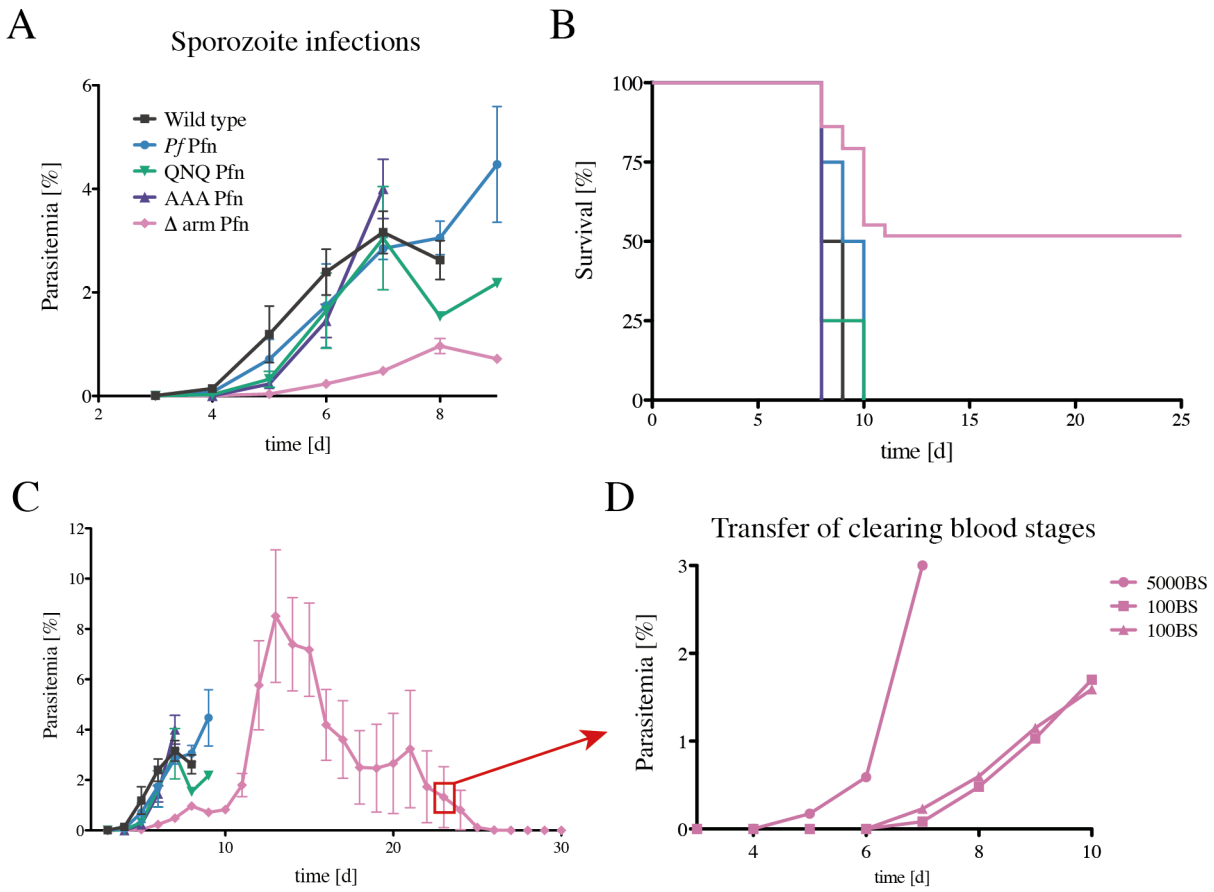

Figure 37: Progression of parasitemia of sporozoite-induced infection of C57BL/6 mice with Δ arm Pfn is unusual. (A) Summaries of parasitemia progression of C57BL/6 mice during the first 9 days after sporozoite infection (by bite and 100 sporozoite injected IV). For Δ arm Pfn, the curves represent a total of 26 mice, whereas in all other groups 4 mice were infected. (B) Survival of C57BL/6 mice from A. Note that 50 % of mice infected with Δ arm Pfn survive the infection. (C) Parasitemia progression of C57BL/6 mice up to 30 days after sporozoite infection. This represents a larger view of the same data as in A. (D) Transfer of iRBCs from Δ arm Pfn infected mice that were about to clear the infection into three naïve mice (red box in C). One mouse received 5000 and two mice received 100 blood stage parasites. All three mice died after blood stage transfer.

In a parallel set of experiments, I included early transfer timepoints. However, parasitemias on day 4-6 were too low to count so I transferred 150 μl of blood from mice infected with Δ arm Pfn sporozoites into naïve mice. I performed the late transfers in two ways: one was done as before, where I transferred 100 iRBCs in PBS from mice that were in the process of

clearing the Δ arm Pfn sporozoite infection. The second late transfer was done in the same way as the early transfer: I injected 150 μl of blood from mice just about to clear (approximately 3 % parasitemia). Interestingly, 9 out of 10 mice that had received transfers of 150 μl survived the infection and showed similar parasitemia progressions as mice that survived Δ arm Pfn sporozoite infections independently of the time of transfer. However, all mice that received 100 Δ arm Pfn iRBCs washed from plasma by diluting them in PBS died of ECM between day 10 and 14. This indicates that some factor(s) in the blood of mice experiencing a Δ arm Pfn sporozoite infection conferred protection against cerebral symptoms.

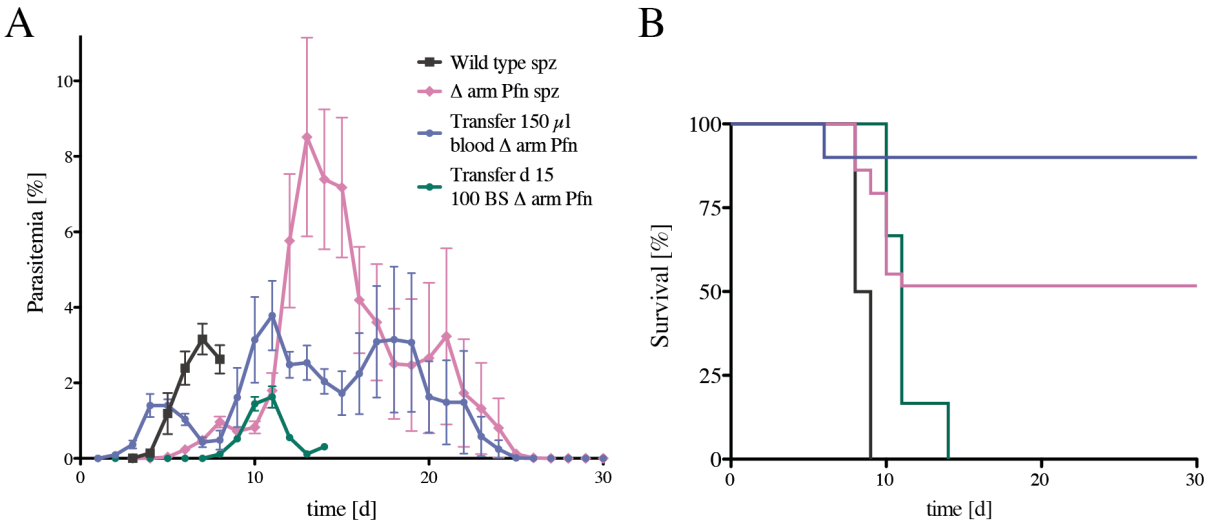

Figure 38: Progression of parasitemia after transfer of almost-cleared iRBCs depends on co- injection of undiluted blood. (A) Mice were infected with wild type sporozoites by bite. Δ arm Pfn infections were either done by bite or by injecting 100 sporozoites IV. Transfers of Δ arm Pfn iRBCs from mice that had almost cleared were done in two ways: First, 150 µl of infected blood was injected IV into naïve mice on days 4-6 (2 mice each) and day 15 (4 mice) these mice are summarized as 'Transfer 150 µl blood Δ arm Pfn' (violet curve); Second, on day 15, 100 iRBCs were injected IV into 6 naïve mice (including the 2 mice from Figure 37D) summarized as 'Transfer d 15 100 BS Δ arm Pfn'. (B) Survival plot of mice from A.

3.5.2 Outcome of Δ arm Pfn sporozoite infection depends on the mouse strain

As C57BL/6 mice succumb to symptoms of ECM (Huang *et al*., 2015) that result – at least in part – from the mice's own immune system, I then used BALB/c mice, known to develop and die of severe anemia or other symptoms such as multi-organ failure, but not ECM upon infection with *Plasmodium berghei* (de Kossodo & Grau, 1993). I infected BALB/c mice with wild type and Δ arm Pfn sporozoites and as expected, none of them developed ECM. The BALB/c mice infected with wild type *P. berghei* ANKA parasites died around day 30 with very high (85 – 98 %) parasitemias (Figure 39). Interestingly, all BALB/c mice infected with

Δ arm Pfn sporozoites recovered and cleared all iRBCs had a similar parasitemia progression as in the C57BL/6 mice. The BALB/c mice reached higher parasitemias than the C57BL/6 mice (up to 45 %). This clearly shows that the 50 % mortality rate of C57BL/6 mice was not caused by a parasite line-specific effect, but was likely caused by strong global inflammatory response.

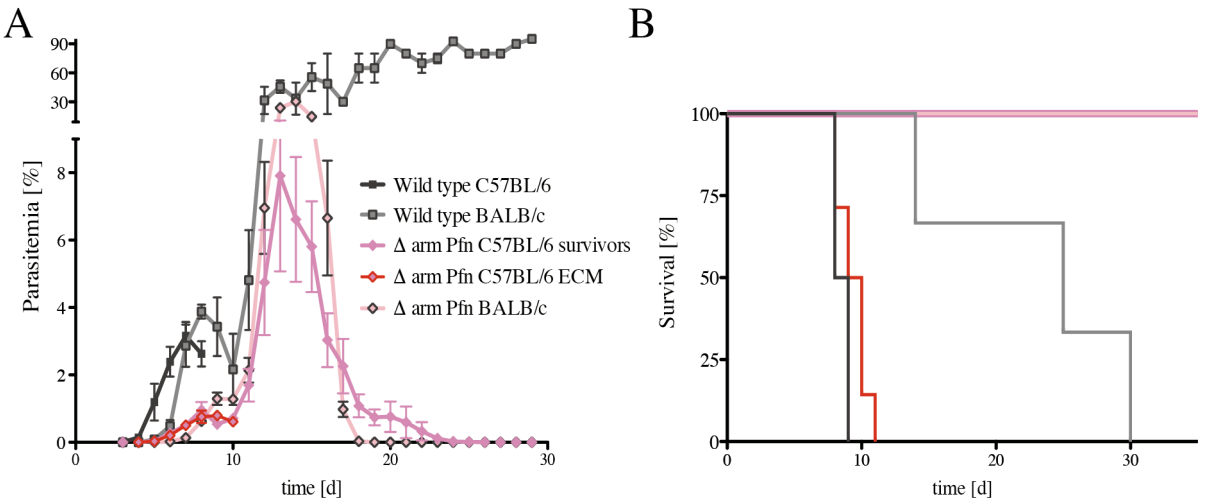

Figure 39: BALB/c mice are not killed by sporozoite-induced Δ arm Pfn infections. (A) Wild type and Δ arm Pfn sporozoites were used to infect BALB/c mice (n=12: 3 wild type and 9 Δ arm Pfn) that were monitored by daily blood smears and compared to infections in C57BL/6 mice. In this graph, mice infected with Δ arm Pfn that succumbed to ECM (red, n=13) and the ones that survived (pink, n=13) are displayed separately. (B) Survival plot of mice in A. Note that 100 % of BALB/c mice survived the infection with Δ arm Pfn sporozoites. Thickness of lines varies for optimal visibility.

3.5.3 Mice that survived Δ arm Pfn sporozoite infections are protected from homologous and heterologous challenges

In order to investigate whether the surviving mice were protected from subsequent infections, we challenged Δ arm Pfn-survivors from both the C57BL/6 and the BALB/c mice with either *P. berghei* ANKA or *P. yoelii* 17XL (lethal strain) iRBCs or *P. berghei* ANKA sporozoites (Table 8). The first exemplary challenge was performed six months after the initial infection with Δ arm Pfn sporozoites and is shown in Figure 40. During the initial infection, four mice had been infected with Δ arm Pfn sporozoites by mosquito bites. As infection rates were so low (17 %, Table 5) only two of these four mice were infected. Thus, the two mice that had not been infected provided naïve controls for the challenge with wild type sporozoites as all four mice were of the same age. As expected, the two previously naïve mice developed parasitemias of 4 and 13 % and died of ECM on day 8. The other two mice that had experienced and cleared the Δ arm Pfn sporozoite-induced infection developed much lower parasitemias of 1 - 1.6 % and cleared the infection by day 12 (Figure 40).

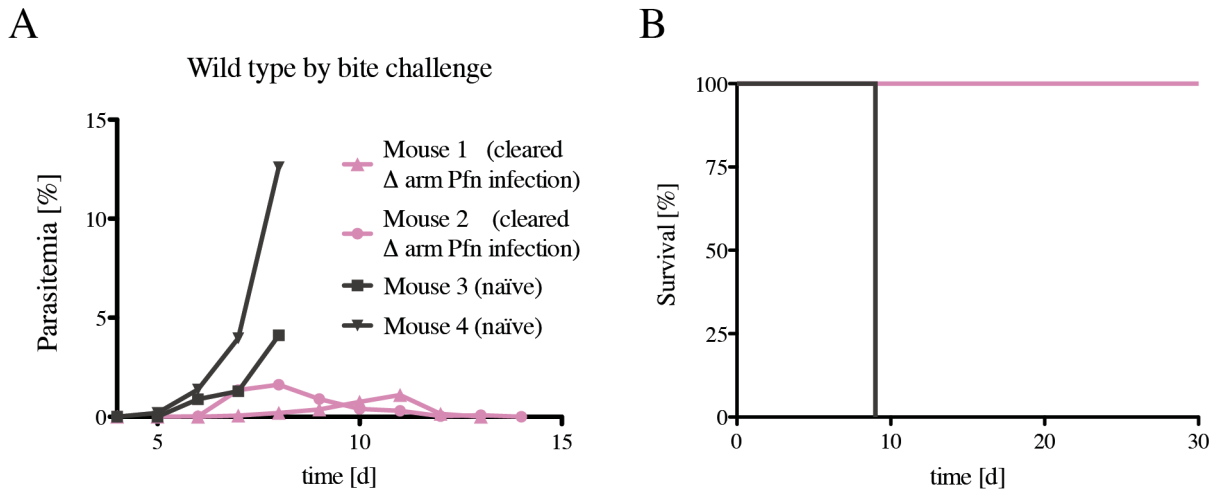

Figure 40: Mice are protected from severe disease after Δ arm Pfn infection. Four C57BL/6 mice from the same shipment and age – two had been infected with Δ arm Pfn, two had remained negative – were challenged with wild type sporozoites six months later. (A) Blood stage development of naïve and Δ arm Pfn-cleared mice. (B) Survival of the two naïve and two Δ arm Pfn-cleared mice from A.

In total, I challenged eight C57BL/6 and nine BALB/c survivor mice and all of them were protected from severe disease and able to resolve the infection (Table 8). Upon challenge, the C57BL/6 mice developed parasitemias between 0.07 and 4.73 % that was cleared within 1-2 weeks. Four out of nine challenged BALB/c mice did not develop microscopically detectable parasitemias. The remaining five BALB/c mice developed parasitemias between 0.6 and 6.1 % that was also cleared within 1-2 weeks. The initial challenge that was performed six months after the initial infection and all other challenges were performed after six weeks.

Table 8: Overview over mice challenged after cleared Δ arm Pfn infections.

Mouse strain	Time since clearance	Challenge	Prepatency	Max. parasitemia [%] (day)	Clearance
C57BL/6	6 months	*Pb*A sporozoites (by bite)	day 7	1.10 (day 11)	day 13
C57BL/6	6 months	*Pb*A sporozoites (by bite)	day 6	1.62 (day 8)	day 14
C57BL/6	6 weeks	*Pb*A sporozoites (by bite)	day 7	0.33 (day 10)	day 12
C57BL/6	6 weeks	*Pb*A sporozoites (by bite)	day 6	0.07 (day 6)	day 7
C57BL/6	6 weeks	*Pb*A 10,000 iRBCs IV	day 4	1.37 (day 7)	day 16
C57BL/6	6 weeks	*Pb*A 10,000 iRBCs IV	day 7	0.33 (day 8)	day 15
C57BL/6	6 weeks	Py 17XL 10,000 iRBCs IV	day 5	1.79 (day 7)	day 9
C57BL/6	6 weeks	Py 17XL 10,000 iRBCs IV	day 3	4.73 (day 5)	day 9
BALB/c	6 weeks	*Pb*A 100 sporozoites IV	-	0	-
BALB/c	6 weeks	*Pb*A 100 sporozoites IV	-	0	-
BALB/c	6 weeks	*Pb*A 100 sporozoites IV	-	0	-
BALB/c	6 weeks	*Pb*A 10,000 iRBCs IV	day 5	6.10 (day 9)	day 11
BALB/c	6 weeks	*Pb*A 10,000 iRBCs IV	day 5	3.40 (day 8)	day 11
BALB/c	6 weeks	*Pb*A 10,000 iRBCs IV	day 6	1.80 (day 10)	day 13
BALB/c	6 weeks	Py 17XL 10,000 iRBCs IV	day 4	0.60 (day 5)	day 6
BALB/c	6 weeks	Py 17XL 10,000 iRBCs IV	-	0	-
BALB/c	6 weeks	Py 17XL 10,000 iRBCs IV	day 4	1.60 (day 5)	day 7

3.6 Profilin Knockout (Pfn KO)

During the work of Kursula et al, profilin could not be knocked out (Kursula *et al.*, 2008a). I repeated the experiment three times using a replacement vector (Figure 12B) lacking the profilin gene but also failed to achieve a clonal parasite carrying a profilin knockout.

3.6.1 Profilin kockout was achieved with a *Plasmo*GEM vector

Recently, the Wellcome Trust Sanger Institute has created the *Plamodium* genetic modification project (*Plasmo*GEM) (Pfander *et al.*, 2011). They produced vectors targeting *P. berghei* genes to either knock them out or tag them and made these vectors available for research purposes free of charge. I used the profilin KO vector (2.6.2) and surprisingly, was able to achieve the knockout and a clonal line in the first attempt (Figure 41).

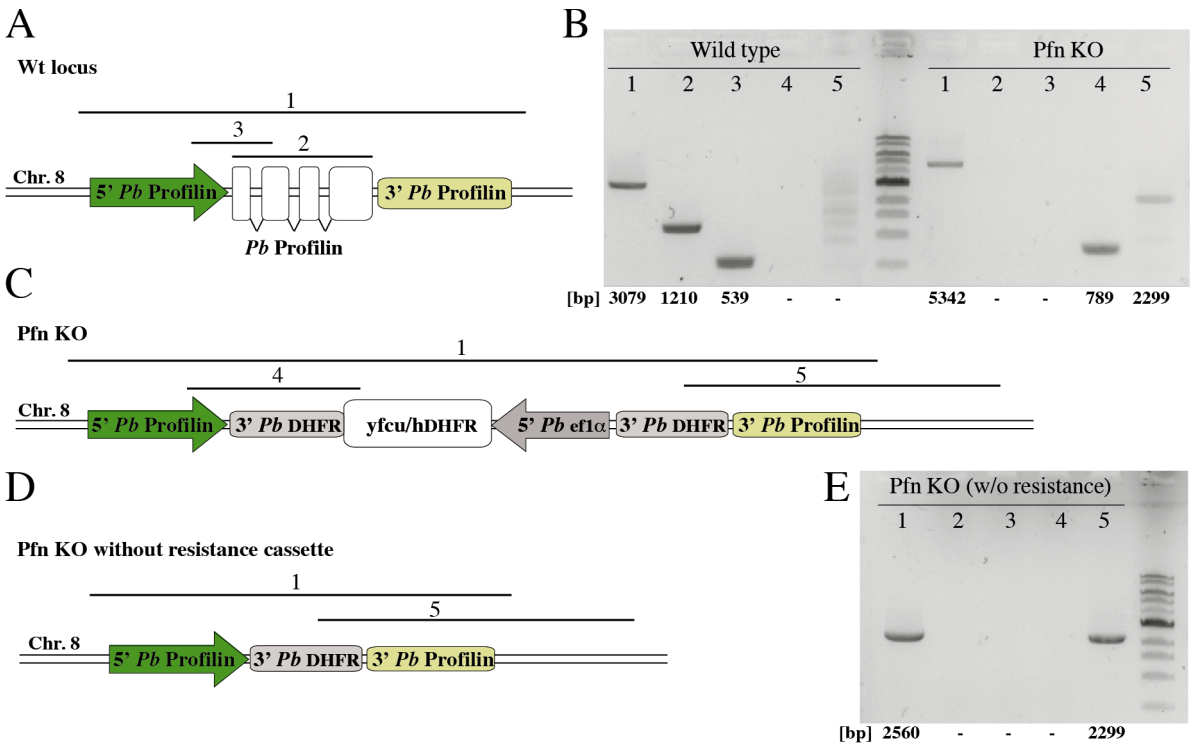

Figure 41: Genomic locus after knock out of *P. berghei* profilin. (A) Layout of the wild type profilin locus. (B) Integration PCR of wild type and Pfn KO parasite lines. Numbers on top of the lanes correspond to black bars indicated in A and C. Fragment 1 and 2 correspond to the previous PCRs (Figure 16) whereas PlasmoGEM had recommended primers for fragments 3-5. Note that fragment 1 is much longer in the Pfn KO than in the wild type. (C) Layout of the profilin locus after successful integration of the knock out vector. Note that the resistance cassette (yFCU/hDHFR) is flanked by two *Pb* DHFR 3'UTRs. (D) Layout of the Pfn KO locus after the resistance cassette was lost due to homologous recombination. (E) PCR of the Pfn KO after the loss of the resistance cassette (fragment 4, compare to B).

In addition to the genomic level, I looked for absence of profilin protein. First, we used an antibody from the Soldati-Favre group in Geneva we obtained as a kind gift. This antibody was reported to recognize *Pb* Pfn even though it was raised against *Pf* Pfn (Pino *et al.*, 2012). However, the antibody stained a myriad of bands possibly including the profilin band (Figure 42A). For generating this antibody, the Soldati group had used purified *Pf* Pfn including a His-tag. Thus, I raised an antibody (2.8.5) against *Pb* Pfn without a His-tag, which produced a much cleaner signal, despite two unspecific bands (Figure 42B).

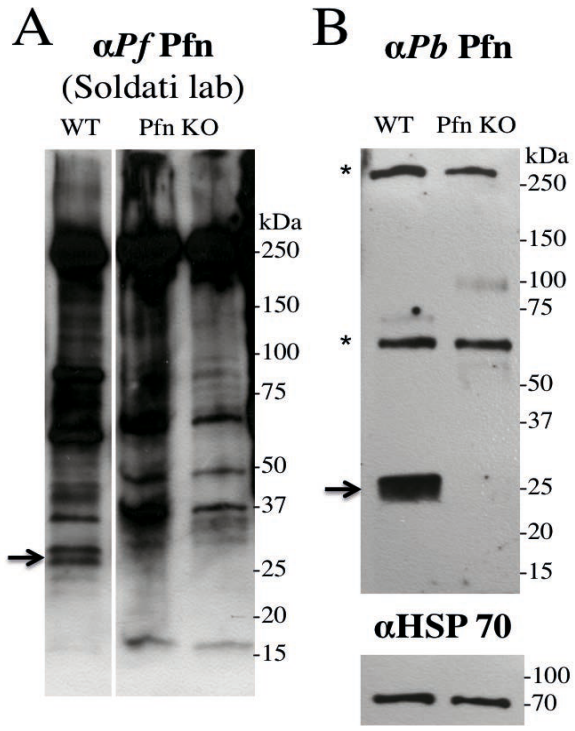

Figure 42: The Pfn KO lacks the profilin protein, showing a true knockout. Western blots of schizont cultures using two different αPfn antibodies. (A) Wild type and two different samples of Pfn KO blood stages were probed with an antibody raised against *P. falciparum* profilin. The arrow points to two bands that have a similar size and either of them could be profilin as both of them are lost in the Pfn KO samples. This antibody was obtained as a gift from the group of Dominique Soldati-Favre in Geneva. The protein used for immunization included the 6xHis-tag from purification. (B) Wild type and Pfn KO blood stages were probed with an antibody that we raised against *Pb* Pfn. We used purified *P. berghei* profilin and cleaved off the 6xHis-tag before raising the antibody. The arrow indicates the profilin band and the asterisks indicate unspecific bands. HSP70 was used as a loading control.

3.6.2 Outcome of infections with Pfn KO blood stage parasite is dose-dependent

During the linear phase of blood stage growth, the Pfn KO blood stage parasites had a very low median multiplication rate of 5.9, even lower than the growth rate of 6.5 in Δ arm Pfn blood stages. However, progression of blood stage infection and survival of the mice was found to be dose-dependent (Figure 43) and the majority of mice (3 out of 4) that had been infected with low doses (100 iRBCs) of Pfn KO iRBCs cleared the infection around day 23. The progression of parasitemia in these mice was almost identical to the progression in surviving mice infected with Δ arm Pfn sporozoites (Figure 37C). In contrast to this, mice that received high initial doses of Pfn KO iRBCs (5000) all died with unusually low levels of parasitemia. This turned infection of mosquito cages into a challenge. The first two attempts to infect mosquito cages failed to result in an infection.

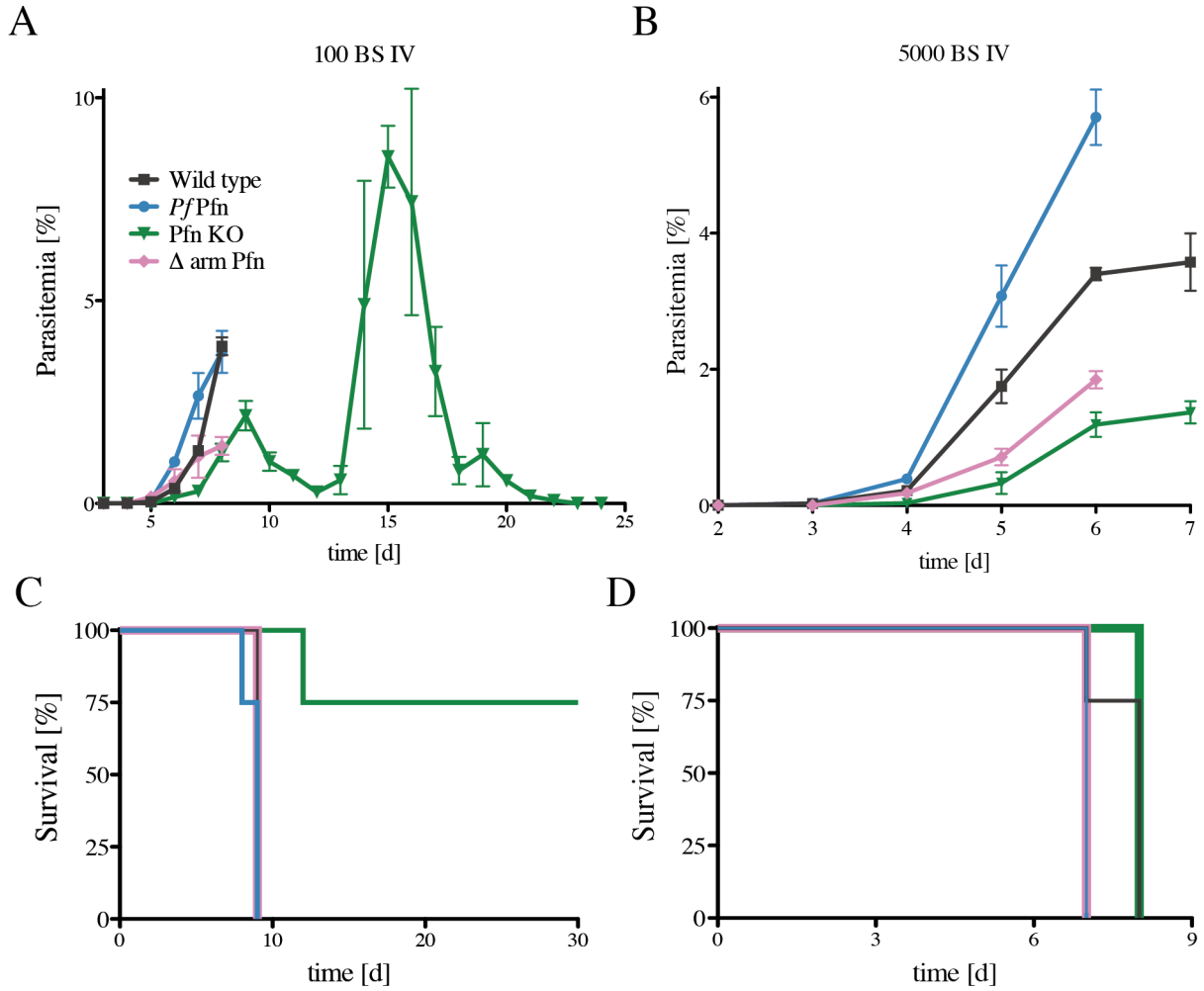

Figure 43: Blood stage growth of Pfn KO parasites is dose dependent. (A) 100 wild type, *Pf* Pfn, Δ arm Pfn and Pfn KO iRBCs were injected into 4 C57BL/6 mice each and their parasitemia was monitored daily. Note that Pfn KO parasites clear from the blood stream. (B) 5000 wild type, *Pf* Pfn, Δ arm Pfn and Pfn KO iRBCs were injected into 4 C57BL/6 mice each and their parasitemia was monitored daily. Note that with this higher dose, Pfn KO parasites (in contrast to A) were not cleared from the blood stream. (C) Survival of mice from A. Note the survival of 3 out of 4 mice that had received 100 Pfn KO iRBCs. (D) Survival of mice from B. Note that for these 5000 iRBCs IV injections none of the mice survived. Lines vary in thickness for optimal visibility.

3.6.3 Pfn KO ookinetes move very slowly and lack intact crystalloid bodies

To pinpoint the problem with infections, we first investigated whether the Pfn KO was able to produce ookinetes. Indeed, Pfn KO ookinetes were formed with normal conversion rates and we were able to observe and track ookinetes (Figure 44). Interestingly, their speed was drastically reduced compared to wild type ookinetes. Additionally, we observed a morphological change in the Pfn KO ookinetes. In wild type ookinetes black vesicles that probably contain hemozoin crystals are highly abundant and are usually distributed throughout the cell. They move around quickly and continuously. In the Pfn KO ookinetes, these vesicles are accumulated at the back and hardly show any movement. Additionally, a

strange cone-shaped structure was visible at their front end (Figure 44C, white arrows and dashed circle).

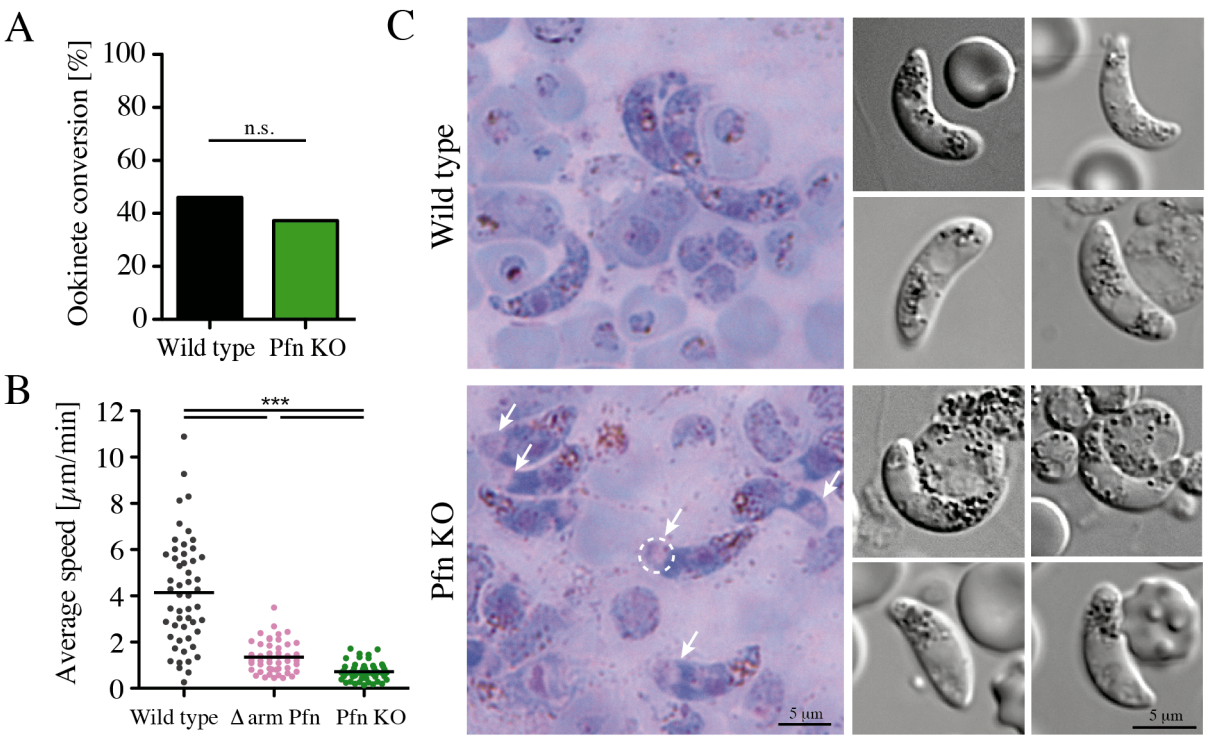

Figure 44: Pfn KO ookinetes are very slow and show an altered morphology. (A) Macrogamete to ookinete conversion was assessed for wild type and Pfn KO. Significance was tested using Fisher's exact test. (B) Wild type, Δ arm Pfn and Pfn KO ookinetes were tracked and their average speeds were calculated. Black lines indicate the median. Significance was tested with a Kruskal-Wallis test. (C) Morphology of wild type and Pfn KO ookinetes in Giemsa-stainings (left) and DIC images (right). In the Pfn KO black vesicles accumulate at the rear end of the cell. The unknown structure appearing at the front end is indicated with a circle and white arrows.

It has been reported that hemozoin-containing vesicles usually cluster around crystalloid bodies, ookinete specific organelles made of a large number of vesicles clustered together in a regular arrangement (Carter *et al.*, 2008, Lemgruber & Lupetti, 2012). As localization of the hemozoin-containing vesicles was altered in Pfn KO ookinetes, we hypothesized that there might be a problem with crystalloid bodies. To monitor crystalloid body integrity in the Pfn KO, I introduced a GFP-tag in a protein (DHHC10) that was recently shown to localize to the two distinct crystalloid bodies in *P. berghei* ookinetes (Santos *et al.*, 2016). The DHHC10-GFP vector was a kind gift from Gunnar Mair. Unfortunately, the integration PCR failed to work even after several attempts at troubleshooting. However, we were able to detect green fluorescence, thus indirectly verifying integration in a proportion of parasites. This was sufficient to localize DHHC10-GFP-positive Pfn KO ookinetes (Figure 45). Interestingly, in the Pfn KO DHHC10 was distributed throughout the cell, with several small bright dots at the rear of the cell, indicating loss of crystalloid body integrity. These smaller accumulations

have also been observed during ookinete development and have been suggested to fuse together to form the crystalloid body (Raine *et al.*, 2007, Saeed *et al.*, 2015). The presence of these small accumulations of DHHC10-GFP in otherwise fully formed ookinetes might hint towards a problem with late stages of crystalloid body formation. In addition to these small concentrations of DHHC10-GFP, a larger accumulation at the front end of the ookinete appeared that was not present in the wild type.

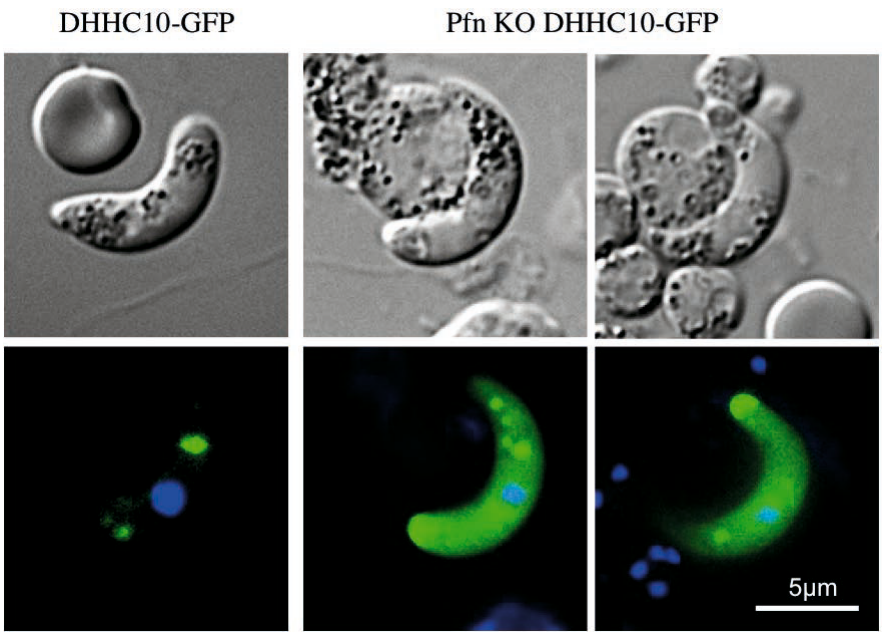

Figure 45: Integrity of crystalloid bodies is compromised in Pfn KO ookinetes. DHHC10-GFP was used as a marker for crystalloid bodies (left). DHHC10 localizes to two dots in normal ookinetes. DHHC10-GFP in the Pfn KO (middle and right) was found in the cytoplasm, at the front of the ookinetes and in small dots throughout the cells. Top row: DIC images; bottom row: merge of GFP-fluorescence (green) and Hoechst staining (blue).

3.6.4 Infection of mosquitoes with Pfn KO is possible

As seen above, Pfn KO ookinetes still showed some remnants of crystalloid bodies, making mosquito infections theoretically possible. To overcome the low multiplication rates and early deaths of the mice infected with Pfn KO parasites, we treated mice with phenylhydrazine prior to infection in order to increase parasitemia and gametocyte levels. Indeed, this led to infected mosquito midguts: we found a mean of 10 oocysts per infected midgut that contained individual nuclei indicating sporulation (Figure 46). We found an average of 160 midgut sporozoites per mosquito that is much lower than even Δ arm Pfn that had an average of 3400 midgut sporozoites per mosquito. However, we could not find sporozoites in the salivary glands, indicating that profilin is essential for sporozoites to reach the salivary glands.

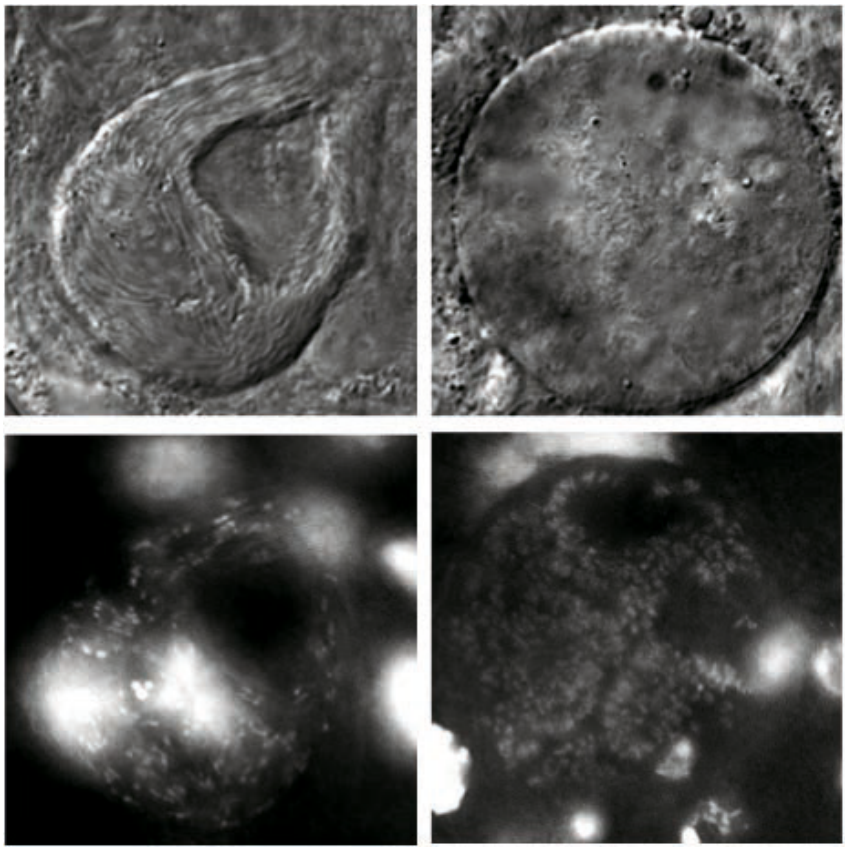

Figure 46: Sporulation occurs in Pfn KO oocysts. Pfn KO oocysts on day 10 post infection. The majority of oocysts was sporulated with visible individual sporozoites tightly packed (top left image). Even in oocysts where sporozoites were not (yet) visible, individual nuclei indicated partial sporulation. Top row: DIC images; bottom row: Hoechst staining.

4 Discussion

In the work leading up to this thesis, I set out to investigate the role of *Plasmodium* profilin in parasite motility. This important ABP is one of a very limited number of ABPs that have been identified in *Plasmodium* so far. However, this reduced pool of ABPs can still enable cell motility of up to 6 µm/s (Munter *et al.*, 2009, Quadt *et al.*, 2016). It might be possible that *Plasmodia* are capable of such high speeds BECAUSE they don't have too many ABPs competing for the regulation of actin. This could mean reduced complexity and thus an increased efficiency for motility.

Even though *Plasmodia* that contain around 5000 genes are less complex than mammalian cells (*e.g.* around 22,000 genes in humans) investigations of the apicomplexan motor machinery underlying gliding motility have only revealed small pieces of this puzzle.

4.1 Profilin is not essential in the blood stage

In contrast to previous reports that indicated that apicomplexan profilins are essential (Kursula *et al.*, 2008a), I was able to show that *Plasmodium berghei* profilin could be knocked out in the blood stage (Figure 41, Figure 42). However, I had also tried and failed three times to produce a knockout with traditional vector design, demonstrating the increased efficiency of recombination when using *Plasmo*GEM vectors that contain very long homology arms. Curiously, in the western blot stained with the α*Pf* Pfn antibody there were a lot of unspecific higher bands but it also showed two bands of the proper size (Figure 42). Both of these bands disappeared in the Pfn KO. When I employed the self-made antibody raised against *Pb* Pfn, only a single band was visible at the expected height. Even so, the band looked rather thick, indicating the possibility of profilin being post-translationally modified. There have been reports on calf profilin being phosphorylated at the C-terminal serine (Hansson *et al.*, 1988, Singh *et al.*, 1996) and plant profilin being phosphorylated at up to four tyrosine residues (Guillen *et al.*, 1999). There is conflicting evidence on whether phosphorylation of profilin enhances or reduces its affinity for actin and poly-L-proline (Krishnan & Moens, 2009). In mice, the penultimate tyrosine residue of profilin-1 (Y129) was reported to be phosphorylated. This phosphorylation was critical for wound-healing related angiogenesis (Fan *et al.*, 2012). *Plasmodium* profilin contains multiple tyrosine residues as well as serine residues at the C-terminus, so it could in principle be phosphorylated. However, although it is present in Apicomplexa, the penultimate tyrosine residue is not present in *Plasmodium* (Figure 8 and 8.3). Also, a recent phosphoproteomic screen did not find

phosphorylated profilin in schizonts, although the protein was found in the regular proteome (Ganter *et al.*, 2017).

Another possibility for the shift in size would be that the second band represents a different isoform of profilin. As only one profilin isoform has been identified at the genomic level, a second isoform could occur through differential splicing as reported for Mouse profilin 2 (Di Nardo *et al.*, 2000). A study in *P. falciparum* looked for alternatively spliced proteins and profilin was not among differentially spliced proteins (Sorber *et al.*, 2011). Thus, it is not very likely that profilin should be alternatively spliced to form an isoform with a slightly different size. There are no reports yet on any other post-translational modification like acetylation or ubiquitination of profilin, but it is in theory possible that this might have caused the second band. In any case, the antibody we raised against *Pb* Pfn resulted in less unspecific bands and stained only one profilin band. In light of this it is possible, that one of the two bands seen with the α*Pf* Pfn antibody is another unspecific band. To be able to say more, further experiments are needed to be sure whether profilin phosphorylation occurs in *Plasmodium*.

Although profilin was not essential in the blood stage, the multiplication rate in Pfn KO parasites was significantly reduced. This was confirmed by independent experiments at *Plasmo*GEM that showed a relative growth rate of 0.57 out of 1 (http://plasmogem.sanger.ac.uk/phenotypes). The low multiplication rate also explains why generating the knockout was not possible with traditional vectors: with lower transfections efficiency, a smaller proportion of parasites was transfected and probably lost as the untransfected wild type parasites multiplied much faster. This has been reported before in *P. berghei* blood stages where profilin had been knocked down (Pino *et al.*, 2012). This study found that merozoite invasion was reduced in profilin knockdown, possibly explaining the lower multiplication rate of Pfn KO blood stages.

4.2 Pfn KO parasites fail to produce salivary gland sporozoites

While salivary gland sporozoites are not present in the Pfn KO line, the Δ arm Pfn line is still able to produce mature and infectious salivary gland sporozoites (Table 5). This indicates that profilin's function is crucial at the mosquito stage. In contrast to the study of Pino *et al.* that reported a reduced capacity of Pfn knockdown parasites to transform into ookinetes (Pino *et al.*, 2012), we found no difference in ookinete conversion between wild type and Pfn KO parasites (Figure 44A). We could show that Pfn KO ookinetes have compromised crystalloid body integrity. The loss of crystalloid bodies impaired oocyst sporulation in some studies (Raine *et al.*, 2007, Saeed *et al.*, 2015) or showed a lack of sporozoites in the salivary glands

in other cases (Carter *et al.*, 2008, Ecker *et al.*, 2008, Pradel *et al.*, 2004). Similar to these latter studies, Pfn KO oocysts showed individual nuclei, and we observed fully formed midgut sporozoites, indicating successful sporulation (Figure 46). Future studies should be able to distinguish whether Pfn KO sporozoites are able to egress from the oocysts by assessing the presence and number of hemolymph sporozoites.

The reason why the Pfn KO parasite line does not produce salivary gland sporozoites could either be due to impaired crystalloid body formation and the already reported subsequent loss of salivary gland invasion (Carter *et al.*, 2008, Ecker *et al.*, 2008, Pradel *et al.*, 2004) or because profilin itself is essential for salivary gland invasion. A study by Sato *et al.* produced a *P. berghei* parasite line strongly overexpressing profilin that interestingly also failed to produce salivary gland sporozoites (Sato *et al.*, 2016). This indicates, that the amount of profilin is critical in parasites as too much profilin as well as its absence lead to similar results. A study involving a different G-actin sequestering protein of *Plasmodium*, called C-CAP (C-terminal domain of the cyclase associated protein), revealed that lack of this protein also led to decreased oocyst numbers (Hliscs *et al.*, 2010). In addition, sporogony was disrupted around day 7 of oocyst development. Also, actin depolymerization factor 2 (ADF2) was knocked out, likewise impairing the development of oocysts (Doi *et al.*, 2010). Another study showed, that *P. berghei* parasites lacking functional actin capping protein also produced slower ookinetes and sporozoites failed to invade salivary glands (Ganter *et al.*, 2009). These studies underline the importance of actin regulation in sporozoite development and salivary gland invasion. Taken together, even though we currently cannot tell whether the lack of salivary gland sporozoites is a profilin-specific consequence or due to the lack of intact crystalloid bodies it seems likely, that profilins influence on actin dynamics contributed at least in part to the phenotype.

4.3 Sporozoites carrying mutations in profilin have altered biochemical and biophysical properties

Whatever the reason for the lack of salivary gland sporozoites, without sporozoites we could not use the Pfn KO line for investigating gliding motility. Also the laser tweezer analysis required salivary gland sporozoites. However, we were able to investigate sporozoites carrying mutations in profilin that would still be able to complete the life cycle. We created two sets of mutants: the first set involved point mutations at and deletion of the arm motif and the second set was comprised of acidic loop chimeras of *Plasmodium* profilin.

4.3.1 Profilin tip mutants reveal that actin-binding of the arm motif is essential for normal gliding motility

The arm motif of *Plasmodium* profilin is present in many apicomplexan parasites (Kursula *et al*., 2008). I was able to find the arm motif in the two photosynthetic free-living algae called chromerids (Figure 8) that are closely related to Apicomplexa (Janouskovec *et al.*, 2013). Hence, the arm motif is probably present in all apicomplexans, as chromerids have likely provided the genetic blueprint for the whole phylum (Woo *et al.*, 2015).

The fact, that the arm motif is still conserved in all these species underlines its importance for actin dynamics in these parasites. We were able to show that the tip of the arm motif in *Plasmodium* is critically involved in actin binding. Biochemically (Figure 22), biophysically (Figure 35) and by computational simulations (Figure 27), even small changes in profilin lead to a visible impact on actin binding or the strength of sporozoites. In polymerization assays, both QNQ Pfn and AAA Pfn did not sequester actin as efficiently as the wildtype (Figure 22), the laser tweezer analysis revealed that sporozoites from both mutants were weaker than wildtype sporozoites and molecular dynamics simulations revealed the loss of the E_{66}^{Pfn} – R_{291}^{Act} salt bridge in the mutants and thus a weaker binding energy.

Interestingly, *in vivo* analysis showed that QNQ Pfn ookinetes and sporozoites are still able to glide like wild type *Pf* Pfn sporozoites whereas AAA Pfn ookinetes and sporozoites moved significantly slower (Figure 24, Figure 26). Also, AAA Pfn sporozoites were drastically reduced in both the number of gliding sporozoites and the quality of their gliding motility as their trajectories much more edgy than in *Pf* Pfn or QNQ Pfn sporozoites (Figure 25). This was unexpected as QNQ Pfn and AAA Pfn had behaved similarly in all other assays.

We hypothesize that this discrepancy is a result of the complete loss of interaction of the AAA arm motif with actin. Without hydrogen bonds at the tip of the arm, even the arm-neighboring interactions that remain largely unchanged in the AAA mutant are not enough to stabilize the arm motif.

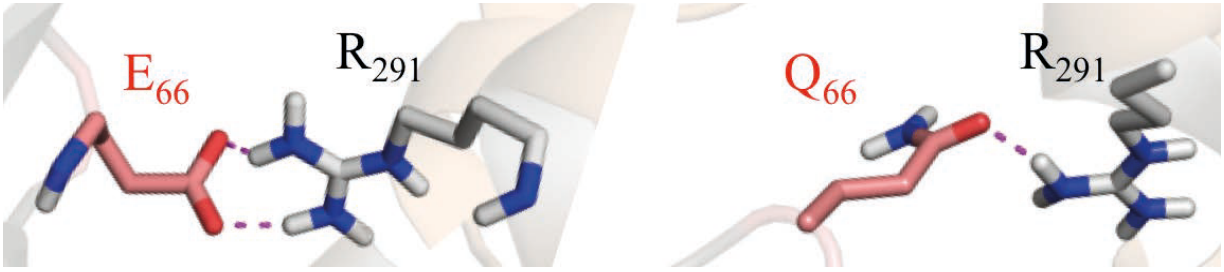

Figure 47: Close-up of hydrogen bonds formed between the tip of the *Plasmodium* profilin arm motif and *Plasmodium* actin. Left: E_{66} from wild type profilin forms two hydrogen bonds with R_{291} of actin. Right: Q66 from the QNQ Pfn mutant forms only one hydrogen bond with R_{291} of actin. Oxygen atoms are colored bright red and nitrogen atoms blue. For orientation within the complex see Figure 27C.

The tip of the arm motif QNQ Pfn (Q_{66}) is still able to form a single hydrogen bond with actin (R_{291}) compared to two hydrogen bonds with a salt bridge (E_{66}) in wildtype profilin (Figure 47).

Interestingly, the reduction of speed of AAA Pfn parasites was less apparent at the ookinete than at the sporozoite stage (Figure 24, Figure 26). This seems puzzling at first, but sporozoites glide ~25 times faster than ookinetes. I believe that the gliding machinery at the ookinete stage does not have to function close to its maximum capacity and thus, small changes can be tolerated more easily and are harder to spot. Presumably, the motor machinery comes much closer to its limit at the sporozoite stage where changes are thus not tolerated as well and more readily detectable than in ookinetes.

At the same time however, gliding motility of the sporozoites is also robust and able to cope with a number of changes (QNQ Pfn) without much perturbation. This robust gliding was seen in the QNQ Pfn mutant - in spite of *in vitro* and *in vivo* measurements clearly showing functional impairments at the molecular level. At a certain threshold however, even gliding motility is affected. This is exemplified in the AAA Pfn mutant that, in addition to a reduced actin sequestration ability and weaker sporozoites, also has significant impairments in gliding motility.

4.3.2 AAA Pfn parasites do not show a reduced infectivity in mice

Surprisingly, we observed that AAA Pfn parasites while having problems with gliding motility in 2D (Figure 25, Figure 26) hardly show a delay in *in vivo* infections (Table 5). This means that they are probably still able to glide reasonably well in 3D. This effect was also observed in sporozoites of the recently described coronin knock out (Bane *et al.*, 2016). It is possible that in 3D environments (like the extracellular matrix of the skin) sporozoites can attach with a much bigger cell surface area than on glass. As observed in laser tweezer experiments, sporozoites are able to exert forces on beads attached to their dorsal side, while being attached to a 2D surface on its ventral side (Quadt *et al.*, 2016), meaning adhesions on at least two sides can be formed at a given time. It is possible that attaching to the extracellular matrix all over its surface aids sporozoites having trouble to glide in 2D in their ability to exert forces and thus to glide. In all other stages AAA Pfn seems to be sufficient for normal development (Table 5, Figure 24). In light of the unusually low multiplication rate and defects in mosquito stage development of the Pfn KO (Figure 44, Figure 45), AAA Pfn must be at least partially able to fulfill its function.

4.3.3 Profilin loop chimeras

We currently know less about the loop chimeras than we know about the tip mutants. The rationale behind the generation of the loop chimeras was to find out why *Pf* Pfn sporozoites move faster than *Pb* Pfn sporozoites (Figure 26). I found that the most divergent region between the two species was the acidic loop (Figure 28). Thus, I generated a version of profilin based on the *P. berghei* backbone but containing the loop from *P. falciparum* (*Pb* Pfn $^{Pf\,loop}$). I also generated a mutant that was built the other way around (*Pf* backbone with *Pb* loop) as a control (*Pf* Pfn $^{Pb\,loop}$). In addition to that, I created a mutant with a loop deletion. As *Toxoplasma gondii* profilin contains a very short loop, instead of simply deleting the whole loop and in order to avoid problems with protein folding I used the corresponding sequence of *Tg* Pfn to replace the longer loop of *Plasmodia* (*Pf* Pfn $^{Tg\,loop}$) (Figure 31F). This could also open up studies of full-length *T. gondii* replacements in *P. berghei* and vice versa.

Against my expectations, the speed of *Pb* Pfn $^{Pf\,loop}$ sporozoites was not elevated as in *Pf* Pfn sporozoites (Figure 33). In fact, *Pb* Pfn $^{Pf\,loop}$ sporozoites moved even slower than wild type sporozoites (0.6 μm/s lower on average). This possibly means that the acidic loop, even though it seems to be the most divergent region between *P. berghei* and *P. falciparum*, was not enough to make sporozoites move faster. The *in vitro* polymerization assays of the loop chimeras included the wild type *Pb* Pfn. Surprisingly, it behaved differently from wild type *Pf* Pfn: *Pb* Pfn displayed much weaker actin sequestration ability than *Pf* Pfn (Figure 31). This could possibly explain why wild type sporozoites (carrying *Pb* Pfn) move slower than *Pf* Pfn sporozoites. If sequestration of actin monomers is naturally weaker in *Pb* Pfn, this might lead to different actin dynamics than with *Pf* Pfn.

Both loop chimeras based on the *Pf* Pfn backbone (*Pf* Pfn $^{Pb\,loop}$ and *Pf* Pfn $^{Tg\,loop}$) had a very similar speed that was 0.9 μm/s below the median speed of their *Pf* Pfn control (Figure 33). In actin polymerization assays, *Pf* Pfn $^{Pb\,loop}$ and *Pf* Pfn $^{Tg\,loop}$ sequestered actin monomers similarly, but slightly worse than *Pf* Pfn (Figure 31).

In general, the polymerization only occurred after a lag phase of 5-10 minutes (Figure 31A) that had not been observed in the tip mutants (Figure 22A). Pig muscle α-actin can vary in these assays and should be extracted as fast as possible. Possibly, the actin was prepared too soon before the assay was performed. As I was performing this assay for the first time, it is likely that I needed more experience to have optimal polymerization conditions. However, the assays of the loop chimeras are comparable with each other and we could still gain valuable insight into the function of the profilin loop chimeras.

Molecular dynamics simulations are still ongoing but preliminary data hint towards an influence of the acidic loop on the stability and orientation of the arm motif. Thus, the loop chimeras could also be impaired in actin binding. This would explain why the loop chimeras seem to mimic the tip mutants and arm deletion mutants' behavior in laser tweezer experiments (Figure 35).

4.3.4 Mutant profilins could possibly lead to longer actin filaments

Strikingly, all profilin mutants showed the same overall trend, when being analyzed with the help of laser tweezers. All mutant sporozoites were weaker that the wildtype, but showed increased rates of retrograde flow (Figure 35). We believe that altered actin dynamics provide the base for this difference. We think that the retrograde flow represents the motion of actin-adhesin complexes that are being moved to the rear of the cell with the help of myosin (Baum *et al.*, 2006).

At first it seemed puzzling that all profilin mutants should behave similarly, since the loop chimeras involved the mutation of a domain that was not expected to be involved in actin binding. However, preliminary molecular dynamics simulations have indicated that the loop chimeras could also be impaired in actin binding. This has led us to speculate on the state of actin filaments in the profilin mutants:

Evidence of actin in the parasite indicates that filaments are probably short (Schmitz *et al*., 2010, Vahokoski *et al*., 2014), (Figure 48). In wild type sporozoites, the force measured with laser tweezers is higher than for sporozoites treated with Jasplakinolide. At the same time, the speed of retrograde flow in wild type sporozoites is lower than in the presence of Jas (Quadt *et al.*, 2016). This could mean that longer filaments speed up retrograde flow, as Jas stabilizes actin filaments (Figure 48). Retrograde flow might be increased as more myosins can bind to longer filaments at a time and thus generate higher flow speeds.

The profilin mutants sequestered actin monomers less than the wildtype, but behaved similarly to sporozoites treated with Jas in the laser tweezer analysis. Thus we hypothesize that more actin monomers can be incorporated into the filament in the profilin mutants. As profilin should not affect the off-rate of actin monomers from the filament, this would lead to longer filaments than in the wild type (Figure 48).

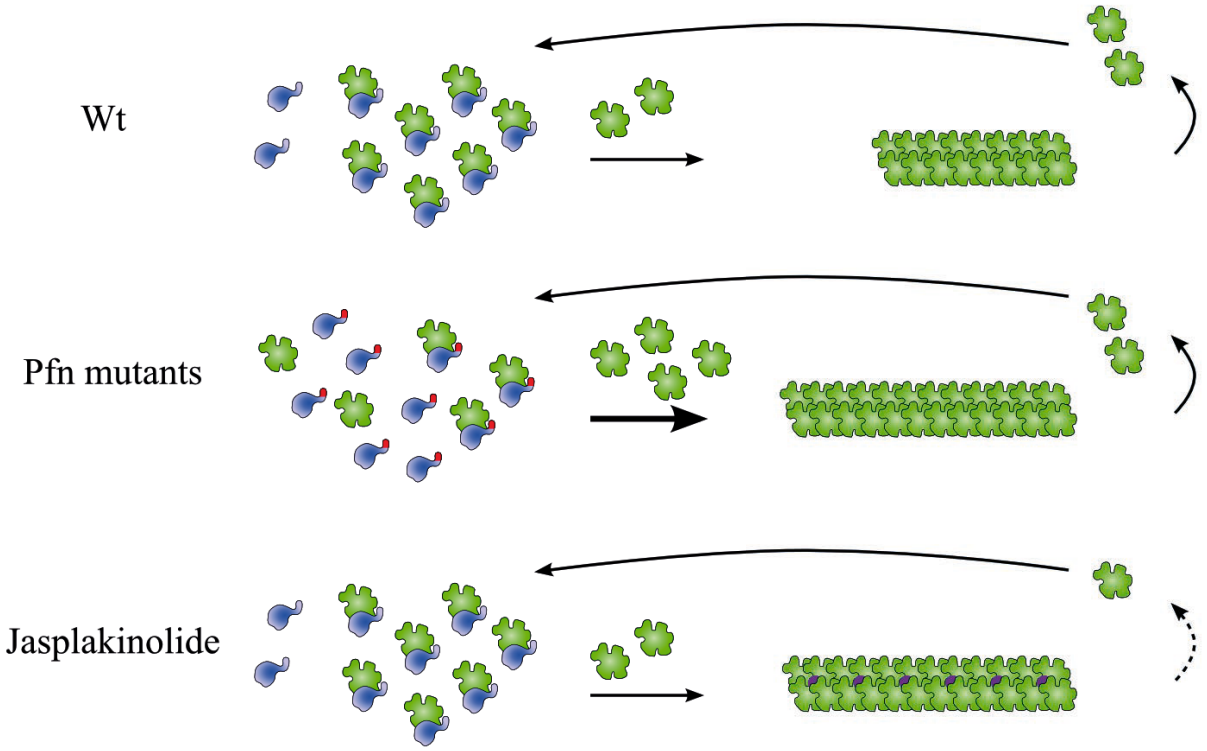

Figure 48: Working hypothesis for the effect of the profilin mutants on actin filaments. In the wild type, most actin monomers (green) are bound to profilin (blue) and a certain amount is incorporated into treadmilling filaments. The profilin mutants display weaker actin binding (red arm motif) and thus have a higher rate of monomer incorporation. With the same off-rate as in the wild type, this might lead to longer filaments. Quadt et al. showed that sporozoites treated with jasplakinolide behaved similarly as sporozoites carrying the profilin mutants (Quadt *et al.*, 2016). As Jas stabilizes filaments (purple dots), this is a good indication that the profilin mutants do lead to longer filaments.

4.3.5 Parameters measured with laser tweezers are insufficient to predict the ability of sporozoites to glide in 2D

The laser tweezer setup allowed us to analyze individual features of the sporozoites: their ability to produce and overcome forces and the speed of retrograde flow. We had previously hypothesized that the sporozoites integrate these two abilities for optimal gliding motility (Quadt *et al.*, 2016). However, although the QNQ Pfn and the AAA Pfn mutant both display low forces and high retrograde flow speeds (Figure 35) they differ in their ability to glide. While the sporozoites carrying AAA Pfn are impaired in their ability to glide in 2D, the sporozoites carrying QNQ Pfn are not. This means that the two parameters provided by the laser tweezer analysis are not enough to predict the quality of gliding motility. We believe that the state of actin filaments, whether it be length, orientation or both, significantly influences the sporozoites ability to glide productively, something that seems to be affected in the AAA Pfn mutant, but not the QNQ Pfn mutant. Indeed, our molecular dynamics simulations have revealed a differential behavior of the two mutants: the QNQ Pfn has a reduced actin binding capacity than wild type profilin, but is still capable of binding to actin

with the tip of the arm motif. The AAA Pfn however, has lost the interaction between its arm motif and actin, which leads to a decreased binding free energy than in QNQ Pfn (Figure 27). This indicates, that the two mutants possibly result in different states of actin that could be the critical factor determining the ability of the sporozoite to glide in 2D.

4.4 Δ arm Pfn

4.4.1 Of all investigated mutant profilins, the arm deletion is impaired the most

In contrast to the tip mutants, the arm deletion had a significantly lower blood stage multiplication rate ($p < 0.01$) of 6.5 compared to 8.9 in wild type parasites (Table 5). The blood stage multiplication rate of the Pfn KO (5.9) is comparable with that of Δ arm Pfn, indicating that Δ arm Pfn might not be able to exert much of a function at the blood stage. This is underlined by the complete lack of actin monomer sequestration ability of Δ arm Pfn (Figure 22). In addition, prepatency of arm deletion parasites in mice after sporozoites challenge was on average 2 days later than for *Pf* Pfn and wild type parasites (Table 5). This increase in prepatency was probably not the result of delayed liver stage development, as preliminary experiments in *in vitro* liver stage assays resulted in merosome formation after 66 - 69 hours (data not shown), a time comparable to the release of wild type merosomes (Stanway *et al.*, 2009). However, the release of merosomes from *in vitro* liver stages unfortunately only worked once. Even so, this suggests that the delay in prepatency of Δ arm Pfn parasites is likely a result of their reduced blood stage multiplication rate (Table 5).

In addition to the lower blood stage growth rate, Δ arm Pfn ookinetes were also significantly impaired. Their speed was reduced 75 % compared to *Pf* Pfn wild type control ookinetes (Figure 24).

Surprisingly, Δ arm Pfn was found to form dimers *in vitro* (Bhargav *et al.*, 2015), a feature that might prevent it from fulfilling its proper function. However, we currently do not know whether dimers (Figure 49A) are formed *in vivo*. Interestingly, dimerization was shown to occur through a process called domain swapping, where two polypeptide chains fold each apparent monomer subunit (Bhargav *et al.*, 2015, Bennett *et al.*, 1995, Figure 49A). This led to the discovery, that profilin can self-assemble from two independently expressed folding units (Bhargav *et al.*, 2015, Figure 49B). The border between the two subunits was found to be located in the arm motif. Most likely, the glycine residue at the turn of the arm motif (G_{68}, Figure 21) enables the polypeptide chain to be flexible enough to bend back on itself to form

the β-hairpin (Bhargav *et al.*, 2015). Interestingly, the glycine residue is conserved in Apicomplexa and chromerids (Figure 8). Loss of the arm motif in the Δ arm Pfn mutant includes this G_{68} residue, which leads to a reduced flexibility of the protein in this region, thus the protein is more easily folded by two separate polypeptide chains thereby avoiding the tight turn of the β-hairpin.

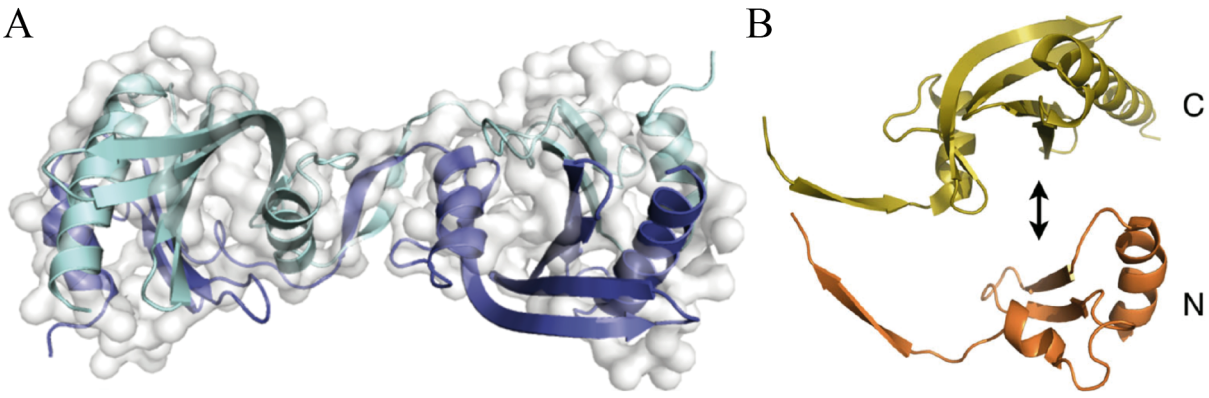

Figure 49: Dimerization and independent folding units of Δ arm Pfn (Bhargav *et al.*, 2015). (A) SAXS outline of the Δ arm Pfn dimer overlaid with its homology model. Dimers are formed through means of domain swapping: the violet and light blue polypeptide chains each form half of a monomer. (B) *Pf* Profilin can spontaneously self-assemble from two independent folding units. The cut-off is located within the arm motif, explaining how the domain swapping in A can occur.

Oligomerization of profilins has been reported in profilin from human platelets, from mugwort pollen as well as human, yeast and birch pollen profilin expressed in *E. coli* (Krishnan & Moens, 2009). Although it was found that profilin oligomers from plant pollen could be more powerful allergens than their monomeric counterpart, the function of profilin oligomerization in cells is not clear (Krishnan & Moens, 2009). Also, in previous studies it was not investigated whether these oligomers are formed through means of domain swapping as it occurs in *Plasmodium* Δ arm Pfn (Figure 49A) where one apparent monomer is comprised of subunits of two polypeptide chains (Bhargav *et al.*, 2015).

It is possible, that arm deletion ookinetes face a problem with crystalloid body integrity similar to the Pfn KO (Figure 45). However, in contrast to Pfn KO ookinetes (Figure 44C) the Δ arm Pfn ookinete morphology was undistinguishable from wild type ookinetes in DIC images or Giemsa stainings and did not display hemozoin-containing vesicles accumulations at their rear end (data not shown). This, as well as the fact that arm deletion sporozoites can produce infectious salivary glands (Table 5), shows that Δ arm Pfn still has residual function even if it does form dimers *in vivo* (Figure 49A).

4.4.2 Sporozoite-induced Δ arm Pfn infections enable mice to clear parasites from their blood

Half of the C57BL/6 mice and all of BALB/c mice were able to overcome and clear sporozoite-induced Δ arm Pfn infections (Figure 37, Figure 39). The difference between these mouse strains suggests that the loss of 50 % of C57BL/6 mice might be due to immunopathology and not due to the parasites *per se* as all BALB/c mice that do not develop EMC survived. Even though injection of Δ arm Pfn iRBCs led to the death of all C57BL/6 mice (Figure 36), avoiding the liver stage by injecting *in vitro* generated merosomes enabled the mice to clear the infection. This points away from a liver stage-specific induction of protection and hints towards a probably dose-dependent effect of iRBCs that could be investigated in future studies by lowering the injected dose of Δ arm Pfn parasites even further (e.g. ≤ 10 iRBCs) to give the mice enough time to develop protective immune responses before developing severe (cerebral) symptoms. Interestingly, another study showed that blood stage parasites lacking both a merozoite surface protein (MSP7) and an aspartic protease (plasmepsin 4) caused very similar parasitemia progression as sporozoite-induced Δ arm Pfn infections, indicating a similar reduction in virulence (Spaccapelo *et al.*, 2011).

The timeline of sporozoite-induced Δ arm Pfn infections (Figure 37) fits with the time it takes to produce antibodies (Hansen *et al.*, 2005). To tackle the question whether antibodies are the main mechanism conveying protection we could transfer plasma of mice having experienced a Δ arm Pfn, wild type or no infection together with wildtype parasites into naïve mice and observe the outcome of these infections. Additionally, mice from cleared Δ arm Pfn infections could be challenged with wildtype parasites after treatment with αIgG-antibodies to inhibit potential antibodies directed against the parasites to see whether that changes the outcome of wild type challenges. Also, Δ arm Pfn infections could be performed in RAG-1 knockout mice that do not produce mature B- or T-cells (Mombaerts *et al.*, 1992) and thus are unable to produce antibodies. In any case, investigating the immune mechanisms of mice against the Δ arm Pfn parasites should involve an experienced immunologist as a collaborator or advisor.

The existing results point towards the potential of the Δ arm Pfn parasites to be used as a sporozoite-transmitted blood-stage inducing experimental vaccine in mice. This (together with the work on the Pfn KO) has inspired further experiments that have evolved as a collaborative effort in the lab and led to the generation of stage-specific profilin knockouts. The overall aim is to preserve profilin during the mosquito stages to enable normal development and salivary gland invasion of sporozoites, but stop profilin expression at the

blood stage to reduce virulence of the parasite inside the vertebrate host. However, this is a proof-of-concept situation and we are not proposing a 1:1 adaptation of profilin mutations or stage-specific knockouts for developing a life attenuated vaccine in humans, especially since *Plasmodium* profilin was shown to be recognized by TLR11/12 heterodimers that are both missing in humans (Gazzinelli *et al.*, 2014) and modulation of virulence is thus expected to be different in humans.

4.5 Conclusion

The structure of *Plasmodium* profilin with its unique motifs has spiked our interest to find out more about its function. For that we used a multidisciplinary approach combining biochemical, biophysical, computational and molecular genetics analyses with live cell imaging of motile parasite stages. It is this combination that paints a much more comprehensive picture of *Plasmodium* profilin. Contrary to assumptions and results from *T. gondii*, I could show that *Plasmodium* profilin is not essential in the blood stage, even though loss of profilin or its arm motif significantly reduced blood stage growth rates. However, I could show that profilin is essential for formation of infectious sporozoites and profilins arm motif is critically involved in actin binding and gliding motility. I also found differences between *P. berghei* and *P. falciparum* profilin that need to be investigated further. Interestingly, loss of the arm motif of profilin reduced parasite virulence enough to enable mice to clear infections with these parasites, showing that the generation of a sporozoite-transmittable blood-stage attenuated vaccine is possible.

5 References

Agnandji ST, Lell B, Fernandes JF, Abossolo BP, Kabwende AL, Adegnika AA, Mordmüller B, Issifou S, Kremsner PG, Loembe MM *et al*. (2014) Efficacy and safety of the RTS,S/AS01 malaria vaccine during 18 months after vaccination: a phase 3 randomized, controlled trial in children and young infants at 11 African sites. PLoS Medicine 11: e1001685. PMID: 25072396.

Agop-Nersesian C, De Niz M, Niklaus L, Prado M, Eickel N, Heussler VT (2017) Shedding of host autophagic proteins from the parasitophorous vacuolar membrane of Plasmodium berghei. Scientific Reports 7: 2191. PMID: 28526861.

Aly AS, Matuschewski K (2005) A malarial cysteine protease is necessary for Plasmodium sporozoite egress from oocysts. The Journal of Experimental Medicine 202: 225-30. PMID: 16027235.

Amino R, Thiberge S, Martin B, Celli S, Shorte S, Frischknecht F, Menard R (2006) Quantitative imaging of Plasmodium transmission from mosquito to mammal. Nature Medicine 12: 220-4. PMID: 16429144.

Andreadaki M, Morgan RN, Deligianni E, Kooij TW, Santos JM, Spanos L, Matuschewski K, Louis C, Mair GR, Siden-Kiamos I (2014) Genetic crosses and complementation reveal essential functions for the Plasmodium stage-specific actin 2 in sporogonic development. Cellular Microbiology 16: 751-67. PMID: 24471657.

Angrisano F, Riglar DT, Sturm A, Volz JC, Delves MJ, Zuccala ES, Turnbull L, Dekiwadia C, Olshina MA, Marapana DS *et al*. (2012) Spatial localisation of actin filaments across developmental stages of the malaria parasite. PloS One 7: e32188. PMID: 22389687.

Baer K, Klotz C, Kappe SH, Schnieder T, Frevert U (2007) Release of hepatic Plasmodium yoelii merozoites into the pulmonary microvasculature. PLoS Pathogens 3: e171. PMID: 17997605.

Bane KS, Lepper S, Kehrer J, Sattler JM, Singer M, Reinig M, Klug D, Heiss K, Baum J, Mueller AK *et al*. (2016) The Actin Filament-Binding Protein Coronin Regulates Motility in Plasmodium Sporozoites. PLoS Pathogens 12: e1005710. PMID: 27409081.

Barnhart EL, Lee KC, Keren K, Mogilner A, Theriot JA (2011) An adhesion-dependent switch between mechanisms that determine motile cell shape. PLoS Biology 9: e1001059. PMID: 21559321.

Baum J, Papenfuss AT, Baum B, Speed TP, Cowman AF (2006) Regulation of apicomplexan actin-based motility. Nature Reviews Microbiology 4: 621-8. PMID: 16845432.

Bennink S, Kiesow MJ, Pradel G (2016) The development of malaria parasites in the mosquito midgut. Cellular Microbiology 18: 905-18. PMID: 27111866.

Bergman LW, Kaiser K, Fujioka H, Coppens I, Daly TM, Fox S, Matuschewski K, Nussenzweig V, Kappe SH (2003) Myosin A tail domain interacting protein (MTIP) localizes to the inner membrane complex of Plasmodium sporozoites. Journal of Cell Science 116: 39-49. PMID: 12456714.

Berro J, Sirotkin V, Pollard TD (2010) Mathematical modeling of endocytic actin patch kinetics in fission yeast: disassembly requires release of actin filament fragments. Molecular Biology of the Cell 21: 2905-15. PMID: 20587776.

Bhargav SP, Vahokoski J, Kallio JP, Torda AE, Kursula P, Kursula I (2015) Two independently folding units of Plasmodium profilin suggest evolution via gene fusion. Cellular and Molecular Life Sciences : CMLS 72: 4193-203. PMID: 26012696.

Billker O, Lindo V, Panico M, Etienne AE, Paxton T, Dell A, Rogers M, Sinden RE, Morris HR (1998) Identification of xanthurenic acid as the putative inducer of malaria development in the mosquito. Nature 392: 289-92. PMID: 9521324.

Billker O, Miller AJ, Sinden RE (2000) Determination of mosquito bloodmeal pH in situ by ion-selective microelectrode measurement: implications for the regulation of malarial gametogenesis. Parasitology 120 (Pt 6): 547-51. PMID: 10874717.

Blackman MJ, Bannister LH (2001) Apical organelles of Apicomplexa: biology and isolation by subcellular fractionation. Molecular and Biochemical Parasitology 117: 11-25. PMID: 11551628.

Blaser H, Reichman-Fried M, Castanon I, Dumstrei K, Marlow FL, Kawakami K, Solnica-Krezel L, Heisenberg CP, Raz E (2006) Migration of zebrafish primordial germ cells: a role for myosin contraction and cytoplasmic flow. Developmental Cell 11: 613-27. PMID: 17084355.

Bouharoun-Tayoun H, Oeuvray C, Lunel F, Druilhe P (1995) Mechanisms underlying the monocyte-mediated antibody-dependent killing of Plasmodium falciparum asexual blood stages. The Journal of Experimental Medicine 182: 409-18. PMID: 7629503.

Bozdech Z, Zhu J, Joachimiak MP, Cohen FE, Pulliam B, DeRisi JL (2003) Expression profiling of the schizont and trophozoite stages of Plasmodium falciparum with a long-oligonucleotide microarray. Genome Biology 4: R9. PMID: 12620119.

Bubb MR, Senderowicz AM, Sausville EA, Duncan KL, Korn ED (1994) Jasplakinolide, a cytotoxic natural product, induces actin polymerization and competitively inhibits the binding of phalloidin to F-actin. The Journal of Biological Chemistry 269: 14869-71. PMID: 8195116.

Bullen HE, Tonkin CJ, O'Donnell RA, Tham WH, Papenfuss AT, Gould S, Cowman AF, Crabb BS, Gilson PR (2009) A novel family of Apicomplexan glideosome-associated proteins with an inner membrane-anchoring role. The Journal of Biological Chemistry 284: 25353-63. PMID: 19561073.

Carlsson L, Nystrom LE, Lindberg U, Kannan KK, Cid-Dresdner H, Lovgren S (1976) Crystallization of a non-muscle actin. Journal of Molecular Biology 105: 353-66. PMID: 972388.

Carlsson L, Nystrom LE, Sundkvist I, Markey F, Lindberg U (1977) Actin polymerizability is influenced by profilin, a low molecular weight protein in non-muscle cells. Journal of Molecular Biology 115: 465-83. PMID: 563468.

Carter V, Shimizu S, Arai M, Dessens JT (2008) PbSR is synthesized in macrogametocytes and involved in formation of the malaria crystalloids. Molecular Microbiology 68: 1560-9. PMID: 18452513.

Chaparro-Olaya J, Margos G, Coles DJ, Dluzewski AR, Mitchell GH, Wasserman MM, Pinder JC (2005) Plasmodium falciparum myosins: transcription and translation during asexual parasite development. Cell Motility and the Cytoskeleton 60: 200-13. PMID: 15754360.

Charras G, Paluch E (2008) Blebs lead the way: how to migrate without lamellipodia. Nature Reviews Molecular Cell Biology 9: 730-6. PMID: 18628785.

Chaudhary A, Chen J, Gu QM, Witke W, Kwiatkowski DJ, Prestwich GD (1998) Probing the phosphoinositide 4,5-bisphosphate binding site of human profilin I. Chemistry & Biology 5: 273-81. PMID: 9578635.

Cohen S, Butcher GA, Crandall RB (1969) Action of malarial antibody in vitro. Nature 223: 368-71. PMID: 4980851.

Combe A, Moreira C, Ackerman S, Thiberge S, Templeton TJ, Menard R (2009) TREP, a novel protein necessary for gliding motility of the malaria sporozoite. International Journal for Parasitology 39: 489-96. PMID: 19000911.

de Koning-Ward TF, Dixon MW, Tilley L, Gilson PR (2016) Plasmodium species: master renovators of their host cells. Nature Reviews Microbiology 14: 494-507. PMID: 27374802.

de Kossodo S, Grau GE (1993) Profiles of cytokine production in relation with susceptibility to cerebral malaria. Journal of Immunology 151: 4811-20. PMID: 8409439.

de Oca MM, Engwerda C, Haque A (2013) Plasmodium berghei ANKA (PbA) infection of C57BL/6J mice: a model of severe malaria. Methods in Molecular Biology 1031: 203-13. PMID: 23824903.

Deligianni E, Morgan RN, Bertuccini L, Kooij TW, Laforge A, Nahar C, Poulakakis N, Schuler H, Louis C, Matuschewski K *et al*. (2011) Critical role for a stage-specific actin in male exflagellation of the malaria parasite. Cellular Microbiology 13: 1714-30. PMID: 21790945.

Di Nardo A, Gareus R, Kwiatkowski D, Witke W (2000) Alternative splicing of the mouse profilin II gene generates functionally different profilin isoforms. Journal of Cell Science 113 Pt 21: 3795-803. PMID: 11034907.

Ding Z, Roy P (2013) Profilin-1 versus profilin-2: two faces of the same coin? Breast Cancer Research 15: 311. PMID: 23827010.

Dobrowolski JM, Niesman IR, Sibley LD (1997) Actin in the parasite Toxoplasma gondii is encoded by a single copy gene, ACT1 and exists primarily in a globular form. Cell Motility and the Cytoskeleton 37: 253-62. PMID: 9227855.

Dobrowolski JM, Sibley LD (1996) Toxoplasma invasion of mammalian cells is powered by the actin cytoskeleton of the parasite. Cell 84: 933-9. PMID: 8601316.

Doi Y, Shinzawa N, Fukumoto S, Okano H, Kanuka H (2010) ADF2 is required for transformation of the ookinete and sporozoite in malaria parasite development. Biochemical and Biophysical Research Communication 397: 668-72. PMID: 20529666.

Douglas RG, Amino R, Sinnis P, Frischknecht F (2015) Active migration and passive transport of malaria parasites. Trends in Parasitology 31: 357-62. PMID: 26001482.

Ecker A, Bushell ES, Tewari R, Sinden RE (2008) Reverse genetics screen identifies six proteins important for malaria development in the mosquito. Molecular Microbiology 70: 209-20. PMID: 18761621.

Egarter S, Andenmatten N, Jackson AJ, Whitelaw JA, Pall G, Black JA, Ferguson DJ, Tardieux I, Mogilner A, Meissner M (2014) The toxoplasma Acto-MyoA motor complex is important but not essential for gliding motility and host cell invasion. PloS One 9: e91819. PMID: 24632839.

Fackler OT, Grosse R (2008) Cell motility through plasma membrane blebbing. The Journal of Cell Biology 181: 879-84. PMID: 18541702.

Falkenburger BH, Jensen JB, Dickson EJ, Suh BC, Hille B (2010) Phosphoinositides: lipid regulators of membrane proteins. The Journal of Physiology 588: 3179-85. PMID: 20519312.

Fan Y, Arif A, Gong Y, Jia J, Eswarappa SM, Willard B, Horowitz A, Graham LM, Penn MS, Fox PL (2012) Stimulus-dependent phosphorylation of profilin-1 in angiogenesis. Nature Cell Biology 14: 1046-56. PMID: 23000962.

Forscher P, Lin CH, Thompson C (1992) Novel form of growth cone motility involving site-directed actin filament assembly. Nature 357: 515-8. PMID: 1608453.

Forscher P, Smith SJ (1988) Actions of cytochalasins on the organization of actin filaments and microtubules in a neuronal growth cone. The Journal of Cell Biology 107: 1505-16. PMID: 3170637.

Francia ME, Striepen B (2014) Cell division in apicomplexan parasites. Nature Reviews Microbiology 12: 125-36. PMID: 24384598.

Frenal K, Marq JB, Jacot D, Polonais V, Soldati-Favre D (2014) Plasticity between MyoC- and MyoA-glideosomes: an example of functional compensation in Toxoplasma gondii invasion. PLoS Pathogens 10: e1004504. PMID: 25393004.

Frenal K, Polonais V, Marq JB, Stratmann R, Limenitakis J, Soldati-Favre D (2010) Functional dissection of the apicomplexan glideosome molecular architecture. Cell Host & Microbe 8: 343-57. PMID: 20951968.

Freund J, Thomson KJ, et al. (1948) Immunization of monkeys against malaria by means of killed parasites with adjuvants. American Journal of Tropical Medicine and Hygiene 28: 1-22. PMID: 18898694.

Frevert U, Engelmann S, Zougbede S, Stange J, Ng B, Matuschewski K, Liebes L, Yee H (2005) Intravital observation of Plasmodium berghei sporozoite infection of the liver. PLoS Biology 3: e192. PMID: 15901208.

Frischknecht F, Baldacci P, Martin B, Zimmer C, Thiberge S, Olivo-Marin JC, Shorte SL, Menard R (2004) Imaging movement of malaria parasites during transmission by Anopheles mosquitoes. Cellular Microbiology 6: 687-94. PMID: 15186404.

Ganter M, Goldberg JM, Dvorin JD, Paulo JA, King JG, Tripathi AK, Paul AS, Yang J, Coppens I, Jiang RH *et al*. (2017) Plasmodium falciparum CRK4 directs continuous rounds of DNA replication during schizogony. Nature Microbiology 2: 17017. PMID: 28211852.

Ganter M, Schuler H, Matuschewski K (2009) Vital role for the Plasmodium actin capping protein (CP) beta-subunit in motility of malaria sporozoites. Molecular Microbiology 74: 1356-67. PMID: 19682250.

Gaskins E, Gilk S, DeVore N, Mann T, Ward G, Beckers C (2004) Identification of the membrane receptor of a class XIV myosin in Toxoplasma gondii. The Journal of Cell Biology 165: 383-93. PMID: 15123738.

Gazzinelli RT, Mendonca-Neto R, Lilue J, Howard J, Sher A (2014) Innate resistance against Toxoplasma gondii: an evolutionary tale of mice, cats, and men. Cell Host & Microbe 15: 132-8. PMID: 24528860.

Ghosh AK, Devenport M, Jethwaney D, Kalume DE, Pandey A, Anderson VE, Sultan AA, Kumar N, Jacobs-Lorena M (2009) Malaria parasite invasion of the mosquito salivary gland requires interaction between the Plasmodium TRAP and the Anopheles saglin proteins. PLoS Pathogens 5: e1000265. PMID: 19148273.

Green JL, Martin SR, Fielden J, Ksagoni A, Grainger M, Yim Lim BY, Molloy JE, Holder AA (2006) The MTIP-myosin A complex in blood stage malaria parasites. Journal of Molecular Biology 355: 933-41. PMID: 16337961.

Grutzke J, Rindte K, Goosmann C, Silvie O, Rauch C, Heuer D, Lehmann MJ, Mueller AK, Brinkmann V, Matuschewski K *et al*. (2014) The spatiotemporal dynamics and membranous features of the Plasmodium liver stage tubovesicular network. Traffic 15: 362-82. PMID: 24423236.

Guillen G, Valdes-Lopez V, Noguez R, Olivares J, Rodriguez-Zapata LC, Perez H, Vidali L, Villanueva MA, Sanchez F (1999) Profilin in Phaseolus vulgaris is encoded by two genes (only one expressed in root nodules) but multiple isoforms are generated in vivo by phosphorylation on tyrosine residues. Plant Journal 19: 497-508. PMID: 10504572.

Hansen DS, Evans KJ, D'Ombrain MC, Bernard NJ, Sexton AC, Buckingham L, Scalzo AA, Schofield L (2005) The natural killer complex regulates severe malarial pathogenesis and influences acquired immune responses to Plasmodium berghei ANKA. Infection and Immunity 73: 2288-97. PMID: 15784573.

Hansson A, Skoglund G, Lassing I, Lindberg U, Ingelman-Sundberg M (1988) Protein kinase C-dependent phosphorylation of profilin is specifically stimulated by phosphatidylinositol bisphosphate (PIP2). Biochemical and Biophysical Research Communication 150: 526-31. PMID: 2829877.

Harding CR, Meissner M (2014) The inner membrane complex through development of Toxoplasma gondii and Plasmodium. Cellular Microbiology 16: 632-41. PMID: 24612102.

Haugwitz M, Noegel AA, Karakesisoglou J, Schleicher M (1994) Dictyostelium amoebae that lack G-actin-sequestering profilins show defects in F-actin content, cytokinesis, and development. Cell 79: 303-14. PMID: 7954798.

Hegge S, Kudryashev M, Smith A, Frischknecht F (2009) Automated classification of Plasmodium sporozoite movement patterns reveals a shift towards productive motility during salivary gland infection. Biotechnology Journal 4: 903-13. PMID: 19455538.

Heintzelman MB, Schwartzman JD (1997) A novel class of unconventional myosins from Toxoplasma gondii. Journal of Molecular Biology 271: 139-46. PMID: 9300060.

Heiss K, Nie H, Kumar S, Daly TM, Bergman LW, Matuschewski K (2008) Functional characterization of a redundant Plasmodium TRAP family invasin, TRAP-like protein, by aldolase binding and a genetic complementation test. Eukaryotic Cell 7: 1062-70. PMID: 18441124.

Hellmann JK, Munter S, Kudryashev M, Schulz S, Heiss K, Muller AK, Matuschewski K, Spatz JP, Schwarz US, Frischknecht F (2011) Environmental constraints guide migration of malaria parasites during transmission. PLoS Pathogens 7: e1002080. PMID: 21698220.

Higashida C, Miyoshi T, Fujita A, Oceguera-Yanez F, Monypenny J, Andou Y, Narumiya S, Watanabe N (2004) Actin polymerization-driven molecular movement of mDia1 in living cells. Science 303: 2007-10. PMID: 15044801.

Hliscs M, Sattler JM, Tempel W, Artz JD, Dong A, Hui R, Matuschewski K, Schuler H (2010) Structure and function of a G-actin sequestering protein with a vital role in malaria oocyst development inside the mosquito vector. The Journal of Biological Chemistry 285: 11572-83. PMID: 20083609.

Holmes KC, Popp D, Gebhard W, Kabsch W (1990) Atomic model of the actin filament. Nature 347: 44-9. PMID: 2395461.

Hopp CS, Chiou K, Ragheb DR, Salman A, Khan SM, Liu AJ, Sinnis P (2015) Longitudinal analysis of Plasmodium sporozoite motility in the dermis reveals component of blood vessel recognition. eLife 4: e007789. PMID: 26271010.

Hotulainen P, Lappalainen P (2006) Stress fibers are generated by two distinct actin assembly mechanisms in motile cells. The Journal of Cell Biology 173: 383-94. PMID: 16651381.

Hou T, Wang J, Li Y, Wang W (2011) Assessing the performance of the MM/PBSA and MM/GBSA methods. 1. The accuracy of binding free energy calculations based on molecular dynamics simulations. Journal of Chemical Information and Modeling 51: 69-82. PMID: 21117705.

Huang BW, Pearman E, Kim CC (2015) Mouse Models of Uncomplicated and Fatal Malaria. Biology Protocols 5. PMID: 26236758.

Ignatev A, Bhargav SP, Vahokoski J, Kursula P, Kursula I (2012) The lasso segment is required for functional dimerization of the Plasmodium formin 1 FH2 domain. PloS One 7: e33586. PMID: 22428073.

Jacot D, Daher W, Soldati-Favre D (2013) Toxoplasma gondii myosin F, an essential motor for centrosomes positioning and apicoplast inheritance. The EMBO Journal 32: 1702-16. PMID: 23695356.

Jacot D, Tosetti N, Pires I, Stock J, Graindorge A, Hung YF, Han H, Tewari R, Kursula I, Soldati-Favre D (2016) An Apicomplexan Actin-Binding Protein Serves as a Connector and Lipid Sensor to Coordinate Motility and Invasion. Cell Host & Microbe 20: 731-743. PMID: 27978434.

Janouskovec J, Horak A, Barott KL, Rohwer FL, Keeling PJ (2013) Environmental distribution of coral-associated relatives of apicomplexan parasites. ISME Journal 7: 444-7. PMID: 23151646.

Jewett TJ, Sibley LD (2003) Aldolase forms a bridge between cell surface adhesins and the actin cytoskeleton in apicomplexan parasites. Molecular Cell 11: 885-94. PMID: 12718875.

Kafsack BF, Rovira-Graells N, Clark TG, Bancells C, Crowley VM, Campino SG, Williams AE, Drought LG, Kwiatkowski DP, Baker DA *et al*. (2014) A transcriptional switch underlies commitment to sexual development in malaria parasites. Nature 507: 248-52. PMID: 24572369.

Kapishnikov S, Weiner A, Shimoni E, Guttmann P, Schneider G, Dahan-Pasternak N, Dzikowski R, Leiserowitz L, Elbaum M (2012) Oriented nucleation of hemozoin at the digestive vacuole membrane in Plasmodium falciparum. Proceedings of the National Academy of Sciences of the United States of America 109: 11188-93. PMID: 22745164.

Kaushansky A, Douglass AN, Arang N, Vigdorovich V, Dambrauskas N, Kain HS, Austin LS, Sather DN, Kappe SH (2015) Malaria parasites target the hepatocyte receptor EphA2 for successful host infection. Science 350: 1089-92. PMID: 26612952.

Kehrer J, Frischknecht F, Mair GR (2016) Proteomic Analysis of the Plasmodium berghei Gametocyte Egressome and Vesicular bioID of Osmiophilic Body Proteins Identifies Merozoite TRAP-like Protein (MTRAP) as an Essential Factor for Parasite Transmission. Molecular & Cellular Proteomics : MCP 15: 2852-62. PMID: 27371728.

Khater EI, Sinden RE, Dessens JT (2004) A malaria membrane skeletal protein is essential for normal morphogenesis, motility, and infectivity of sporozoites. The Journal of Cell Biology 167: 425-32. PMID: 15533999.

King CA (1988) Cell motility of sporozoan protozoa. Parasitology Today 4: 315-9. PMID: 15463014.

Klug D, Frischknecht F (2017) Motility precedes egress of malaria parasites from oocysts. eLife 6: e19157. PMID: 28115054.

Koblansky AA, Jankovic D, Oh H, Hieny S, Sungnak W, Mathur R, Hayden MS, Akira S, Sher A, Ghosh S (2013) Recognition of profilin by Toll-like receptor 12 is critical for host resistance to Toxoplasma gondii. Immunity 38: 119-30. PMID: 23246311.

Kovar DR, Pollard TD (2004) Insertional assembly of actin filament barbed ends in association with formins produces piconewton forces. Proceedings of the National Academy of Sciences of the United States of America 101: 14725-30. PMID: 15377785.

Krishnan K, Moens PDJ (2009) Structure and functions of profilins. Biophysical Reviews 1: 71-81. PMID: 28509986.

Kucera K, Koblansky AA, Saunders LP, Frederick KB, De La Cruz EM, Ghosh S, Modis Y (2010) Structure-based analysis of Toxoplasma gondii profilin: a parasite-specific motif is required for recognition by Toll-like receptor 11. Journal of Molecular Biology 403: 616-29. PMID: 20851125.

Kudryashev M, Lepper S, Baumeister W, Cyrklaff M, Frischknecht F (2010a) Geometric constrains for detecting short actin filaments by cryogenic electron tomography. PMC Biophysics 3: 6. PMID: 20214767.

Kudryashev M, Lepper S, Stanway R, Bohn S, Baumeister W, Cyrklaff M, Frischknecht F (2010b) Positioning of large organelles by a membrane- associated cytoskeleton in Plasmodium sporozoites. Cellular Microbiology 12: 362-71. PMID: 19863555.

Kudryashev M, Munter S, Lemgruber L, Montagna G, Stahlberg H, Matuschewski K, Meissner M, Cyrklaff M, Frischknecht F (2012) Structural basis for chirality and directional motility of Plasmodium sporozoites. Cellular Microbiology 14: 1757-68. PMID: 22776715.

Kursula I, Kursula P, Ganter M, Panjikar S, Matuschewski K, Schuler H (2008a) Structural basis for parasite-specific functions of the divergent profilin of Plasmodium falciparum. Structure 16: 1638-48. PMID: 19000816.

Kursula P, Kursula I, Massimi M, Song YH, Downer J, Stanley WA, Witke W, Wilmanns M (2008b) High-resolution structural analysis of mammalian profilin 2a complex formation with two physiological ligands: the formin homology 1 domain of mDia1 and the proline-rich domain of VASP. Journal of Molecular Biology 375: 270-90. PMID: 18001770.

Lammermann T, Afonso PV, Angermann BR, Wang JM, Kastenmuller W, Parent CA, Germain RN (2013) Neutrophil swarms require LTB4 and integrins at sites of cell death in vivo. Nature 498: 371-5. PMID: 23708969.

Lammermann T, Bader BL, Monkley SJ, Worbs T, Wedlich-Soldner R, Hirsch K, Keller M, Forster R, Critchley DR, Fassler R *et al*. (2008) Rapid leukocyte migration by integrin-independent flowing and squeezing. Nature 453: 51-5. PMID: 18451854.

Lammermann T, Sixt M (2009) Mechanical modes of 'amoeboid' cell migration. Current Opinion in Cell Biology 21: 636-44. PMID: 19523798.

Langhorne J, Buffet P, Galinski M, Good M, Harty J, Leroy D, Mota MM, Pasini E, Renia L, Riley E *et al*. (2011) The relevance of non-human primate and rodent malaria models for humans. Malaria Journal 10: 23. PMID: 21288352.

Langhorne J, Ndungu FM, Sponaas AM, Marsh K (2008) Immunity to malaria: more questions than answers. Nature Immunology 9: 725-32. PMID: 18563083.

Langreth SG, Peterson E (1985) Pathogenicity, stability, and immunogenicity of a knobless clone of Plasmodium falciparum in Colombian owl monkeys. Infection and Immunity 47: 760-6. PMID: 3882566.

Le Roch KG, Johnson JR, Florens L, Zhou Y, Santrosyan A, Grainger M, Yan SF, Williamson KC, Holder AA, Carucci DJ *et al*. (2004) Global analysis of transcript and protein levels across the Plasmodium falciparum life cycle. Genome research 14: 2308-18. PMID: 15520293.

Lemgruber L, Kudryashev M, Dekiwadia C, Riglar DT, Baum J, Stahlberg H, Ralph SA, Frischknecht F (2013) Cryo-electron tomography reveals four-membrane architecture of the Plasmodium apicoplast. Malaria Journal 12: 25. PMID: 23331966.

Lemgruber L, Lupetti P (2012) Crystalloid body, refractile body and virus-like particles in Apicomplexa: what is in there? Parasitology 139: 285-93. PMID: 22217113.

Lindner SE, Swearingen KE, Harupa A, Vaughan AM, Sinnis P, Moritz RL, Kappe SH (2013) Total and putative surface proteomics of malaria parasite salivary gland sporozoites. Molecular & Cellular Proteomics : MCP 12: 1127-43. PMID: 23325771.

Long CA, Zavala F (2017) Immune Responses in Malaria. Cold Spring Harbor Perspectives in Medicine: a025577. PMID: 28389518.

Lu J, Pollard TD (2001) Profilin binding to poly-L-proline and actin monomers along with ability to catalyze actin nucleotide exchange is required for viability of fission yeast. Molecular Biology of the Cell 12: 1161-75. PMID: 11294914.

Lyke KE, Ishizuka AS, Berry AA, Chakravarty S, DeZure A, Enama ME, James ER, Billingsley PF, Gunasekera A, Manoj A *et al*. (2017) Attenuated PfSPZ Vaccine induces strain-transcending T cells and durable protection against heterologous controlled human malaria infection. Proceedings of the National Academy of Sciences of the United States of America 114: 2711-2716. PMID: 28223498.

Machesky LM, Atkinson SJ, Ampe C, Vandekerckhove J, Pollard TD (1994a) Purification of a cortical complex containing two unconventional actins from Acanthamoeba by affinity chromatography on profilin-agarose. The Journal of Cell Biology 127: 107-15. PMID: 7929556.

Machesky LM, Cole NB, Moss B, Pollard TD (1994b) Vaccinia virus expresses a novel profilin with a higher affinity for polyphosphoinositides than actin. Biochemistry 33: 10815-24. PMID: 8075084.

Machesky LM, Poland TD (1993) Profilin as a potential mediator of membrane-cytoskeleton communication. Trends in Cell Biology 3: 381-5. PMID: 14731655.

Magnani M, Stocchi V, Cucchiarini L, Chiarantini L, Fornaini G (1986) Red blood cell phagocytosis and lysis following oxidative damage by phenylhydrazine. Cell Biochemistry and Function 4: 263-9. PMID: 2947735.

Mann T, Beckers C (2001) Characterization of the subpellicular network, a filamentous membrane skeletal component in the parasite Toxoplasma gondii. Molecular and Biochemical Parasitology 115: 257-68. PMID: 11420112.

Margos G, Siden-Kiamos I, Fowler RE, Gillman TR, Spaccapelo R, Lycett G, Vlachou D, Papagiannakis G, Eling WM, Mitchell GH *et al*. (2000) Myosin A expressions in sporogonic stages of Plasmodium. Molecular and Biochemical Parasitology 111: 465-9. PMID: 11163454.

Marsick BM, Flynn KC, Santiago-Medina M, Bamburg JR, Letourneau PC (2010) Activation of ADF/cofilin mediates attractive growth cone turning toward nerve growth factor and netrin-1. Developmental Neurobiology 70: 565-88. PMID: 20506164.

Matuschewski K, Mota MM, Pinder JC, Nussenzweig V, Kappe SH (2001) Identification of the class XIV myosins Pb-MyoA and Py-MyoA and expression in Plasmodium sporozoites. Molecular and Biochemical Parasitology 112: 157-61. PMID: 11166399.

Mbengue A, Yam XY, Braun-Breton C (2012) Human erythrocyte remodelling during Plasmodium falciparum malaria parasite growth and egress. British Journal of Haematology 157: 171-9. PMID: 22313394.

McFadden GI (2011) The apicoplast. Protoplasma 248: 641-50. PMID: 21165662.

Meibalan E, Marti M (2016) Biology of Malaria Transmission. Cold Spring Harbor Perspectives in Medicine 7 (3): a025452. PMID: 27836912.

Meissner M, Schluter D, Soldati D (2002) Role of Toxoplasma gondii myosin A in powering parasite gliding and host cell invasion. Science 298: 837-40. PMID: 12399593.

Menard R, Tavares J, Cockburn I, Markus M, Zavala F, Amino R (2013) Looking under the skin: the first steps in malarial infection and immunity. Nature Reviews Microbiology 11: 701-12. PMID: 24037451.

Metzler WJ, Bell AJ, Ernst E, Lavoie TB, Mueller L (1994) Identification of the poly-L-proline-binding site on human profilin. The Journal of Biological Chemistry 269: 4620-5. PMID: 8308034.

Mitchison TJ, Cramer LP (1996) Actin-based cell motility and cell locomotion. Cell 84: 371-9. PMID: 8608590.

Moll K LI, Perlmann H, Scherf A, Wahlgren M. (eds) (2008) Methods in Malaria Research. Paris, France.

Mombaerts P, Iacomini J, Johnson RS, Herrup K, Tonegawa S, Papaioannou VE (1992) RAG-1-deficient mice have no mature B and T lymphocytes. Cell 68: 869-77. PMID: 1547488.

Morahan BJ, Wang L, Coppel RL (2009) No TRAP, no invasion. Trends in Parasitology 25: 77-84. PMID: 19101208.

Moreira CK, Templeton TJ, Lavazec C, Hayward RE, Hobbs CV, Kroeze H, Janse CJ, Waters AP, Sinnis P, Coppi A (2008) The Plasmodium TRAP/MIC2 family member, TRAP-Like Protein (TLP), is involved in tissue traversal by sporozoites. Cellular Microbiology 10: 1505-16. PMID: 18346224.

Morrissette NS, Sibley LD (2002) Cytoskeleton of apicomplexan parasites. Microbiology and Molecular Biology Reviews 66: 21-38. PMID: 11875126.

Mota MM, Pradel G, Vanderberg JP, Hafalla JC, Frevert U, Nussenzweig RS, Nussenzweig V, Rodriguez A (2001) Migration of Plasmodium sporozoites through cells before infection. Science 291: 141-4. PMID: 11141568.

Mueller AK, Camargo N, Kaiser K, Andorfer C, Frevert U, Matuschewski K, Kappe SH (2005a) Plasmodium liver stage developmental arrest by depletion of a protein at the parasite-host interface. Proceedings of the National Academy of Sciences of the United States of America 102: 3022-7. PMID: 15699336.

Mueller AK, Labaied M, Kappe SH, Matuschewski K (2005b) Genetically modified Plasmodium parasites as a protective experimental malaria vaccine. Nature 433: 164-7. PMID: 15580261.

Munter S, Sabass B, Selhuber-Unkel C, Kudryashev M, Hegge S, Engel U, Spatz JP, Matuschewski K, Schwarz US, Frischknecht F (2009) Plasmodium sporozoite motility is modulated by the turnover of discrete adhesion sites. Cell Host & Microbe 6: 551-62. PMID: 20006843.

Muthinja MJ, Ripp J, Hellmann JK, Haraszti T, Dahan N, Lemgruber L, Battista A, Schutz L, Fackler OT, Schwarz US *et al*. (2017) Microstructured Blood Vessel Surrogates Reveal Structural Tropism of Motile Malaria Parasites. Advanced Healthcare Materials 6, 1601178. PMID: 28117558.

Nussenzweig RS, Vanderberg J, Most H, Orton C (1967) Protective immunity produced by the injection of x-irradiated sporozoites of plasmodium berghei. Nature 216: 160-2. PMID: 6057225.

Osier FH, Fegan G, Polley SD, Murungi L, Verra F, Tetteh KK, Lowe B, Mwangi T, Bull PC, Thomas AW *et al*. (2008) Breadth and magnitude of antibody responses to multiple Plasmodium falciparum merozoite antigens are associated with protection from clinical malaria. Infection and Immunity 76: 2240-8. PMID: 18316390.

Otomo T, Tomchick DR, Otomo C, Panchal SC, Machius M, Rosen MK (2005) Structural basis of actin filament nucleation and processive capping by a formin homology 2 domain. Nature 433: 488-94. PMID: 15635372.

Otterbein LR, Graceffa P, Dominguez R (2001) The crystal structure of uncomplexed actin in the ADP state. Science 293: 708-11. PMID: 11474115.

Pardee JD, Spudich JA (1982) Purification of muscle actin. Methods in Enzymology 85 Pt B: 164-81. PMID: 7121269.

Paul AS, Egan ES, Duraisingh MT (2015) Host-parasite interactions that guide red blood cell invasion by malaria parasites. Current Opinion in Hematology 22: 220-6. PMID: 25767956.

Periz J, Whitelaw J, Harding C, Gras S, Del Rosario Minina MI, Latorre-Barragan F, Lemgruber L, Reimer MA, Insall R, Heaslip A *et al*. (2017) Toxoplasma gondii F-actin forms an extensive filamentous network required for material exchange and parasite maturation. eLife 6: e24119. PMID: 28322189.

Perrin BJ, Ervasti JM (2010) The actin gene family: function follows isoform. Cytoskeleton 67: 630-4. PMID: 20737541.

Pfander C, Anar B, Schwach F, Otto TD, Brochet M, Volkmann K, Quail MA, Pain A, Rosen B, Skarnes W *et al*. (2011) A scalable pipeline for highly effective genetic modification of a malaria parasite. Nature Methods 8: 1078-82. PMID: 22020067.

Pimenta PF, Touray M, Miller L (1994) The journey of malaria sporozoites in the mosquito salivary gland. The Journal of Eukaryotic Microbiology 41: 608-24. PMID: 7866385.

Pinder JC, Fowler RE, Dluzewski AR, Bannister LH, Lavin FM, Mitchell GH, Wilson RJ, Gratzer WB (1998) Actomyosin motor in the merozoite of the malaria parasite, Plasmodium falciparum: implications for red cell invasion. Journal of Cell Science 111 (Pt 13): 1831-9. PMID: 9625746.

Pino P, Sebastian S, Kim EA, Bush E, Brochet M, Volkmann K, Kozlowski E, Llinas M, Billker O, Soldati-Favre D (2012) A tetracycline-repressible transactivator system to study essential genes in malaria parasites. Cell Host & Microbe 12: 824-34. PMID: 23245327.

Plattner F, Yarovinsky F, Romero S, Didry D, Carlier MF, Sher A, Soldati-Favre D (2008) Toxoplasma profilin is essential for host cell invasion and TLR11-dependent induction of an interleukin-12 response. Cell Host & Microbe 3: 77-87. PMID: 18312842.

Pollard TD, Borisy GG (2003) Cellular motility driven by assembly and disassembly of actin filaments. Cell 112: 453-65. PMID: 12600310.

Porta JC, Borgstahl GE (2012) Structural basis for profilin-mediated actin nucleotide exchange. Journal of Molecular Biology 418: 103-16. PMID: 22366544.

Pradel G, Hayton K, Aravind L, Iyer LM, Abrahamsen MS, Bonawitz A, Mejia C, Templeton TJ (2004) A multidomain adhesion protein family expressed in Plasmodium falciparum is essential for transmission to the mosquito. The Journal of Experimental Medicine 199: 1533-44. PMID: 15184503.

Prado M, Eickel N, De Niz M, Heitmann A, Agop-Nersesian C, Wacker R, Schmuckli-Maurer J, Caldelari R, Janse CJ, Khan SM *et al*. (2015) Long-term live imaging reveals cytosolic immune responses of host hepatocytes against Plasmodium infection and parasite escape mechanisms. Autophagy 11: 1561-79. PMID: 26208778.

Prudencio M, Rodriguez A, Mota MM (2006) The silent path to thousands of merozoites: the Plasmodium liver stage. Nature Reviews Microbiology 4: 849-56. PMID: 17041632.

Prugnolle F, Durand P, Neel C, Ollomo B, Ayala FJ, Arnathau C, Etienne L, Mpoudi-Ngole E, Nkoghe D, Leroy E *et al*. (2010) African great apes are natural hosts of multiple related malaria species, including Plasmodium falciparum. Proceedings of the National Academy of Sciences of the United States of America 107: 1458-63. PMID: 20133889.

Quadt KA, Streichfuss M, Moreau CA, Spatz JP, Frischknecht F (2016) Coupling of Retrograde Flow to Force Production During Malaria Parasite Migration. ACS Nano 10: 2091-102. PMID: 26792112.

Raine JD, Ecker A, Mendoza J, Tewari R, Stanway RR, Sinden RE (2007) Female inheritance of malarial lap genes is essential for mosquito transmission. PLoS Pathogens 3 (3): e30. PMID: 17335349.

Ramasamy R (2014) Zoonotic malaria - global overview and research and policy needs. Frontiers in Public Health 2: 123. PMID: 25184118.

Ream RA, Theriot JA, Somero GN (2003) Influences of thermal acclimation and acute temperature change on the motility of epithelial wound-healing cells (keratocytes) of tropical, temperate and Antarctic fish. Journal of Experimental Biology 206: 4539-51. PMID: 14610038.

Renkawitz J, Schumann K, Weber M, Lammermann T, Pflicke H, Piel M, Polleux J, Spatz JP, Sixt M (2009) Adaptive force transmission in amoeboid cell migration. Nature Cell Biology 11: 1438-43. PMID: 19915557.

Ribeiro JM, Francischetti IM (2003) Role of arthropod saliva in blood feeding: sialome and post-sialome perspectives. Annual Review of Entomology 48: 73-88. PMID: 12194906.

Riley EM, Couper KN, Helmby H, Hafalla JC, de Souza JB, Langhorne J, Jarra WB, Zavala F (2010) Neuropathogenesis of human and murine malaria. Trends in Parasitology 26: 277-8. PMID: 20338809.

Robson KJ, Hall JR, Jennings MW, Harris TJ, Marsh K, Newbold CI, Tate VE, Weatherall DJ (1988) A highly conserved amino-acid sequence in thrombospondin, properdin and in proteins from sporozoites and blood stages of a human malaria parasite. Nature 335: 79-82. PMID: 3045563.

Romero S, Le Clainche C, Didry D, Egile C, Pantaloni D, Carlier MF (2004) Formin is a processive motor that requires profilin to accelerate actin assembly and associated ATP hydrolysis. Cell 119: 419-29. PMID: 15507212.

Russell ES, Neufeld EF, Higgins CT (1951) Comparison of normal blood picture of young adults from 18 inbred strains of mice. Proceedings of the Society for Experimental Biology and Medicine Society for Experimental Biology and Medicine 78: 761-6. PMID: 14912022.

Saeed S, Tremp AZ, Dessens JT (2015) Biogenesis of the crystalloid organelle in Plasmodium involves microtubule-dependent vesicle transport and assembly. International Journal for Parasitology 45: 537-47. PMID: 25900212.

Samatey FA, Matsunami H, Imada K, Nagashima S, Shaikh TR, Thomas DR, Chen JZ, Derosier DJ, Kitao A, Namba K (2004) Structure of the bacterial flagellar hook and implication for the molecular universal joint mechanism. Nature 431: 1062-8. PMID: 15510139.

Sanders PR, Cantin GT, Greenbaum DC, Gilson PR, Nebl T, Moritz RL, Yates JR, 3rd, Hodder AN, Crabb BS (2007) Identification of protein complexes in detergent-resistant membranes of Plasmodium falciparum schizonts. Molecular and Biochemical Parasitology 154: 148-57. PMID: 17553576.

Santos JM, Duarte N, Kehrer J, Ramesar J, Avramut MC, Koster AJ, Dessens JT, Frischknecht F, Chevalley-Maurel S, Janse CJ *et al*. (2016) Maternally supplied S-acyl-transferase is required for crystalloid organelle formation and transmission of the malaria parasite. Proceedings of the National Academy of Sciences of the United States of America 113: 7183-8. PMID: 27303037.

Sato Y, Hliscs M, Dunst J, Goosmann C, Brinkmann V, Montagna GN, Matuschewski K (2016) Comparative Plasmodium gene overexpression reveals distinct perturbation of sporozoite transmission by profilin. Molecular Biology of the Cell 27: 2234-44. PMID: 27226484.

Schmitz S, Schaap IA, Kleinjung J, Harder S, Grainger M, Calder L, Rosenthal PB, Holder AA, Veigel C (2010) Malaria parasite actin polymerization and filament structure. The Journal of Biological Chemistry 285: 36577-85. PMID: 20826799.

Schneider D, Shahabuddin M (2000) Malaria parasite development in a Drosophila model. Science 288: 2376-9. PMID: 10875925.

Schrevel J, Asfaux-Foucher G, Hopkins JM, Robert V, Bourgouin C, Prensier G, Bannister LH (2008) Vesicle trafficking during sporozoite development in Plasmodium berghei: ultrastructural evidence for a novel trafficking mechanism. Parasitology 135: 1-12. PMID: 17908361.

Schuler H, Matuschewski K (2006) Regulation of apicomplexan microfilament dynamics by a minimal set of actin-binding proteins. Traffic 7: 1433-9. PMID: 17010119.

Schuler H, Mueller AK, Matuschewski K (2005) A Plasmodium actin-depolymerizing factor that binds exclusively to actin monomers. Molecular Biology of the Cell 16: 4013-23. PMID: 15975905.

Seder RA, Chang LJ, Enama ME, Zephir KL, Sarwar UN, Gordon IJ, Holman LA, James ER, Billingsley PF, Gunasekera A *et al*. (2013) Protection against malaria by intravenous immunization with a nonreplicating sporozoite vaccine. Science 341: 1359-65. PMID: 23929949.

Shen B, Sibley LD (2014) Toxoplasma aldolase is required for metabolism but dispensable for host-cell invasion. Proceedings of the National Academy of Sciences of the United States of America 111: 3567-72. PMID: 24550496.

Siden-Kiamos I, Ganter M, Kunze A, Hliscs M, Steinbuchel M, Mendoza J, Sinden RE, Louis C, Matuschewski K (2011) Stage-specific depletion of myosin A supports an essential role in motility of malarial ookinetes. Cellular Microbiology 13: 1996-2006. PMID: 21899701.

Sidjanski S, Vanderberg JP (1997) Delayed migration of Plasmodium sporozoites from the mosquito bite site to the blood. American Journal of Tropical Medicine and Hygiene 57: 426-9. PMID: 9347958.

Silvestrini F, Alano P, Williams JL (2000) Commitment to the production of male and female gametocytes in the human malaria parasite Plasmodium falciparum. Parasitology 121 Pt 5: 465-71. PMID: 11128797.

Sinden RE, Talman A, Marques SR, Wass MN, Sternberg MJ (2010) The flagellum in malarial parasites. Current Opinion in Microbiology 13: 491-500. PMID: 20566299.

Singer M, Frischknecht F (2017) Time for Genome Editing: Next-Generation Attenuated Malaria Parasites. Trends in Parasitology 33: 202-213. PMID: 27793562.

Singh SS, Chauhan A, Murakami N, Styles J, Elzinga M, Chauhan VP (1996) Phosphoinositide-dependent in vitro phosphorylation of profilin by protein kinase C. Phospholipid specificity and localization of the phosphorylation site. Journal of Receptors and Signal Transduction 6: 77-86. PMID: 9015863.

Sinha A, Hughes KR, Modrzynska KK, Otto TD, Pfander C, Dickens NJ, Religa AA, Bushell E, Graham AL, Cameron R *et al*. (2014) A cascade of DNA-binding proteins for sexual commitment and development in Plasmodium. Nature 507: 253-7. PMID: 24572359.

Skillman KM, Daher W, Ma CI, Soldati-Favre D, Sibley LD (2012) Toxoplasma gondii profilin acts primarily to sequester G-actin while formins efficiently nucleate actin filament formation in vitro. Biochemistry 51: 2486-95. PMID: 22397711.

Skillman KM, Diraviyam K, Khan A, Tang K, Sept D, Sibley LD (2011) Evolutionarily divergent, unstable filamentous actin is essential for gliding motility in apicomplexan parasites. PLoS pathogens 7: e1002280. PMID: 21998582.

Small JV, Herzog M, Anderson K (1995) Actin filament organization in the fish keratocyte lamellipodium. The Journal of Cell Biology 129: 1275-86. PMID: 7775574.

Sohn RH, Chen J, Koblan KS, Bray PF, Goldschmidt-Clermont PJ (1995) Localization of a binding site for phosphatidylinositol 4,5-bisphosphate on human profilin. The Journal of Biological Chemistry 270: 21114-20. PMID: 7673143.

Sorber K, Dimon MT, DeRisi JL (2011) RNA-Seq analysis of splicing in Plasmodium falciparum uncovers new splice junctions, alternative splicing and splicing of antisense transcripts. Nucleic Acids Research 39: 3820-35. PMID: 21245033.

Spaccapelo R, Aime E, Caterbi S, Arcidiacono P, Capuccini B, Di Cristina M, Dottorini T, Rende M, Bistoni F, Crisanti A (2011) Disruption of plasmepsin-4 and merozoites surface protein-7 genes in Plasmodium berghei induces combined virulence-attenuated phenotype. Scientific Reports 1: 39. PMID: 22355558.

Stanisic DI, Good MF (2015) Whole organism blood stage vaccines against malaria. Vaccine 33: 7469-75. PMID: 26428451.

Stanway RR, Graewe S, Rennenberg A, Helm S, Heussler VT (2009) Highly efficient subcloning of rodent malaria parasites by injection of single merosomes or detached cells. Nature Protocols 4: 1433-9. PMID: 19745825.

Steinbuechel M, Matuschewski K (2009) Role for the Plasmodium sporozoite-specific transmembrane protein S6 in parasite motility and efficient malaria transmission. Cellular Microbiology 11: 279-88. PMID: 19016774.

Sterling CR, Aikawa M, Vanderberg JP (1973) The passage of Plasmodium berghei sporozoites through the salivary glands of Anopheles stephensi: an electron microscope study. Journal of Parasitology 59: 593-605. PMID: 4578977.

Sturm A, Amino R, van de Sand C, Regen T, Retzlaff S, Rennenberg A, Krueger A, Pollok JM, Menard R, Heussler VT (2006) Manipulation of host hepatocytes by the malaria parasite for delivery into liver sinusoids. Science 313: 1287-90. PMID: 16888102.

Sultan AA, Thathy V, Frevert U, Robson KJ, Crisanti A, Nussenzweig V, Nussenzweig RS, Menard R (1997) TRAP is necessary for gliding motility and infectivity of plasmodium sporozoites. Cell 90: 511-22. PMID: 9267031.

Tavares J, Formaglio P, Thiberge S, Mordelet E, Van Rooijen N, Medvinsky A, Menard R, Amino R (2013) Role of host cell traversal by the malaria sporozoite during liver infection. The Journal of Experimental Medicine 210: 905-15. PMID: 23610126.

Tossavainen H, Pihlajamaa T, Huttunen TK, Raulo E, Rauvala H, Permi P, Kilpelainen I (2006) The layered fold of the TSR domain of P. falciparum TRAP contains a heparin binding site. Protein science : a Publication of the Protein Society 15: 1760-8. PMID: 16815922.

Tsuji M, Mattei D, Nussenzweig RS, Eichinger D, Zavala F (1994) Demonstration of heat-shock protein 70 in the sporozoite stage of malaria parasites. Parasitology Research 80: 16-21. PMID: 8153120.

Vahokoski J, Bhargav SP, Desfosses A, Andreadaki M, Kumpula EP, Martinez SM, Ignatev A, Lepper S, Frischknecht F, Siden-Kiamos I *et al*. (2014) Structural differences explain diverse functions of Plasmodium actins. PLoS Pathogens 10: e1004091. PMID: 24743229.

Valenta R, Duchene M, Ebner C, Valent P, Sillaber C, Deviller P, Ferreira F, Tejkl M, Edelmann H, Kraft D *et al*. (1992) Profilins constitute a novel family of functional plant pan-allergens. The Journal of Experimental Medicine 175: 377-85. PMID: 1370681.

van Dijk MR, Douradinha B, Franke-Fayard B, Heussler V, van Dooren MW, van Schaijk B, van Gemert GJ, Sauerwein RW, Mota MM, Waters AP *et al*. (2005) Genetically attenuated, P36p-deficient malarial sporozoites induce protective immunity and apoptosis of infected liver cells. Proceedings of the National Academy of Sciences of the United States of America 102: 12194-9. PMID: 16103357.

Vanderberg JP (1974) Studies on the motility of Plasmodium sporozoites. The Journal of Protozoology 21: 527-37. PMID: 4138523.

Vanderberg JP, Frevert U (2004) Intravital microscopy demonstrating antibody-mediated immobilisation of Plasmodium berghei sporozoites injected into skin by mosquitoes. International journal for Parasitology 34: 991-6. PMID: 15313126.

Vaughan AM, Kappe SHI (2017) Malaria Parasite Liver Infection and Exoerythrocytic Biology. Cold Spring Harbor Perspectives in Medicine 7 (6): a025486. PMID: 28242785.

Verheyen EM, Cooley L (1994) Profilin mutations disrupt multiple actin-dependent processes during Drosophila development. Development 120: 717-28. PMID: 7600952.

Vicente-Manzanares M, Ma X, Adelstein RS, Horwitz AR (2009) Non-muscle myosin II takes centre stage in cell adhesion and migration. Nature Reviews Molecular Cell Biology 10: 778-90. PMID: 19851336.

Vinson VK, De La Cruz EM, Higgs HN, Pollard TD (1998) Interactions of Acanthamoeba profilin with actin and nucleotides bound to actin. Biochemistry 37: 10871-80. PMID: 9692980.

Vlachou D, Schlegelmilch T, Runn E, Mendes A, Kafatos FC (2006) The developmental migration of Plasmodium in mosquitoes. Current Opinion in Genetics & Development 16: 384-91. PMID: 16793259.

Vlachou D, Zimmermann T, Cantera R, Janse CJ, Waters AP, Kafatos FC (2004) Real-time, in vivo analysis of malaria ookinete locomotion and mosquito midgut invasion. Cellular Microbiology 6: 671-85. PMID: 15186403.

Wang YL (1985) Exchange of actin subunits at the leading edge of living fibroblasts: possible role of treadmilling. The Journal of Cell Biology 101: 597-602. PMID: 4040521.

Wegner A (1976) Head to tail polymerization of actin. Journal of Molecular Biology 108: 139-50. PMID: 1003481.

White NJ, Turner GD, Medana IM, Dondorp AM, Day NP (2010) The murine cerebral malaria phenomenon. Trends in Parasitology 26: 11-5. PMID: 19932638.

Whitelaw JA, Latorre-Barragan F, Gras S, Pall GS, Leung JM, Heaslip A, Egarter S, Andenmatten N, Nelson SR, Warshaw DM *et al*. (2017) Surface attachment, promoted by the actomyosin system of Toxoplasma gondii is important for efficient gliding motility and invasion. BMC Biology 15: 1. PMID: 28100223.

WHO (2016) World Malaria Report. In Licence: CC BY-NC-SA 30 IGO, Geneva: World Health Organization

WHO (2017) Malaria vaccine: WHO position paper, January 2016 - Recommendations. Vaccine: S0264410X16309823 PMID: 28385607.

Wilson CA, Tsuchida MA, Allen GM, Barnhart EL, Applegate KT, Yam PT, Ji L, Keren K, Danuser G, Theriot JA (2010) Myosin II contributes to cell-scale actin network treadmilling through network disassembly. Nature 465: 373-7. PMID: 20485438.

Witke W (2004) The role of profilin complexes in cell motility and other cellular processes. Trends in Cell Biology 14: 461-9. PMID: 15308213.

Witke W, Sutherland JD, Sharpe A, Arai M, Kwiatkowski DJ (2001) Profilin I is essential for cell survival and cell division in early mouse development. Proceedings of the National Academy of Sciences of the United States of America 98: 3832-6. PMID: 11274401.

Wolven AK, Belmont LD, Mahoney NM, Almo SC, Drubin DG (2000) In vivo importance of actin nucleotide exchange catalyzed by profilin. The Journal of Cell Biology 150: 895-904. PMID: 10953013.

Woo YH, Ansari H, Otto TD, Klinger CM, Kolisko M, Michalek J, Saxena A, Shanmugam D, Tayyrov A, Veluchamy A *et al*. (2015) Chromerid genomes reveal the evolutionary path from photosynthetic algae to obligate intracellular parasites. eLife 4: e06974. PMID: 26175406.

Yam PT, Wilson CA, Ji L, Hebert B, Barnhart EL, Dye NA, Wiseman PW, Danuser G, Theriot JA (2007) Actin-myosin network reorganization breaks symmetry at the cell rear to spontaneously initiate polarized cell motility. The Journal of Cell Biology 178: 1207-21. PMID: 17893245.

Yarovinsky F, Zhang D, Andersen JF, Bannenberg GL, Serhan CN, Hayden MS, Hieny S, Sutterwala FS, Flavell RA, Ghosh S *et al*. (2005) TLR11 activation of dendritic cells by a protozoan profilin-like protein. Science 308: 1626-9. PMID: 15860593.

Yusuf NA, Green JL, Wall RJ, Knuepfer E, Moon RW, Schulte-Huxel C, Stanway RR, Martin SR, Howell SA, Douse CH *et al*. (2015) The Plasmodium Class XIV Myosin, MyoB, Has a Distinct Subcellular Location in Invasive and Motile Stages of the Malaria Parasite and an Unusual Light Chain. The Journal of Biological Chemistry 290: 12147-64. PMID: 25802338.

6 Publications and achievements

Part of this work has been published in:

Moreau CA, Bhargav SP, Kumar H, Quadt KA, Piirainen H, Strauss L, Kehrer J, Streichfuss M, Spatz JP, Wade RC, Kursula I, Frischknecht F (2017) A unique profilin-actin interface is important for malaria parasite motility. PLoS pathogens 13: e1006412. PMID: 28552953.

Other publications:

Quadt KA, Streichfuss M, Moreau CA, Spatz JP, Frischknecht F (2016) Coupling of Retrograde Flow to Force Production During Malaria Parasite Migration. ACS nano 10: 2091-102. PMID: 26792112.

Santos JM, Egarter S, Zuzarte-Luis V, Kumar H, Moreau CA, Kehrer J, Pinto A, Costa MD, Franke-Fayard B, Janse CJ, Frischknecht F, Mair GR (2017) Malaria parasite LIMP protein regulates sporozoite gliding motility and infectivity in mosquito and mammalian hosts. eLife 6: e24109. PMID: 28525314.

Further achievements:

Cover image of PloS Pathogens issue June 2017

Poster award at the Conference for Actin Dynamics, Regensburg organized by the DGZ (German Society for Cell Biology)

Poster award at the 3rd Heidelberg Forum for young life scientists conference

Teaching microscopy at EMBO Practical Course: Imaging infection and immunity, CSIR Pretoria, South Africa

Oral presentation during the European Cytoskeletal Forum - Cell Adhesion and Migration, Conference, Cambridge, UK

7 Danksagung

Ich bin sehr vielen Menschen, die mich in den letzten Jahren auf die eine oder andere Weise begleitet und unterstützt haben zu großem Dank verpflichtet:

Allen voran Freddy, Danke für Führung, Chancen, Freiheit und Freundschaft, dafür, dass Du meine ungefilterte Meinung schätzt und mir ein Vorbild für mehr Gelassenheit bist.

Professor Lanzer, für Unterstützung in TAC meetings und den Glauben an meine Fähigkeiten. Danke an Marcel Deponte und Volker Lohmann für ihren Rat und immer präzise Antworten auf alle meine Fragen.

Ich danke Silvia Portugal für ihre große Flexibilität, kurzfristige Verfügbarkeit für die Prüfungskommision und Unterstützung bei Fragen zur Immunologie. Ich danke auch Steeve Boulant für die Teilnahme an meiner Prüfungskommission.

Ich danke unseren Kollaboratoren Professor Rebecca Wade und Professor Inari Kursula, sowie meinen Kollegen und guten Freunden Hirdesh Kumar (*in silico* Simulationen) und Bhargav Saligram Prabhakar (*in vitro* Biochemie). Danke Bhargav für die tolle Zeit in Oulu.

Ich möchte besonders Madlen Konert und Léanne Strauß danken. Ich habe großes Glück, so fähige Praktikanten wie Euch gehabt zu haben. Ihr wart eine große Unterstützung während meiner Arbeit im Labor, bei der Datenauswertung und für die (sehr nötige) gute Stimmung.
Ich danke Hanna Roth und Samantha Ebersoll für die Hilfe bei der Datenauswertung.

Ich danke meiner Frau Katharina, für die Analyse meiner Mutanten mit den optischen Pinzetten und für deine Mit-Leidenschaft für Profilin. Ich danke Dir für die endlose Unterstützung, aufbauenden und immer positiven Worte, dein großes Herz und vor allem, dass Du mich zu einem besseren Menschen machst.

Ich danke Simone Lepper und Mirko Singer dafür, dass sie mir ihr fundiertes Wissen beigebracht und mich die Techniken der AG Frischknecht eingeweiht haben. Ich danke auch Jessica Kehrer für eine tolle Zeit in Südafrika und großartige Zusammenarbeit (working with experts!). Außerdem danke ich Miriam Reinig und Julia Sattler für die Unterstützung bei der Arbeit an Profilin.
Ich danke besonders Ross Douglas für die Korrektur meiner Arbeit, konstruktive Diskussionen und Unterstützung mit PyMol und der Kollaboration mit Rebecca Wade.
Ich danke Romy Alisch, Daria Camozzi, Leandro Lemgruber, Noa Dahan, Mendi Muthinja und Claudia Kuss für ein jederzeit offenes Ohr und die wunderbare Freundschaft.

Ich danke Ann-Kristin Müller, Kirsten Heiss, Britta Nyboer, Priyanka Fernandes und Roland Frank sowie Miriam Griesheimer und Sandra Niebel für Unterstützung.

Ich danke Dennis Klug, Konrad Beyer, Saskia Egarter, Ben Spreng, Verena Staudacher, Linda Liedgens, Sandra Specht und Cletus Wezena sowie allen anderen Mitgliedern der AG Frischknecht und Deponte für gute Stimmung im Labor und im Büro.

Ein ganz besonderer Dank geht an meine Familie und vor allem an meine Eltern für ihre umfangreiche Unterstützung und ihren Glauben an mich.

Ich danke Birthe für die jahrelange tolle Freundschaft. Man sagt, dass Freundschaften die länger als 7 Jahre halten für immer sind. So kann ich mich auf gemeinsame Kochabende und Tassen Tee mit meiner besten Freundin und liebstem Herzensmenschen freuen wenn wir beide schon alt und grau sind.

Danke, Carla und Yvonne für die gemeinsamen Gespräche (mit oder ohne Tränen) in der Küche und die großartige, unvergessliche Zeit zusammen in DER Heidelberger Frauen-WG. Danke an Johannes, my brother from another mother für die lustigen Ginflut-Abende, Crêpe-Sonntage und Unterstützung bei Wifi- und Computerproblemen. Ohne Dich hätte mein MacBook die Leistung der Doktorarbeit (Word und gleichzeitig 50 Tabs im Browser) nicht bringen können!

8 Appendix

8.1 Macro for automated intensity measurements

```
//start with z-projection sum slices
//run("Duplicate...", "title=12-1 duplicate channels=2 slices=1-35");
//run("Z Project...", "start=1 stop=235 projection=[Sum Slices]");
run("Duplicate...", "title=[12] duplicate");
setMinAndMax(0, 65536); //equalizes different min/max in channels
run("16-bit");
run("Duplicate...", "title=[background mask] duplicate");
run("Median...", "radius=5");
run("Auto Threshold", "method=Huang white");
run("Divide...", "value=255.000");
run("Duplicate...", "title=[sample mask] duplicate");
selectWindow("background mask");
run("Multiply...", "value=255.000");
run("Invert");
run("Divide...", "value=255.000");
imageCalculator("Multiply create", "12","sample mask");
run("Duplicate...", "title=[sample] duplicate");
imageCalculator("Multiply create", "12","background mask");
run("Duplicate...", "title=[background] duplicate");
selectWindow("sample");
run("Measure");
run("Subtract...", "value=1");
run("Measure");
selectWindow("background");
run("Measure");
run("Subtract...", "value=1");
run("Measure");
selectWindow("sample");
close();
selectWindow("Result of 12");
close();
selectWindow("Result of 12");
close();
selectWindow("background mask");
close();
selectWindow("background");
close();
selectWindow("sample mask");
close();
selectWindow("12");
close();
//selectWindow("SUM_12-1");
//close();
//selectWindow("12-1");
//close();
```

8.2 Primer

Number	Description	T_{anneal}	Sequence
	Profilin wild type and arm mutations		
356	*Pb* Pfn fw NotI	48	ATTTGCGGCCGCAAAATGGAAGAATATTCATGGG
357	*Pb* Pfn rv XbaI w stop	56	GCTCTAGATTATGCGGCACCTGTATCAG
358	*Pb* Pfn rv XbaI w/o stop	55	GCTCTAGATGCTGCTGCTGCTGCGGCACCTGTATCAG
359	*Pf* Pfn QNQ, AAA, Δarm fw NotI	55	ATTTGCGGCCGCAAAATGGCAGAGGAGTATTCTTGG
360	*Pf* Pfn QNQ, AAA, Δarm rv XbaI w stop	56	GCTCTAGATTACTGTGAGCTTTCTGCCAG
361	*Pf* Pfn QNQ, AAA, Δarm rv XbaI w/o stop	54	GCTCTAGATGCTGCTGCTGCCTGTGAGCTTTCTGCCAG
364	*Pf* Pfn rv XbaI w stop	54	GCTCTAGATGCTGCTGCTGCTTGACTGCTTTCAGCTAGC
365	*Pf* Pfn fw NotI	54	ATTTGCGGCCGCAAAATGGCAGAAGAATATTCATGGG
366	Primer for sequencing, binds in mCherry	56	TCACCTTCAGCTTGGCG
418	*Pf* Pfn rv XbaI w stop	56	GCTCTAGACTATTGACTGCTTTCAGCTAGC
	Pfn homology regions		
367	*Pb* Pfn 3'UTR rv KpnI	55	GGGGTACCCACACATTGGCATTATATAGAAATTGAG
368	*Pb* Pfn 5'UTR fw SacII	46	TCCCCGCGGGAGATATTACACATTGCTAC
369	*Pb* Pfn 5'UTR rv NotI	55	TAAAGCGGCCGCTTTATTATCTTAAAAATTATTTATATAATATGATG
375	Integration test in front of *Pb* Pfn 5'UTR fw	56	GGTGCACACTCATTTGAATGTG
376	Integration test behind *Pb* Pfn 3'UTR rv	56	CAAGTTCTTTCCTCATGTGTTCATG
412	*Pb* Profilin 3'UTR fw ClaI	45	CCATCGATAATAAAGAAAATATTATAAAAATGTG
	Pfn // mCh		
553	*Pb* Pfn mCh rv NotI	56	ATTTGCGGCCGCAAAATGGAAGAATATTCATGGGAAAATT
554	mCherry fw BamHI	55	CGGGATCCTTACTTGTACAGCTCGTCCATG
	Pfn Loop Swaps		
555	*Pb* Pfn with *Pf* loop 1a rev LS1	62/48	CAAAATTTGGGTCACTCTCTTCACCCTGTGCTACGCATTCATATAC
556	*Pb* Pfn with *Pf* loop 1b fw LS1	62/56	CACAGGGTGAAGAGAGTGACCCAAATTTTGATAAATGGTCTCTTTTTTATAAAGAAGA
717	*Pf* Pfn with *Pb* loop 1a rv LS2	62/48	TCAAAGTCTGGATTATTTTCATCGGGGGTAGCTACACAAGCATAGA
718	*Pf* Pfn with *Pb* loop 1b fw LS2	62/56	AGCTACCCCCGATGAAAATAATCCAGACTTTGATAAATGGTCACTTTTTTATAAAGAAGATT
816	*Pf* Pfn with *Tg* loop 1a rv LS3	60/72	CAGCTTGGACCATCCGTCATCATCATCAGCCGCCGCGGCGAAGACAACTCCATCTTCTTCCG AAGCTAATC
817	*Pf* Pfn with *Tg* loop 1b fw LS3	60/72	TTCGCCGCGGCGGCTGATGATGATGACGGATGGTCCAAGCTGTATAAAGAAGATTATGATA AGTTGAAGATGAAAATGGTAC

	LS mutants in pETM-11		
1009	*Pb* Pfn rv XhoI	56	CCGCTCGAGTTATGCGGCACCTGTATCAG
1011	*Pf* Pfn rv XhoI	56	CCGCTCGAGTTATGCTGCTGCTGCTTGA
1045	*Pb* fw NcoI as start	56	CATGCCATGGAAGAATATTCATGGGAAAATTTTTTAAAT
1046	*Pf* fw NcoI as start	55	CATGCCATGGCAGAGGAGTATTCTTGG
	Pfn-mCherry short linker		
P1263	$Pfn^{+/-i}$ mCh rv 1a	48/62	CGCCCTTGCTCACGCCGCCGCCGCCTGCGGCACCTG
P1264	$Pfn^{+/-i}$ mCh fw 1b	56/62	CAGGTGCCGCAGGCGGCGGCGGCGTGAGCAAGGGCG
	Pfn KO (*Plasmo*GEM)		
P586	Gateway 1	47	CATACTAGCCATTTTATGTG
P587	Gateway 2	48	CTTTGGTGACAGATACTAC
P1090	*Pb* Pfn QCR1	62	TCATCGGGGGTTGCTACGCA
P1091	*Pb* Pfn QCR2	59	GCGTAAGGCTTCGTCCGTTT

8.3 Profilin sequence alignment

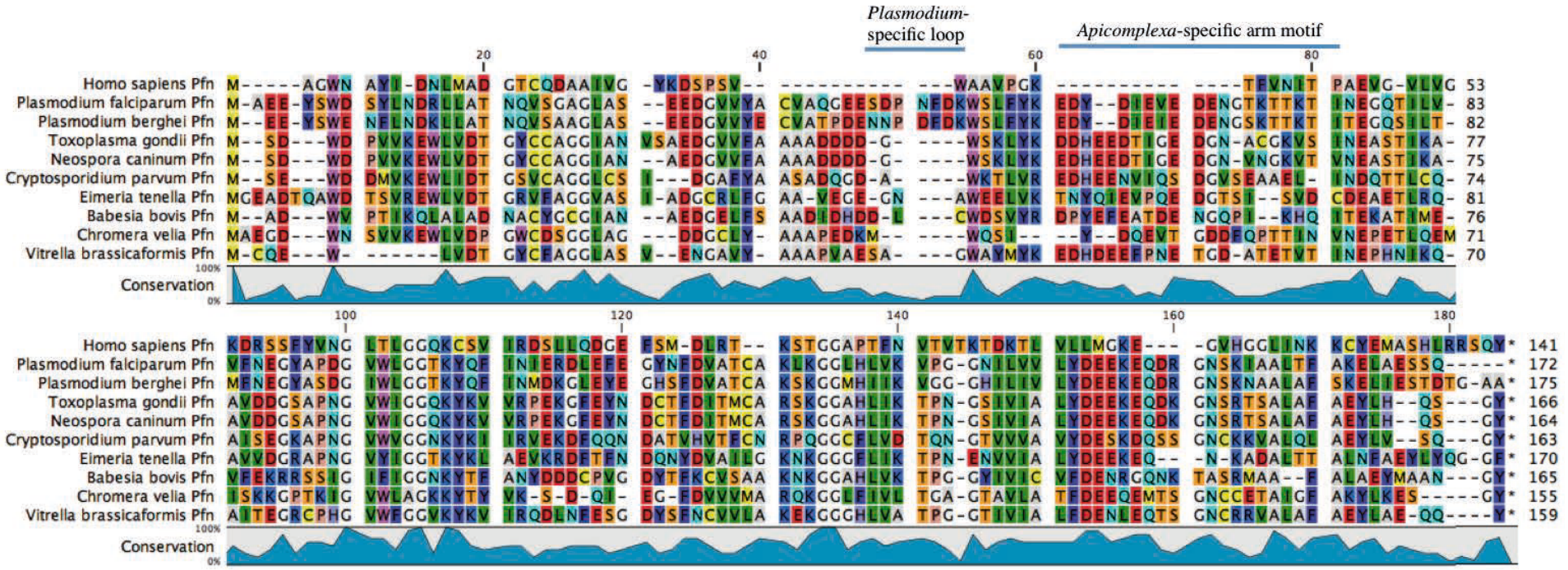

Larger view of Figure 8: Amino acid sequence alignment of human profilin (top) with several apicomplexan profilins (middle) and profilin from the two ancestral chromerids (bottom). The *Plasmodium*-specific acidic loop and the β-hairpin extension (arm motif) are indicated above their respective sequences. The level of sequence conservation is show below in blue. Note the labeled unique features and the corresponding gaps in the human sequence. A larger version of this figure can be found in the appendix. Alignment was created using the CLC Main Workbench software version 5.1 (CLC bio).